Technical Report	455
	W. M. Libbey
Theory of Active Nonreciprocal Networks	4 February 1969

Lincoln Laboratory

MASSACHUSETTS INSTITUTE OF TECHNOLOGY

Lexington, Massachusetts

MASSACHUSETTS INSTITUTE OF TECHNOLOGY
LINCOLN LABORATORY

THEORY OF ACTIVE NONRECIPROCAL NETWORKS

W. M. LIBBEY

Group 44

TECHNICAL REPORT 455

4 FEBRUARY 1969

LEXINGTON   MASSACHUSETTS
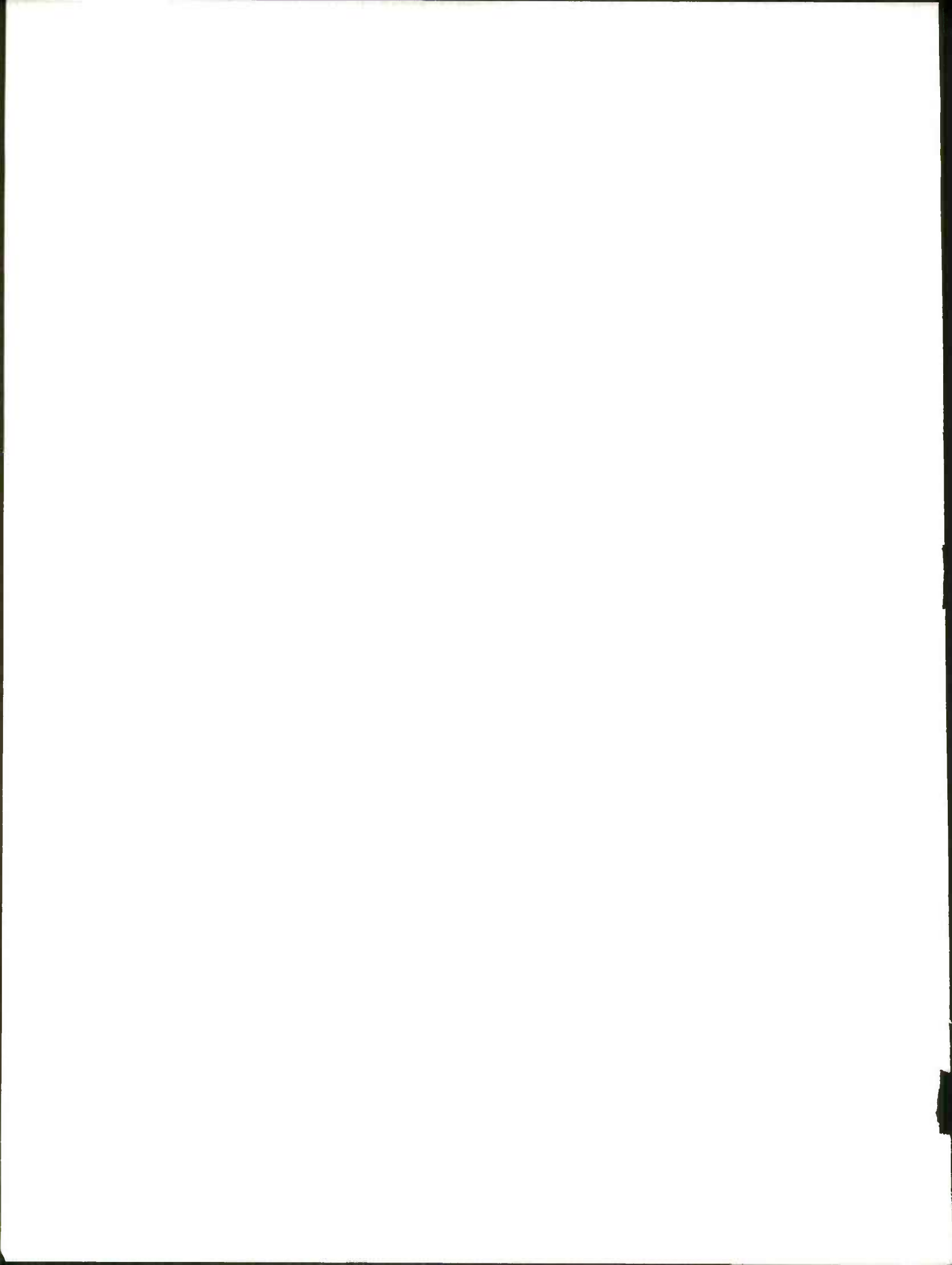
THEORY OF ACTIVE NONRECIPROCAL NETWORKS[†]

ABSTRACT

This investigation sets forth theory and experimental data for active nonreciprocal networks. A simple way is shown of achieving nonreciprocity using a magnetic field device exhibiting small amounts of differential phase shift. In the theoretical treatment, use is made of scattering parameters. The effect on nonreciprocity of having cascaded and parallel connected elements is considered. How matching and scattering from various junctions influences nonreciprocity is included. Two simple devices exhibiting nonreciprocity are discussed in detail: a differential amplifier, and a differential attenuator; and a procedure is given for their use in active network synthesis. For these devices, the meander line is the nonreciprocal element utilizing a magnetic field. A new meander-line design is presented, realizing a desired impedance, based on recent data on odd- and even-mode velocities along coupled microstrips.

From the experimental work, data are reported on a meander line showing impedance characteristics which are in good agreement with theory and showing the amount of differential phase shift possible. To realize an element with loss, an experimental bilateral microstrip attenuator is described whose resistances are short silver-deposited lines. Measurements show satisfactory matching for a 6-dB model. A complete design is given for a microstrip differential attenuator using the loss and nonreciprocal elements mentioned operating near 3 GHz. Scattering parameters measured on a model differential attenuator show very close agreement with theory. Data are presented on both the differential attenuation and the insertion loss of this realized model.

A theoretical analysis is given in Appendix A of two lossless three-port circuits capable of exhibiting nonreciprocity using small amounts of differential phase shift. The analysis demonstrates that relations between variables exist that will allow perfect matching at input and output ports and will allow the desired nonreciprocity without depending entirely on the existence of circulation.

[†] This report is based on a thesis of the same title submitted to the Faculty of the Worcester Polytechnic Institute, Worcester, Massachusetts, on 5 December 1968 in partial fulfillment of the requirements for the Degree of Doctor of Philosophy in Electrical Engineering.

CONTENTS

THEORY OF ACTIVE NONRECIPROCAL NETWORKS

I. INTRODUCTION

Much has been written concerning a class of electrical networks which may be characterized as being bilateral, passive, linear, and composed of finite lumped elements. The theory has been developed to such a degree that various mathematical disciplines have been established whereby these networks may be synthesized directly from a given analytic function.

This report is concerned with a different and more general class of networks for which bilateralness, or reciprocity, is no longer a requirement. At least for a part of the development, the restriction of passivity is also to be removed. Further, since the intended application is at microwave frequencies, elements possessing distributed rather than lumped parameters are utilized. Thus, this less restrictive class of networks is identified as being nonreciprocal, active, and linear (at least within a limited operating range).

In the following sections, the theory of active nonreciprocal two-port networks is extended to include those whose transmission characteristics may be interchanged by a simple switching scheme. The theory shows that nonreciprocal forward-to-backward gain may be achieved by the proper interconnection of active elements and of passive elements that do not exhibit reciprocal phase delay. A basic active circuit is described using the minimum number of components necessary for the existence of such nonreciprocal characteristics. A second device exhibiting nonreciprocal forward-to-backward attenuation is also predicted by the theory. For the latter device, a design is given together with an analysis of data from an experimental model. In Appendix A, two types of imperfect circulators are analyzed as three-port nonreciprocal lossless devices. Appendix B consists of a listing of programs written in Fortran H language specifically for the IBM-360 computer installation at Lincoln Laboratory. Finally, a bibliography pertinent to this report is included as Appendix C.

The remainder of this section is devoted to describing the nature and scope of this specific investigation of active nonreciprocal network theory. As a first step, to obtain the proper perspective, a brief discussion is given of several pertinent contributions to the theory from other investigators.

A. Work of Previous Investigators

Information is available in the literature dealing with the analysis and synthesis of nonreciprocal circuits, various active devices which include conventional tunnel-diode amplifiers, and distributed parameter microstrip transmission lines.

1. Nonreciprocity

Nonreciprocity results from the interaction of a signal magnetic field with a magnetized medium. Thus, a way exists of controlling nonreciprocal phase by reversing a steady magnetic field. If the terminal characteristics of a network are dependent upon nonreciprocal phase, then the terminal characteristics themselves may be switched by such a magnetic bias.

Su[1]† and Carlin, et al.,[2-5] have demonstrated the realization of desired nonreciprocity in conventional active network synthesis. However, these realizations are totally predicated upon the use of a gyrator capable of exhibiting a full 180° of nonreciprocal phase shift. Wenzel[6] and others have shown how microwave reciprocal and nonreciprocal filters may be designed using techniques of modern network synthesis.

Several passive devices are available that do not display equal bilateral phase delay; moreover, unlike the gyrator, these devices may have only a few degrees of nonreciprocal phase. Little information is available on the application of these devices to network theory. One such device, the meander line, is analyzed by Hair and Roome.[7]

2. Active Devices

Single-port nonlinear devices exhibiting negative resistance have been reported in the technical literature for many decades. Although they are considered unstable, they have been applied in many useful ways. Of these negative resistances available today, the Gunn[8] device, the Read[9] avalanche diode, the L. S. A.[10] (limited space-charge accumulation) mode device, and the tunnel diode[11, 12] have been shown to hold promise for the future.

Increasing interest has been created in the very active field of microwave transmission by use of physically small active devices similar to the tunnel diode operating at higher and higher frequencies. Certainly, tunnel diodes are not new, for these particular devices have been applied successfully ever since the discovery of the phenomenon of tunneling by Esaki.[13] Two basic amplifiers are in use today: the transmission type, utilizing the concept of a two-port negative resistance; and the reflection type, utilizing the concept of a one-port negative resistance. In the latter, some additional device is required with which to separate the waves incident upon and reflected from the negative resistance. Scanlan[14] shows the use of three- and four-port ideal circulators with which to perform the separation. On the other hand, Gallagher[15] shows a matched pair of negative resistors in conjunction with a 90° 3-dB hybrid junction as a means to this end.

3. Microstrip Transmission Lines

The interconnection of elements at microwave frequencies is most easily accomplished today by the distributed parameter microstrip line consisting of a single narrow strip separated from a ground plane by a slab of dielectric. The properties of these microstrip lines were first set forth by Wheeler.[16] The characteristics of propagation along two such microstrips coupled together have been analyzed recently by Weiss and Bryant.[17]

Jones and Bolljahn[18] worked out design equations for various filter configurations using coupled lines in the strip-line transmission scheme where normal modes propagate along lines with the same velocity. Similar physical configurations exist in the microstrip transmission

---

† Numbered references are listed at the end of this report on p. 66.

2

scheme, but here, owing to a dielectric-air boundary, the normal modes propagate with different velocities. Differences in propagation velocity certainly alter the predicted filter response of a given configuration. These filter design equations have not been modified for the microstrip system.

4. Periodic Sections

No information is available concerning networks of periodic structure where each iteration is itself an active nonreciprocal section.

B. Statement of the Problem

This study deals specifically with a desired network of potentially periodic structure operating at microwave frequencies. Each individual section is to be a basic active network capable of producing nonreciprocal gain by utilizing nonreciprocal phase-shift elements. Such a section thus can provide some degree of unilateral gain in a direction determined by the elements which exhibit a small amount of nonreciprocal phase shift. Since the nonreciprocal phase shift is reversed by inverting a magnetic field, the unilateral gain through the network will also be considered switchable.

C. Objectives

The objectives of this report are: (1) to contribute to the body of knowledge of active nonreciprocal network theory sufficiently to allow the prediction of basic configurations that exhibit some degree of unilateral and switchable gain with small amounts of nonreciprocal phase shift; and (2) to reduce to practicality one of the devices predicted, thus to substantiate the theoretical development.

II. THEORY

In this section, the theory of active nonreciprocal networks is developed sufficiently to predict several models which show interesting characteristics. The effect of mismatched active elements and different junctions on these nonreciprocal characteristics is considered. A simple procedure is set forth whereby these devices might be utilized in the area of active network synthesis. Throughout the analysis, liberal use is made of the scattering formalism.

A. Definitions

1. Scattering Parameters

One manner in which to characterize a two-port network is given by

$$E_s^1 = S_{11}E_i^1 + S_{12}E_i^2 \tag{1}$$

and

$$E_s^2 = S_{21}E_i^1 + S_{22}E_i^2 \tag{2}$$

where E_i^1 is the complex wave amplitude incident on port 1, E_i^2 is the complex amplitude incident on port 2, E_s^1 is the complex wave amplitude scattered from port 1, E_s^2 is the wave scattered from port 2, and S_{11}, S_{12}, S_{21}, and S_{22} are the directional-coupling or scattering parameters. The ordered double subscript, i.e., S_{12}, is intended to mean scattering referred to

3

port 1 from port 2. Examination of Eqs. (1) and (2) shows that S_{11} and S_{22} have the significance of input reflection coefficients, while S_{21} and S_{12} are the forward and backward transmission coefficients, respectively.

Equations (1) and (2) may be combined in a single matrix equation as

$$\left. \begin{matrix} E_s^1 \\ E_s^2 \end{matrix} \right] = \left[\begin{matrix} S_{11} & S_{12} \\ S_{21} & S_{22} \end{matrix} \right] \left. \begin{matrix} E_i^1 \\ E_i^2 \end{matrix} \right] \tag{3}$$

or

$$\left. \begin{matrix} E_s^1 \\ E_s^2 \end{matrix} \right] = [S] \left. \begin{matrix} E_i^1 \\ E_i^2 \end{matrix} \right] . \tag{4}$$

2. Unitarity

Certain useful relations between the scattering parameters may be derived by considering the energy relations at the driving-point terminals of a given multi-port network.

The total real power delivered to any network may be written in matrix form as

$$P = \text{Re}\left(I^*\right]_t \times E]\right) \tag{5}$$

where $I^*]_t$ is the conjugate transpose or so-called Hermitian conjugate of the matrix I]. If the network is lossless, P must vanish. On substituting the scattering parameters for $I^*]_t$ and assuming that the driving-point impedance is identical at each terminal of the multi-port network, the condition for zero power loss becomes

$$[S^*]_t [S] = [U] \tag{6}$$

or

$$[S] [S^*]_t = [U] \tag{7}$$

where [U] is a unit diagonal matrix. Thus, the scattering matrix itself representing a lossless network is unitary.

In order to satisfy the equality indicated in either Eq. (6) or (7), $S^*]_t$ must be the inverse of the scattering matrix, i.e., $[S]^{-1}$. The determinant of such a matrix must have a unit magnitude.

A condition such as unitarity is often a valuable asset in the algebraic simplification of matrix manipulations, and will be used in the development that follows.

3. Reciprocity

Of the several possible identities which come from the expansion of Eqs. (6) and (7), the following two will suffice to illustrate reciprocity:

$$\left| S_{11} \right|^2 + \left| S_{12} \right|^2 = 1 \tag{8}$$

and

$$\left| S_{11} \right|^2 + \left| S_{21} \right|^2 = 1 \quad . \tag{9}$$

4

Clearly, then, for a lossless network $|S_{12}| = |S_{21}|$, which serves to illustrate the fact that the only nonreciprocity possible is in the arguments of these transmission coefficients.

The visible effect of reciprocity or nonreciprocity on a scattering matrix is the symmetrical condition of the matrix about the principal diagonal. If the matrix is symmetrical, the network is bilateral; however, if there is dissymmetry about the main diagonal, the network possesses some degree of nonreciprocity.

4. Differential Phase

A particular network which is lossless, hence satisfying the unitarity condition, and nonreciprocal only to the extent that the argument of S_{12} does not equal the argument of S_{21}, is said to exhibit differential phase shift. If the phase delay in the forward transmission direction is $\epsilon^{-j\varphi_-}$, the phase delay in the reverse transmission direction is $\epsilon^{-j\varphi_+}$, and the two-port network is matched at both ports, then the scattering matrix for this device is

$$[S] = \begin{bmatrix} 0 & \epsilon^{-j\varphi_+} \\ \epsilon^{-j\varphi_-} & 0 \end{bmatrix} . \tag{10}$$

It is noted the matrix of Eq. (10) demonstrates nonreciprocity by the dissymmetry of phase about the main diagonal; however, owing to the fact that the network is lossless, $|S_{12}| = |S_{21}|$.

The two directional phase angles φ_+ and φ_- will appear many times in the analysis to follow. In order to assist in simplifying as much as possible, a differential phase factor is defined as

$$\delta = \epsilon^{-j[(\varphi_+ - \varphi_-)/2]} . \tag{11}$$

B. Circuit Configurations

Of the many possible methods of interconnecting individual elements to achieve nonreciprocal or differential gain, perhaps the simplest to consider is the cascade or tandem connection.

1. Cascade Connection

Figure 1 shows a cascading of three obstacles or scatterers, a bilateral amplifier with which to make the total circuit active, and a matched element exhibiting differential phase.
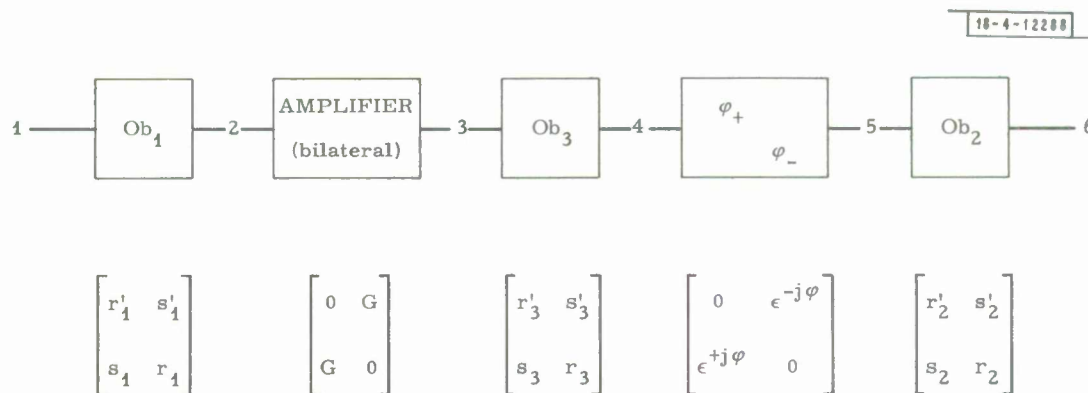
Fig. 1. General cascade connection.

Theorem I.

Any number of circuit elements consisting of lossless scattering obstacles, bilateral ampli-fiers, and elements exhibiting differential phase when cascaded together produce at most nonrec-iprocity in the arguments of the overall transmission characteristics. The magnitudes of the transmission parameters are always equal. If a cascaded circuit is to show nonreciprocal am-plitudes, it then follows that such nonreciprocity must be present in one or more of the elements cascaded together.

Proof.

The input-output waves at the various numbered junctions of the general cascade connection of Fig. 1 are related by directional-coupling parameters and are given in matrix form by

$$
\begin{bmatrix} E_s^1 \\ E_s^2 \end{bmatrix} = \begin{bmatrix} r_1' & s_1' \\ s_1 & r_1 \end{bmatrix} \begin{bmatrix} E_i^1 \\ E_i^2 \end{bmatrix} \tag{12}
$$

$$
\begin{bmatrix} E_s^2 \\ E_s^3 \end{bmatrix} = \begin{bmatrix} 0 & G \\ G & 0 \end{bmatrix} \begin{bmatrix} E_i^2 \\ E_i^3 \end{bmatrix} \tag{13}
$$

$$
\begin{bmatrix} E_s^3 \\ E_s^4 \end{bmatrix} = \begin{bmatrix} r_3' & s_3' \\ s_3 & r_3 \end{bmatrix} \begin{bmatrix} E_i^3 \\ E_i^4 \end{bmatrix} \tag{14}
$$

$$
\begin{bmatrix} E_s^4 \\ E_s^5 \end{bmatrix} = \begin{bmatrix} 0 & \epsilon^{-j\varphi} \\ \epsilon^{+j\varphi} & 0 \end{bmatrix} \begin{bmatrix} E_i^4 \\ E_i^5 \end{bmatrix} \tag{15}
$$

and

$$
\begin{bmatrix} E_s^5 \\ E_s^6 \end{bmatrix} = \begin{bmatrix} r_2' & s_2' \\ s_2 & r_2 \end{bmatrix} \begin{bmatrix} E_i^5 \\ E_i^6 \end{bmatrix} . \tag{16}
$$

A change in notation has been adopted for this proof to avoid confusion where there are several similar double subscript scattering terms — for example, five different S_{11} terms. In addition, the notation for the differential phase is altered slightly to simplify the handling of this proof.

It is advantageous to rewrite each matrix equation in a transmission form relating the inci-dent and scattered waves at one terminal to the incident and scattered waves at the opposite ter-minal. This may be accomplished by expanding each matrix equation indicated and recollecting terms to yield

$$\begin{bmatrix} E_i^1 \\ E_s^1 \end{bmatrix} = \begin{bmatrix} -\dfrac{r_1}{s_1} & \dfrac{1}{s_1} \\ \left(s_1' - \dfrac{r_1' r_1}{s_1}\right) & \dfrac{r_1'}{s_1} \end{bmatrix} \begin{bmatrix} E_i^2 \\ E_s^2 \end{bmatrix} \tag{17}$$

$$\begin{bmatrix} E_i^2 \\ E_s^2 \end{bmatrix} = \begin{bmatrix} 0 & 1/G \\ G & 0 \end{bmatrix} \begin{bmatrix} E_i^3 \\ E_s^3 \end{bmatrix} \tag{18}$$

$$\begin{bmatrix} E_i^3 \\ E_s^3 \end{bmatrix} = \begin{bmatrix} -\dfrac{r_3}{s_3} & \dfrac{1}{s_3} \\ \left(s_3' - \dfrac{r_3' r_3}{s_3}\right) & \dfrac{r_3'}{s_3} \end{bmatrix} \begin{bmatrix} E_i^4 \\ E_s^4 \end{bmatrix} \tag{19}$$

$$\begin{bmatrix} E_i^4 \\ E_s^4 \end{bmatrix} = \begin{bmatrix} 0 & \epsilon^{-j\varphi} \\ \epsilon^{-j\varphi} & 0 \end{bmatrix} \begin{bmatrix} E_i^5 \\ E_s^5 \end{bmatrix} \tag{20}$$

and

$$\begin{bmatrix} E_i^5 \\ E_s^5 \end{bmatrix} = \begin{bmatrix} -\dfrac{r_2}{s_2} & \dfrac{1}{s_2} \\ \left(s_2' - \dfrac{r_2' r_2}{s_2}\right) & \dfrac{r_2'}{s_2} \end{bmatrix} \begin{bmatrix} E_i^6 \\ E_s^6 \end{bmatrix} \; . \tag{21}$$

At an interface between successive elements indicated in Fig. 1, waves must be continuous across the boundary. Thus, a wave scattered to the left becomes the wave incident from the left, etc. This means that E_i^2 from Eq. (17), for example, is identically equal to E_s^2 in Eq. (18). Satisfying the boundary condition requires merely the inversion of the rows of a given transmission matrix equation. Substituting each successive inverted equation into Eq. (17) forms

$$\begin{bmatrix} E_i^1 \\ E_s^1 \end{bmatrix} = \begin{bmatrix} -\dfrac{r_1}{s_1} & \dfrac{1}{s_1} \\ \left(s_1' - \dfrac{r_1' r_1}{s_1}\right) & \dfrac{r_1'}{s_1} \end{bmatrix} \begin{bmatrix} G & 0 \\ 0 & 1/G \end{bmatrix} \begin{bmatrix} \left(s_3' - \dfrac{r_3' r_3}{s_3}\right) & \dfrac{r_3'}{s_3} \\ -\dfrac{r_3}{s_3} & \dfrac{1}{s_3} \end{bmatrix}$$

$$\times \begin{bmatrix} \epsilon^{-j\varphi} & 0 \\ 0 & \epsilon^{-j\varphi} \end{bmatrix} \begin{bmatrix} \left(s_2' - \dfrac{r_2' r_2}{s_2}\right) & \dfrac{r_2'}{s_2} \\ -\dfrac{r_2}{s_2} & \dfrac{1}{s_2} \end{bmatrix} \begin{bmatrix} E_i^6 \\ E_s^6 \end{bmatrix} \; . \tag{22}$$

Equation (22) may be simplified by applying the condition of unitarity to each of the three lossless scattering obstacles as

$$s_1' s_1 - r_1' r_1 = \epsilon^{-j\beta_1} \qquad (23)$$

$$s_2' s_2 - r_2' r_2 = \epsilon^{-j\beta_2} \qquad (24)$$

and

$$s_3' s_3 - r_3' r_3 = \epsilon^{-j\beta_3} \qquad (25)$$

since the determinant of each matrix involved must have a magnitude of one. Equation (22) now becomes

$$
\begin{bmatrix} E_i^1 \\ E_s^1 \end{bmatrix} = \frac{1}{s_1 s_2 s_3}
\begin{bmatrix} -r_1 & 1 \\ \epsilon^{-j\beta_1} & r_1' \end{bmatrix}
\begin{bmatrix} G & 0 \\ 0 & 1/G \end{bmatrix}
\begin{bmatrix} \epsilon^{-j\beta_3} & r_3' \\ -r_3 & 1 \end{bmatrix}
\begin{bmatrix} \epsilon^{-j\varphi} & 0 \\ 0 & \epsilon^{-j\varphi} \end{bmatrix}
$$

$$
\times
\begin{bmatrix} \epsilon^{-j\beta_2} & r_2' \\ -r_2 & 1 \end{bmatrix}
\begin{bmatrix} E_i^6 \\ E_s^6 \end{bmatrix} . \qquad (26)
$$

Performing the indicated matrix multiplication and then rewriting the resulting transmission-form equation in scattering form gives

$$
\begin{bmatrix} E_s^1 \\ E_s^6 \end{bmatrix} =
\begin{bmatrix}
\dfrac{\left(r_2' \epsilon^{-j(\beta_1+\beta_3)} + r_3' \epsilon^{-j\beta_1} \right) G + (-r_1' r_2' r_3 + r_1') \frac{1}{G}}{\left(-r_1 r_2' \epsilon^{-j\beta_3} - r_1 r_3' \right) G + (-r_2' r_3 + 1) \frac{1}{G}}
&
\dfrac{s_1' s_2' s_3' \epsilon^{-j\varphi}}{\left(-r_1 r_2' \epsilon^{-j\beta_3} - r_1 r_3' \right) G + (-r_2' r_3 + 1) \frac{1}{G}}
\\[4ex]
\dfrac{s_1 s_2 s_3 \epsilon^{+j\varphi}}{\left(-r_1 r_2' \epsilon^{-j\beta_3} - r_1 r_3' \right) G + (-r_2' r_3 + 1) \frac{1}{G}}
&
\dfrac{\left(r_1 \epsilon^{-j(\beta_2+\beta_3)} - r_1 r_2 r_3' \right) G + \left(r_3 \epsilon^{-j\beta_2} + r_2 \right) \frac{1}{G}}{\left(-r_1 r_2' \epsilon^{-j\beta_3} - r_1 r_3' \right) G + (-r_2' r_3 + 1) \frac{1}{G}}
\end{bmatrix}
\begin{bmatrix} E_i^1 \\ E_i^6 \end{bmatrix} \qquad (27)
$$

Of particular interest is the ratio of the overall S_{21} and S_{12} terms, which becomes

$$\frac{S_{21}}{S_{12}} = \frac{s_1 s_2 s_3 \, \epsilon^{+j2\varphi}}{s_1' s_2' s_3'} . \qquad (28)$$

Owing to the fact that each of the three obstacles was lossless such that $|s_1| = |s_1'|$, $|s_2| = |s_2'|$, and $|s_3| = |s_3'|$, it is evident that

$$|S_{21}| = |S_{12}| . \qquad (29)$$

The only amount of nonreciprocity ever possible exists in differing arguments of the S_{12} and S_{21}.

8

Regardless of what selection is made from among lossless scatterers, bilateral amplifiers, or differential phase shifters, the analysis of a cascaded group of these elements always yields an equation similar to Eq. (28). Thus, the magnitude of the overall transmission parameters is always the same as shown by Eq. (29).

It should be noted that the bilateral amplification G can only scale the magnitudes of S_{12} and S_{21}, since this term appears in the denominator common to the two coefficients. The author has worked out the case where the bilateral amplifier is not matched but rather is mismatched by differing amounts at the two ports. The extra r-terms to properly account for the mismatch appear in the numerator of S_{11} and S_{22}, and also appear as an extra complexity of the denominator common to all scattering coefficients. Thus, reflections in cascade caused by mismatching cannot aid in obtaining nonreciprocity from differential phase but only to the scaling of S_{12} and S_{21}.

If the numerator and denominator terms of Eq. (28) could be obtained in some sort of additive form rather than in the product form, then there would be a possibility that the ratio of S_{21}/S_{12} was not always of unit magnitude.

2. Parallel-Parallel Connection

From the previous results, it would seem, in addition to scattering waves, that provision should be made for an additional conductive path through the network. The simple parallel-parallel connection provides for this.

Theorem II.

If a wave is split by a scattering junction, and if one resulting component wave is amplified while the other component is altered by a differential phase element, and if the waves are brought together again in such a way that multiple feedback paths exist, then nonreciprocal gain is possible. The parallel arrangement indicated is necessary for nonreciprocity and is also sufficient.

Proof.

The following analysis will suffice to demonstrate the fulfillment of the necessity.

The circuit arrangement of Fig. 2 shows two junctions for splitting and recombining the signal, a single differential phase-shift element, and a bilateral amplifier or active device, as required by Theorem II.
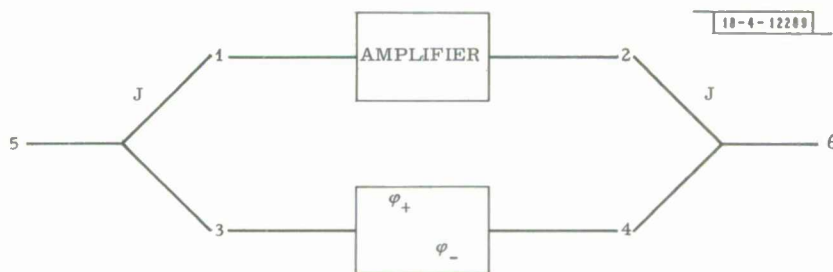
$$J = \begin{bmatrix} -1/3 & 2/3 & 2/3 \\ 2/3 & -1/3 & 2/3 \\ 2/3 & 2/3 & -1/3 \end{bmatrix} \qquad S_{amp} = \begin{bmatrix} 0 & G \\ G & 0 \end{bmatrix} \qquad S_{\varphi} = \begin{bmatrix} 0 & \epsilon^{-j\varphi_+} \\ \epsilon^{-j\varphi_-} & 0 \end{bmatrix}$$

Fig. 2. Parallel-parallel circuit arrangement.

There is no loss in apparent generality if the simplest junction is used first in the analysis which favors reduced algebraic manipulation. One of the simplest junctions is formed by the converging of three identical lossless transmission lines. The two junctions shown are then considered to be completely symmetrical and lossless. Owing to the use of lossless lines, the scattering coefficients are represented by real numbers, hence simplifying algebraic manipulation. The terminal relations of such a symmetrical junction are

$$
\begin{bmatrix} E_s^1 \\ E_s^3 \\ E_s^5 \end{bmatrix} = [J] \begin{bmatrix} E_i^1 \\ E_i^3 \\ E_i^5 \end{bmatrix} \tag{30}
$$

and

$$
\begin{bmatrix} E_s^2 \\ E_s^4 \\ E_s^6 \end{bmatrix} = [J] \begin{bmatrix} E_i^2 \\ E_i^4 \\ E_i^6 \end{bmatrix} \tag{31}
$$

where $[J]$ represents the scattering matrix of the symmetrical junction[†] given by

$$
\begin{bmatrix} J_{11} & J_{12} & J_{13} \\ J_{21} & J_{22} & J_{23} \\ J_{31} & J_{32} & J_{33} \end{bmatrix} = \begin{bmatrix} -1/3 & 2/3 & 2/3 \\ 2/3 & -1/3 & 2/3 \\ 2/3 & 2/3 & -1/3 \end{bmatrix} . \tag{32}
$$

The upper branch of Fig. 2 is designated by

$$
\begin{bmatrix} E_s^1 \\ E_s^2 \end{bmatrix} = \begin{bmatrix} s_{11} & s_{12} \\ s_{21} & s_{22} \end{bmatrix} \begin{bmatrix} E_i^1 \\ E_i^2 \end{bmatrix} \tag{33}
$$

and the lower circuit branch is similarly designated by

$$
\begin{bmatrix} E_s^3 \\ E_s^4 \end{bmatrix} = \begin{bmatrix} s'_{11} & s'_{12} \\ s'_{21} & s'_{22} \end{bmatrix} \begin{bmatrix} E_i^3 \\ E_i^4 \end{bmatrix} . \tag{34}
$$

[†] C. G. Montgomery, R. H. Dicke, and E. M. Purcell, Principles of Microwave Circuits (McGraw-Hill, New York, 1948), p. 427.

With reference to the right-hand junction, it is evident that E_i^2 referred to in Eq. (31) is the same as E_s^2 in Eq. (33), and E_i^4 in Eq. (31) is the same wave as E_s^4 in Eq. (34). Similarly, E_s^2 in Eq. (31) is identical to E_i^2 of Eq. (33), and E_s^4 of Eq. (31) is the same as E_i^4 of Eq. (34). Upon making the indicated changes in Eq. (31) and collecting similar terms, a set of three equations relating incident and reflected waves at the junction may be written as

$$E_i^2 = J_{11}(s_{21}E_i^1 + s_{22}E_i^2) + J_{12}(s'_{21}E_i^3 + s'_{22}E_i^4) + J_{13}E_i^6 \tag{35}$$

$$E_i^4 = J_{21}(s_{21}E_i^1 + s_{22}E_i^2) + J_{22}(s'_{21}E_i^3 + s'_{22}E_i^4) + J_{23}E_i^6 \tag{36}$$

$$E_s^6 = J_{31}(s_{21}E_i^1 + s_{22}E_i^2) + J_{32}(s'_{21}E_i^3 + s'_{22}E_i^4) + J_{33}E_i^6 \quad . \tag{37}$$

Referring now to the left-hand junction, it is easily recognized that E_i^1 in Eq. (30) is E_s^1 in Eq. (33), E_i^3 in Eq. (30) is E_s^3 in Eq. (34), E_s^3 in Eq. (30) is E_i^3 of Eq. (34), and E_s^1 of Eq. (30) is E_i^1 of Eq. (33). Making these substitutions into Eq. (30) and collecting terms generates three equations describing the left-hand junction as

$$E_i^1 = J_{11}(s_{11}E_i^1 + s_{12}E_i^2) + J_{12}(s'_{11}E_i^3 + s'_{12}E_i^4) + J_{13}E_i^5 \tag{38}$$

$$E_i^3 = J_{21}(s_{11}E_i^1 + s_{12}E_i^2) + J_{22}(s'_{11}E_i^3 + s'_{12}E_i^4) + J_{23}E_i^5 \tag{39}$$

$$E_s^5 = J_{31}(s_{11}E_i^1 + s_{12}E_i^2) + J_{32}(s'_{11}E_i^3 + s'_{12}E_i^4) + J_{33}E_i^5 \quad . \tag{40}$$

Equations (37) and (40) show that the overall scattering parameters may be specified if E_i^1, E_i^2, E_i^3, and E_i^4 can be obtained as functions of E_i^5 and E_i^6. Equations (35), (36), (38), and (39) form a set from which the indicated four variables may be obtained by solution of simultaneous equations. It will be assumed at the outset that $s_{11} = s_{22} = s'_{11} = s'_{22} = 0$. There is, of course, a significant saving in algebra by such an assumption. As an example of the calculation involved,

$$E_i^3 = \frac{\begin{vmatrix} -\frac{1}{3}s_{21} & -1 & -\frac{2}{3}E_i^6 & 0 \\ \frac{2}{3}s_{21} & 0 & -\frac{2}{3}E_i^6 & -1 \\ -1 & -\frac{1}{3}s_{12} & -\frac{2}{3}E_i^5 & \frac{2}{3}s'_{12} \\ 0 & \frac{2}{3}s_{12} & -\frac{2}{3}E_i^5 & -\frac{1}{3}s'_{12} \end{vmatrix}}{\begin{vmatrix} -\frac{1}{3}s_{21} & -1 & \frac{2}{3}s'_{21} & 0 \\ \frac{2}{3}s_{21} & 0 & -\frac{1}{3}s'_{21} & -1 \\ -1 & -\frac{1}{3}s_{12} & 0 & \frac{2}{3}s'_{12} \\ 0 & \frac{2}{3}s_{12} & -1 & -\frac{1}{3}s'_{12} \end{vmatrix}} \quad . \tag{41}$$

11

The solution is

$$E_i^3 = \frac{(\frac{2}{9} s_{21}s_{12} + \frac{4}{9} s'_{12}s_{21} - \frac{2}{3}) E_i^5 + (\frac{2}{9} s_{12}s'_{12}s_{21} + \frac{2}{9} s'_{12} - \frac{4}{9} s_{12}) E_i^6}{-\frac{3}{27} s_{12}s'_{12}s_{21}s'_{21} + \frac{1}{9} s_{12}s_{21} + \frac{4}{9} s'_{12}s_{21} + \frac{4}{9} s_{12}s'_{21} + \frac{1}{9} s'_{12}s'_{21} - 1} \quad . \quad (42)$$

Assembling all the E_i terms in Eqs. (40) and (37) yields a matrix equation of the proper form as

$$\begin{bmatrix} E_s^5 \\ E_s^6 \end{bmatrix} = [S] \begin{bmatrix} E_i^5 \\ E_i^6 \end{bmatrix} \quad (43)$$

where [S] refers to the overall circuit parameters. Of particular interest are the S_{12} and S_{21} terms which become, from Eqs. (40) and (37),

$$S_{12} = J_{31}s_{12}[E_i^6 \text{ part of } E_i^2] + J_{32}s'_{12}[E_i^6 \text{ part of } E_i^4]$$

$$= \frac{4}{9} s_{12}s'_{12}s_{21} + \frac{4}{9} s_{12}s'_{12}s'_{21} - \frac{4}{9} s_{12} - \frac{4}{9} s'_{12} \quad (44)$$

and

$$S_{21} = J_{31}s_{21}[E_i^5 \text{ part of } E_i^1] + J_{32}s'_{21}[E_i^5 \text{ part of } E_i^3]$$

$$= \frac{4}{9} s'_{12}s_{21}s'_{21} + \frac{4}{9} s_{12}s_{21}s'_{21} - \frac{4}{9} s'_{21} - \frac{4}{9} s_{21} \quad . \quad (45)$$

The ratio of Eq. (44) to Eq. (45) is

$$\frac{S_{12}}{S_{21}} = \frac{s_{12}(s'_{12}s'_{21} - 1) + s'_{12}(s_{12}s_{21} - 1)}{s_{21}(s'_{12}s'_{21} - 1) + s'_{21}(s_{12}s_{21} - 1)} \quad . \quad (46)$$

The character of Eq. (46), in displaying sums and differences of phasor scattering terms, shows no guarantee that the numerator and denominator are always equal in magnitude. The possibility that $S_{12} \neq S_{21}$ proves the necessity of the parallel-parallel arrangement.

The following proves the sufficiency of the parallel arrangement and determines conditions that must exist for nonreciprocal gain to be possible.

It may be assumed that the upper branch of the circuit of Fig. 2 is an amplifier characterized by

$$[S] = \begin{bmatrix} 0 & G\epsilon^{j\alpha} \\ G\epsilon^{j\alpha} & 0 \end{bmatrix} \quad (47)$$

where G is the amplification constant, and $\epsilon^{j\alpha}$ is the amplifier phase delay. Further, it is assumed that the differential phase element occupies the lower branch of the same Fig. 2 and is given by

$$[S'] = \begin{bmatrix} 0 & \epsilon^{j\alpha'}\epsilon^{j\varphi} \\ \epsilon^{j\alpha'}\epsilon^{-j\varphi} & 0 \end{bmatrix} \tag{48}$$

where $\epsilon^{j\alpha'}$ represents some common insertion phase, and $\epsilon^{\pm j\varphi}$ is the differential phase. By substituting the proper terms and making use of the identity $\epsilon^{j(2\alpha')} - 1 = 2j\epsilon^{j\alpha'}\sin\alpha'$, Eq. (46) becomes

$$\frac{S_{12}}{S_{21}} = \frac{G\epsilon^{j\alpha}2j\sin\alpha' + \epsilon^{j\varphi}(G^2\epsilon^{j2\alpha} - 1)}{G\epsilon^{j\alpha}2j\sin\alpha' + \epsilon^{-j\varphi}(G^2\epsilon^{j2\alpha} - 1)} \quad . \tag{49}$$

The form of Eq. (49) is

$$\frac{\xi + \epsilon^{j\varphi}\eta}{\xi + \epsilon^{-j\varphi}\eta}$$

and the ratio

$$\frac{\xi}{\eta} = \frac{G\epsilon^{j\alpha}2j\sin\alpha'}{G^2\epsilon^{j2\alpha} - 1} \quad . \tag{50}$$

If ξ and η are related by a real number, then the magnitude of Eq. (49) is unity, and no differential gain is ever possible. If, on the other hand, ξ/η can be complex, this proves the sufficiency of the parallel circuit in creating differential gain.

Substitution for the exponentials in Eq. (50) gives

$$\frac{\xi}{\eta} = \frac{2jG(\cos\alpha + j\sin\alpha)\sin\alpha'}{G^2(\cos\alpha + j\sin\alpha)^2 - 1} \quad . \tag{51}$$

By inverting, dividing, collecting of terms and simplifying, the ratio becomes

$$\frac{\xi}{\eta} = \frac{1}{\left(\dfrac{G}{2}\dfrac{\sin\alpha}{\sin\alpha'} + \dfrac{1}{2G}\dfrac{\sin\alpha}{\sin\alpha'}\right) - j\left(\dfrac{G}{2}\dfrac{\cos\alpha}{\sin\alpha'} - \dfrac{1}{2G}\dfrac{\cos\alpha}{\sin\alpha'}\right)} \quad . \tag{52}$$

It may be determined from this equation that (1) if G is not 1.0, or that (2) α is not $n(\pi/2)$ where n is odd, ξ/η cannot be totally real and thus the magnitude of Eq. (49) is guaranteed something other than unity. These conditions on Eq. (52) are sufficient to allow differential gain. It is to be noted from Eq. (52) that the nonreal condition can be met with $\alpha = 0$. Thus, in this analysis, the amplifier does not need to have additional phase delay.

Corollary.

The minimum number of components required to achieve the desired nonreciprocal gain is four.

The specification is for two junctions with which to split the conducting waves, one amplifier or active device to provide gain, and one differential phase element for control.

Scattering Matrix.

The complete scattering matrix for the overall circuit parameters of Eq. (43) is shown in Fig. 3. First it is noted the matrix does not possess symmetry about the principal diagonal, which indicates the presence of nonreciprocity. Second, if all terms containing φ_+ are interchanged for φ_- and vice-versa, the matrix terms would switch about the main diagonal, indicating a swap (end for end) of the network transmission characteristics.

13

$$
\begin{bmatrix}
\dfrac{(3G^2+1)\,\epsilon^{-j(\varphi_+ + \varphi_-)} + G^2 - 4G\epsilon^{-j\varphi_-} - 4G\epsilon^{-j\varphi_+} + 3}{(1-G^2)\,\epsilon^{-j(\varphi_+ + \varphi_-)} + 4G\epsilon^{-j\varphi_+} + 4G\epsilon^{-j\varphi_-} + G^2 - 9} & \dfrac{4(G^2-1)\,\epsilon^{-j\varphi_+} + 4G\epsilon^{-j(\varphi_+ + \varphi_-)} - 4G}{(1-G^2)\,\epsilon^{-j(\varphi_+ + \varphi_-)} + 4G\epsilon^{-j\varphi_+} + 4G\epsilon^{-j\varphi_-} + G^2 - 9} \\[4ex]
\dfrac{4(G^2-1)\,\epsilon^{-j\varphi_-} + 4G\epsilon^{-j(\varphi_+ + \varphi_-)} - 4G}{(1-G^2)\,\epsilon^{-j(\varphi_+ + \varphi_-)} + 4G\epsilon^{-j\varphi_+} + 4G\epsilon^{-j\varphi_-} + G^2 - 9} & \dfrac{(3G^2+1)\,\epsilon^{-j(\varphi_+ + \varphi_-)} + G^2 - 4G\epsilon^{-j\varphi_-} - 4G\epsilon^{-j\varphi_+} + 3}{(1-G^2)\,\epsilon^{-j(\varphi_+ + \varphi_-)} + 4G\epsilon^{-j\varphi_+} + 4G\epsilon^{-j\varphi_-} + G^2 - 9}
\end{bmatrix}
$$

Fig. 3. Complete scattering matrix for overall circuit parameters of Eq. (43).

14

C. Matching Constraint

The fact that the present application is for a periodic structure of identical interconnected networks raises the question concerning each input reflection parameter S_{11}. If this term and S_{22} are made to vanish, this would greatly simplify the present analysis. Further, Theorem I demonstrated that there will be no sacrifice of nonreciprocal gain by constraining the impedance to a match.

In order for S_{11} to vanish, the numerator must be zero, i.e.,

$$3G^2 \epsilon^{-j(\varphi_+ + \varphi_-)} + G^2 - 4G\left(\epsilon^{-j\varphi_-} + \epsilon^{-j\varphi_+}\right) + \epsilon^{-j(\varphi_+ + \varphi_-)} + 3 = 0 \quad . \tag{53}$$

It should be noted here that the gain of the amplifier required for this matched constraint is a function of the junction parameters and the two phase shifts, φ_+ and φ_-.

In order to simplify Eq. (53) as much as possible, a term representing the average insertion phase of any component is defined as

$$\epsilon = \epsilon^{-j[(\varphi_+ + \varphi_-)/2]} \quad . \tag{54}$$

With the use of this definition and the definition of differential phase factor given in Eq. (11), we may rewrite Eq. (53) as

$$(3G^2 + 1)\,\epsilon^2 - 4G(\epsilon\delta^* + \epsilon\delta) + (G^2 + 3) = 0 \tag{55}$$

where δ^* represents the conjugate of δ. Regrouping these terms yields a quadratic equation in the complex amplifier gain required as

$$G^2(3\epsilon^2 + 1) + G(-8\epsilon\,\mathrm{Re}\,\delta) + (\epsilon^2 + 3) = 0 \quad . \tag{56}$$

Solving this quadratic,

$$G = \frac{4\epsilon\,\mathrm{Re}\,\delta}{3\epsilon^2 + 1} \pm \sqrt{\frac{16\epsilon^2\,\mathrm{Re}^2\,\delta}{(3\epsilon^2 + 1)^2} - \frac{\epsilon^2 + 3}{3\epsilon^2 + 1}} \quad . \tag{57}$$

This is a particular type quadratic wherein the two roots are reciprocal conjugates of one another. This may be demonstrated by considering the terms from the quadratic Eq. (56) that identify the product of the two roots as

$$r_1 r_2 = \frac{\epsilon^2 + 3}{3\epsilon^2 + 1} = \frac{1}{\epsilon^2} \frac{\epsilon^2 + 3}{(\epsilon^*)^2 + 3} \tag{58}$$

where ϵ^2 is complex but of unit magnitude, and $(\epsilon^*)^2$ is its conjugate. It should be noted that the magnitude of this product is unity. The argument of the $r_1 r_2$ product is

$$\arg(r_1 r_2) = \tan^{-1}\frac{\mathrm{Im}\,\epsilon^2}{3 + \mathrm{Re}\,\epsilon^2} - \tan^{-1}\frac{\mathrm{Im}\,(\epsilon^*)^2}{3 + \mathrm{Re}\,(\epsilon^*)^2} - 2\tan^{-1}\frac{\mathrm{Im}\,\epsilon}{\mathrm{Re}\,\epsilon} \tag{59}$$

but the second term is conjugate to the first; so,

$$\arg(r_1 r_2) = 2\left(\tan^{-1}\frac{\mathrm{Im}\,\epsilon^2}{3 + \mathrm{Re}\,\epsilon^2} - \tan^{-1}\frac{\mathrm{Im}\,\epsilon}{\mathrm{Re}\,\epsilon}\right) \quad . \tag{60}$$

Hence, the two roots are reciprocal in magnitude but of conjugate angles.

15

Fig. 4. Computer solution for magnitude of amplifier gain G as a function of insertion phase ε and differential phase factor δ satisfying matching constraint of Eq. (53).

DIFFERENTIAL PHASE FACTOR δ (deg)

AVERAGE INSERTION PHASE ε (deg)	5	10	15	20	25	30	35	40	45	50	55	60	65
180	1.00	1.00	1.00	1.00	1.00	1.00	1.00	1.00	1.00	1.00	1.00	1.00	1.00
175	1.00	1.00	1.00	1.00	1.00	1.00	1.00	1.00	1.00	1.00	1.00	1.00	1.00
170	1.13	1.00	1.00	1.00	1.00	1.00	1.00	1.00	1.00	1.00	1.00	1.00	1.00
165	1.23	1.16	1.00	1.00	1.00	1.00	1.00	1.00	1.00	1.00	1.00	1.00	1.00
160	1.34	1.28	1.16	1.00	1.00	1.00	1.00	1.00	1.00	1.00	1.00	1.00	1.00
155	1.45	1.40	1.32	1.15	1.00	1.00	1.00	1.00	1.00	1.00	1.00	1.00	1.00
150	1.58	1.53	1.46	1.34	1.11	1.00	1.00	1.00	1.00	1.00	1.00	1.00	1.00
145	1.71	1.67	1.60	1.50	1.35	1.00	1.00	1.00	1.00	1.00	1.00	1.00	1.00
140	1.86	1.82	1.76	1.66	1.53	1.34	1.00	1.00	1.00	1.00	1.00	1.00	1.00
135	2.03	1.99	1.92	1.83	1.71	1.54	1.31	1.00	1.00	1.00	1.00	1.00	1.00
130	2.21	2.17	2.11	2.02	1.89	1.74	1.54	1.24	1.00	1.00	1.00	1.00	1.00
125	2.41	2.37	2.31	2.22	2.09	1.94	1.75	1.51	1.08	1.00	1.00	1.00	1.00
120	2.63	2.59	2.52	2.43	2.31	2.15	1.97	1.74	1.45	1.00	1.00	1.00	1.00
115	2.87	2.82	2.75	2.66	2.53	2.37	2.19	1.96	1.69	1.31	1.00	1.00	1.00
110	3.11	3.06	2.99	2.89	2.76	2.60	2.40	2.18	1.91	1.58	1.00	1.00	1.00
105	3.34	3.29	3.21	3.11	2.97	2.80	2.61	2.38	2.11	1.79	1.36	1.00	1.00
100	3.53	3.49	3.41	3.30	3.15	2.98	2.78	2.54	2.27	1.95	1.55	1.00	1.00
95	3.67	3.62	3.54	3.42	3.28	3.10	2.89	2.65	2.38	2.06	1.67	1.00	1.00
90	3.72	3.67	3.58	3.47	3.32	3.15	2.94	2.69	2.41	2.09	1.71	1.00	1.00
85	3.67	3.62	3.54	3.42	3.28	3.10	2.89	2.65	2.38	2.06	1.67	1.00	1.00
80	3.53	3.49	3.41	3.30	3.15	2.98	2.78	2.54	2.27	1.95	1.55	1.00	1.00
75	3.34	3.29	3.21	3.11	2.97	2.80	2.61	2.38	2.11	1.79	1.36	1.00	1.00
70	3.11	3.06	2.99	2.89	2.76	2.60	2.40	2.18	1.91	1.58	1.00	1.00	1.00
65	2.87	2.82	2.75	2.66	2.53	2.37	2.19	1.96	1.69	1.31	1.00	1.00	1.00
60	2.63	2.59	2.52	2.43	2.31	2.15	1.97	1.74	1.45	1.00	1.00	1.00	1.00
55	2.41	2.37	2.31	2.22	2.09	1.94	1.75	1.51	1.08	1.00	1.00	1.00	1.00
50	2.21	2.17	2.11	2.02	1.89	1.74	1.54	1.24	1.00	1.00	1.00	1.00	1.00
45	2.03	1.99	1.92	1.83	1.71	1.54	1.31	1.00	1.00	1.00	1.00	1.00	1.00
40	1.86	1.82	1.76	1.66	1.53	1.34	1.00	1.00	1.00	1.00	1.00	1.00	1.00
35	1.71	1.67	1.60	1.50	1.35	1.00	1.00	1.00	1.00	1.00	1.00	1.00	1.00
30	1.56	1.53	1.46	1.34	1.15	1.00	1.00	1.00	1.00	1.00	1.00	1.00	1.00
25	1.45	1.40	1.32	1.16	1.00	1.00	1.00	1.00	1.00	1.00	1.00	1.00	1.00
20	1.34	1.28	1.16	1.00	1.00	1.00	1.00	1.00	1.00	1.00	1.00	1.00	1.00
15	1.23	1.16	1.00	1.00	1.00	1.00	1.00	1.00	1.00	1.00	1.00	1.00	1.00
10	1.13	1.00	1.00	1.00	1.00	1.00	1.00	1.00	1.00	1.00	1.00	1.00	1.00
5	1.00	1.00	1.00	1.00	1.00	1.00	1.00	1.00	1.00	1.00	1.00	1.00	1.00

A program was written for the Lincoln Laboratory IBM-360 computer in order to solve for values of G as a function of the average insertion phase ϵ and the differential phase factor δ. The program is shown in Appendix B, Fig. B-1. Inasmuch as the objective is to produce nonreciprocal gain, the program selects the larger of the two roots of the above quadratic.

Figure 4 shows the results of the computer solution for the magnitude of the vector amplifier gain G for small values of differential phase factor and for various values of the insertion phase. Of particular significance is the fact that magnitudes on this gain profile, required to satisfy the matching constraint, are relatively small. No nonreciprocal gain is possible if G = 1; therefore, the valid solutions all lie within the horseshoe-shaped boundary indicated by the dashed line.

The limited ranges of the variables ϵ and δ may be identified with various conditions applied to the basic quadratic Eq. (57). Valid solutions for G > 1 as identified in Fig. 4 exist only when the radical term of Eq. (57) is real. When the radical term is either zero or imaginary, G = 1, which does not satisfy condition 1 of Eq. (52); thus, nonreciprocity is not possible.

Particular arguments of G are required to satisfy the matching constraint. Figure 5 shows the profile of G angles required for given variables ϵ and δ. Here again, the horseshoe curve has been repeated to bound those values that satisfy the requirement for G > 1.

It should be noted that the coordinates of this horseshoe boundary curve may be defined quite easily. To this end, Eq. (57) may be rewritten restricting its application to the solution boundary where the magnitude of G is 1.0 as

$$|1|\angle\Theta = \frac{4\epsilon \text{ Re } \delta}{3\epsilon^2 + 1} \pm \sqrt{\frac{16\epsilon^2 \text{ Re}^2 \delta}{(3\epsilon^2 + 1)^2} - \frac{\epsilon^2 + 3}{3\epsilon^2 + 1}} \qquad (61)$$

where Θ is the angle on G. Factoring an ϵ out of this equation and assembling the radical terms gives

$$|1|\angle\Theta = \epsilon\left[\frac{4 \text{ Re } \delta \pm \sqrt{16 \text{ Re}^2 \delta - (6 \text{ Re } \epsilon^2 + 10)}}{3\epsilon^2 + 1}\right] \qquad (62)$$

The bracketed quantity is required to be of magnitude 1.0. Assume that the radical term is imaginary, i.e., $16 \text{ Re}^2 \delta < (6 \text{ Re } \epsilon^2 + 10)$. The bracket now has a magnitude of 1. This means

$$\text{Re } \epsilon^2 = \frac{16 \text{ Re}^2 \delta}{6} - 1.667 \qquad (63)$$

is the relation defining the coordinates of the boundary of the dashed curves utilized in Figs. 4 and 5.

The diagram of Fig. 6 illustrates how the various areas of the gain profile of Fig. 4 and the angle profile of Fig. 5 are related to the conditions on the radical term of Eq. (62).

Other general areas of the insertion phase — differential phase space might be expected to yield additional solutions still within the matching constraint. An examination of Eq. (56) shows this to be true in that any addition or subtraction of 180° to the variable δ yields the identical condition, since only the real part of δ is involved. Further, the addition of multiples of 180° to the variable ϵ provides the same magnitudes of G, but, as Eq. (62) shows, the argument of G will depend on these 180° multipliers. The possible cyclic repetitions of the solution areas are shown in Fig. 7.

17

AVERAGE INSERTION PHASE ε (deg)

DIFFERENTIAL PHASE FACTOR δ (deg)

Fig. 5. Computer solution for argument of amplifier gain G required to satisfy matching constraint as a function of ε and δ.

Fig. 6. Diagram identifying areas of gain profiles of Figs. 4 and 5 with certain constraints on Eq. (59).
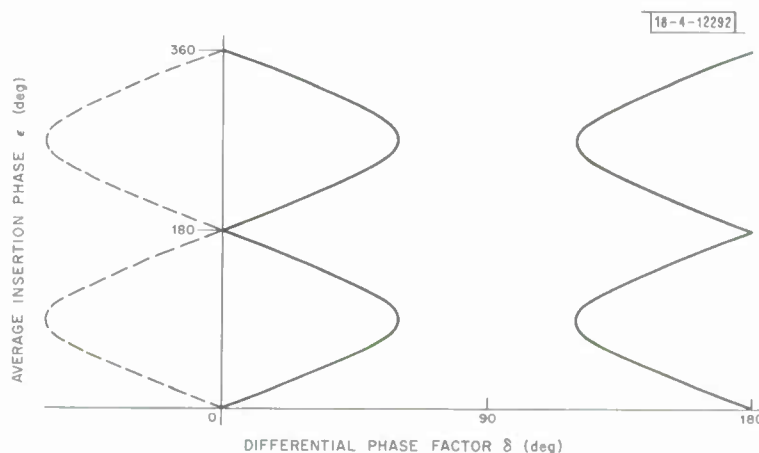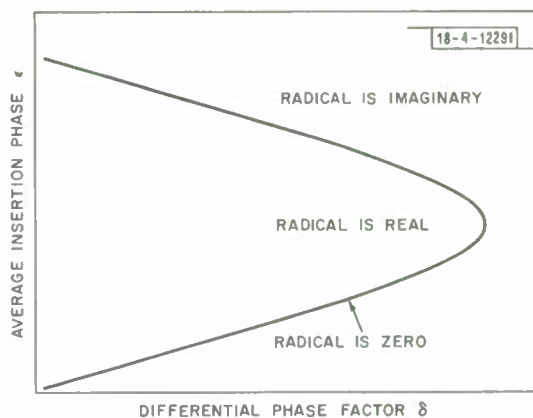
Fig. 7. Diagram illustrating cyclic repetitions of valid solution areas of gain profile as a function of ϵ and δ.

D. Matched Differential Amplifier

Having determined that a range of G does exist for which a matched input and output is possible for potential iterations of the minimum-element basic circuit configuration, it remains to show what range of nonreciprocal gain is possible.

1. Range of S_{12}

A modified computer program was written to determine values of G, S_{12}, and S_{21} over smaller increments of the variables of insertion phase and differential phase factor in order to show more smoothly what variations exist in the parameters.

Figure 8 shows the results of the computer solution for S_{12}. Here, the magnitude of S_{12} is displayed as a function of the average insertion phase ϵ, and the differential phase factor δ. Superimposed on this resultant array is a contour map of equal S_{12} magnitudes. A pole of the function is in evidence near the value of $\epsilon = 55°$ and $\delta = 35°$, where the reverse transmission parameter S_{12} reaches a high value.
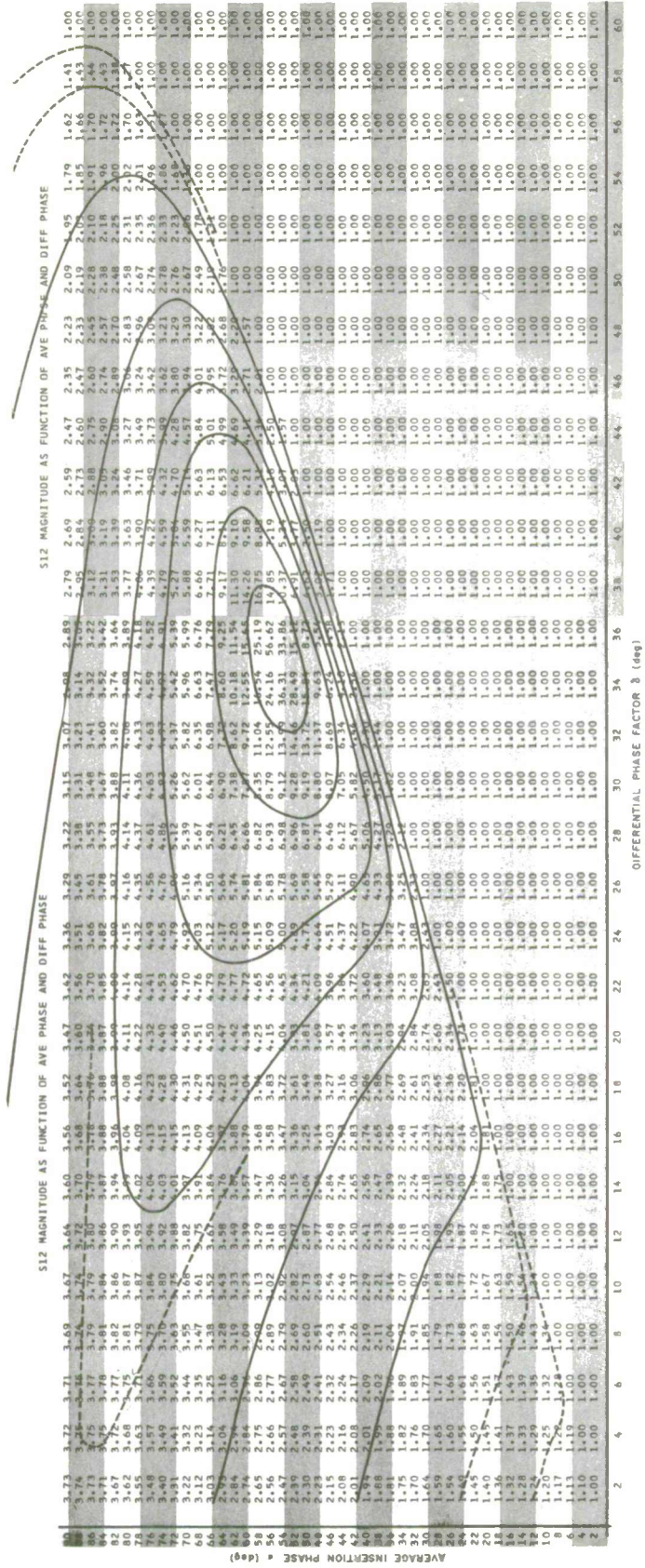
Fig. 8. Computer solution for transmission parameter S_{12} with contours of equal S_{12} magnitude.

20

Attention is still drawn to the fact that the absolute gain of the actual circuit amplifier is still only 3.7 at most. The fact that S_{12} has such a high value in the vicinity of the pole is caused by the denominator of the expression tending to zero.

2. Range of S_{21}

Figure 9 shows the computer results for S_{21} with variables of smaller increments. Again, superimposed on the array is a contour map of equal S_{21} magnitudes. Unlike the array of the previous transmission parameter, there is no pole of the function in evidence; moreover, the values of S_{21} magnitude are, in general, more nearly the values of the circuit amplifier gain. This function seems to be quite regular over the range of interest.

3. Ratio of S_{21}/S_{12}

Of special significance is the ratio of the forward-to-reverse transmission scattering parameters. This determines the magnitude of the nonreciprocal gain possible.

Figure 10 shows such a ratio over the range of the original computer program variables. Spectacular, of course, is the point represented by the presence of the singularity of S_{12}, i. e., $\epsilon = 55°$ and $\delta = 35°$, where the nonreciprocal gain ratio S_{21}/S_{12} is 1:0.01. It is necessary to keep in mind, however, that all values of S_{12} and S_{21} are >1 within any range where the differential amplifier is matched. This represents gain in both directions. The ratio of gains, i. e., S_{21}/S_{12}, is the nonreciprocity desired.

Attention is called to the fact that Fig. 10 shows no nonreciprocal gain to be possible when the insertion phase is either 90° or 180°, a result predicted by the sufficiency condition proved on p. 13.

E. Matched Differential Attenuator

Referring again to the constraint of a matched input and, because of the symmetry in the scattering matrix of Fig. 3, a matched output, we will recall that the necessary amplifier gain required was one complex root from a special quadratic, Eq. (57). The theoretical development of the matched differential amplifier was based solely on the selection of the larger of the two reciprocal conjugate roots.

Owing to the character of the quadratic equation, the alternate root for any given ϵ and δ must have a magnitude <1. Thus, the required match is produced by an "amplifier" having a bilateral "gain" $G < 1$, or bilateral loss. The computer program was modified to select the smaller root; this modification is shown in Appendix B, Fig. B-2.

1. Range of S_{21}

The range of values of the forward transmission parameter is shown in Fig. 11 as a function of the variable insertion phase ϵ and differential phase factor δ. Because the values of G are reciprocal to those used previously, the magnitude of a given value of S_{21} is the reciprocal of that obtained with the same ϵ and δ as before. This means that all S_{21} values are <1 within the range where a match can be effected.

S21 MAGNITUDE AS FUNCTION OF AVE PHASE AND DIFF PHASE

S21 MAGNITUDE AS FUNCTION OF AVE PHASE AND DIFF PHASE

AVERAGE INSERTION PHASE ε (deg)

DIFFERENTIAL PHASE FACTOR δ (deg)
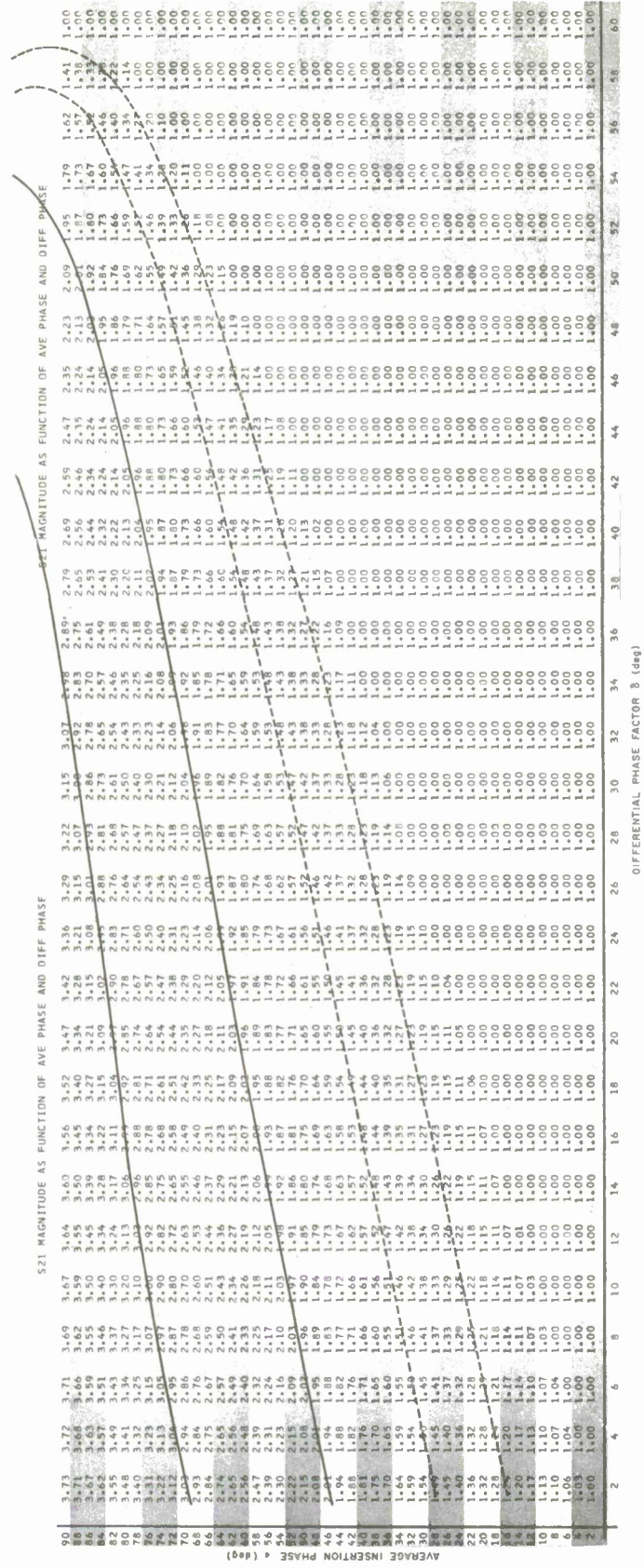
Fig. 9. Computer solution for transmission parameter S_{21} with contours of equal S_{21} magnitude.

AVERAGE INSERTION PHASE ε (deg) vs. DIFFERENTIAL PHASE FACTOR δ (deg)

ε \ δ	5	10	15	20	25	30	35	40	45	50	55	60	65
180	1.00	1.00	1.00	1.00	1.00	1.00	1.00	1.00	1.00	1.00	1.00	1.00	1.00
175	1.00	1.00	1.00	1.00	1.00	1.00	1.00	1.00	1.00	1.00	1.00	1.00	1.00
170	1.18	1.00	1.00	1.00	1.00	1.00	1.00	1.00	1.00	1.00	1.00	1.00	1.00
165	1.17	1.44	1.00	1.00	1.00	1.00	1.00	1.00	1.00	1.00	1.00	1.00	1.00
160	1.17	1.42	1.74	1.00	1.00	1.00	1.00	1.00	1.00	1.30	1.00	1.00	1.00
155	1.17	1.41	1.77	1.95	1.73	1.00	1.00	1.00	1.00	1.00	1.00	1.00	1.00
150	1.18	1.41	1.75	2.30	3.09	1.00	1.00	1.00	1.00	1.00	1.00	1.00	1.00
145	1.18	1.41	1.75	2.31	3.35	3.80	1.00	1.00	1.00	1.00	1.00	1.00	1.00
140	1.18	1.42	1.76	2.31	3.38	5.83	1.00	1.00	1.00	1.00	1.00	1.00	1.00
135	1.19	1.43	1.77	2.31	3.34	6.46	3.29	1.00	1.00	1.00	1.00	1.00	1.00
130	1.19	1.44	1.77	2.31	3.22	5.77	9.39	2.20	1.00	1.00	1.00	1.00	1.00
125	1.19	1.44	1.77	2.28	3.00	4.64	73.51	4.85	1.26	1.00	1.00	1.00	1.00
120	1.19	1.43	1.75	2.22	2.68	3.59	9.12	6.73	2.67	1.00	1.00	1.00	1.00
115	1.18	1.41	1.70	2.09	2.30	2.76	4.82	4.84	3.14	1.68	1.00	1.00	1.00
110	1.17	1.36	1.61	1.91	1.91	2.12	3.17	3.23	2.73	1.97	1.00	1.00	1.00
105	1.14	1.30	1.48	1.69	1.55	1.64	2.28	2.30	2.14	1.82	1.36	1.00	1.00
100	1.10	1.21	1.32	1.44	1.25	1.28	1.70	1.71	1.65	1.52	1.32	1.00	1.00
95	1.05	1.11	1.16	1.21	1.00	1.00	1.30	1.30	1.28	1.24	1.17	1.00	1.00
90	0.95	1.00	1.00	1.00	0.80	0.78	1.00	1.00	0.78	1.00	1.00	1.00	1.00
85	0.91	0.90	0.86	0.83	0.64	0.61	0.77	0.77	0.61	0.81	0.86	1.00	1.00
80	0.88	0.83	0.75	0.69	0.52	0.47	0.59	0.59	0.47	0.66	0.76	1.00	1.00
75	0.86	0.77	0.68	0.59	0.44	0.36	0.44	0.44	0.37	0.55	0.74	1.00	1.00
70	0.85	0.73	0.62	0.52	0.37	0.28	0.32	0.31	0.32	0.51	1.00	1.00	1.00
65	0.84	0.71	0.59	0.48	0.33	0.22	0.21	0.21	0.37	0.60	1.00	1.00	1.00
60	0.84	0.70	0.57	0.45	0.31	0.17	0.11	0.15	0.80	1.00	1.00	1.00	1.00
55	0.84	0.70	0.56	0.44	0.30	0.15	0.01	0.21	1.00	1.00	1.00	1.00	1.00
50	0.84	0.70	0.56	0.43	0.30	0.17	0.11	0.45	1.00	1.00	1.00	1.00	1.00
45	0.84	0.70	0.57	0.43	0.30	0.26	0.30	1.00	1.00	1.00	1.00	1.00	1.00
40	0.85	0.70	0.57	0.43	0.32	1.00	1.00	1.00	1.00	1.00	1.00	1.00	1.00
35	0.85	0.71	0.57	0.44	0.58	1.00	1.00	1.00	1.00	1.30	1.00	1.00	1.00
30	0.85	0.71	0.57	0.51	1.00	1.00	1.00	1.00	1.00	1.00	1.00	1.00	1.00
25	0.85	0.71	0.57	1.00	1.00	1.00	1.00	1.00	1.00	1.00	1.00	1.00	1.00
20	0.85	0.71	0.57	1.00	1.00	1.00	1.00	1.00	1.00	1.00	1.00	1.00	1.00
15	0.85	0.70	1.00	1.00	1.00	1.00	1.00	1.00	1.00	1.00	1.00	1.00	1.00
10	1.00	1.00	1.00	1.00	1.00	1.00	1.00	1.00	1.00	1.00	1.00	1.00	1.00
5	1.00	1.00	1.00	1.00	1.00	1.00	1.00	1.00	1.00	1.00	1.00	1.00	1.00

DIFFERENTIAL PHASE FACTOR δ (deg)

AVERAGE INSERTION PHASE ε (deg)

Fig. 10. Computer solution for ratio of forward-to-reverse transmission scattering parameters.

23

DIFFERENTIAL PHASE FACTOR δ (deg)

ε (deg)	5	10	15	20	25	30	35	40	45	50	55	60	65
180	1.00	1.00	1.00	1.00	1.00	1.00	1.00	1.00	1.00	1.00	1.00	1.00	1.00
175	1.00	1.00	1.00	1.00	1.00	1.00	1.00	1.00	1.00	1.00	1.00	1.00	1.00
170	0.78	1.00	1.00	1.00	1.00	1.00	1.00	1.00	1.00	1.00	1.00	1.00	1.00
165	0.73	0.64	1.00	1.00	1.00	1.00	1.00	1.00	1.00	1.00	1.00	1.00	1.00
160	0.67	0.60	0.53	1.00	1.00	1.00	1.00	1.00	1.00	1.00	1.00	1.00	1.00
155	0.62	0.56	0.48	0.48	1.00	1.00	1.00	1.00	1.00	1.00	1.00	1.00	1.00
150	0.58	0.52	0.44	0.37	0.55	1.00	1.00	1.00	1.00	1.00	1.00	1.00	1.00
145	0.53	0.48	0.41	0.33	0.27	1.00	1.00	1.00	1.00	1.00	1.00	1.00	1.00
140	0.49	0.44	0.38	0.31	0.23	0.22	1.00	1.00	1.00	1.00	1.00	1.00	1.00
135	0.45	0.40	0.35	0.28	0.21	0.13	0.26	1.00	1.00	1.00	1.00	1.00	1.00
130	0.41	0.37	0.32	0.26	0.19	0.11	0.08	0.40	1.00	1.00	1.00	1.00	1.00
125	0.38	0.34	0.29	0.24	0.19	0.11	0.01	0.16	0.76	1.00	1.00	1.00	1.00
120	0.34	0.31	0.27	0.23	0.18	0.13	0.07	0.10	0.30	0.50	1.00	1.00	1.00
115	0.32	0.29	0.26	0.22	0.19	0.15	0.12	0.13	0.23	0.37	1.00	1.00	1.00
110	0.30	0.27	0.25	0.22	0.20	0.18	0.17	0.18	0.23	0.36	1.00	1.00	1.00
105	0.28	0.26	0.24	0.23	0.22	0.21	0.21	0.23	0.27	0.39	0.59	1.00	1.00
100	0.27	0.26	0.25	0.24	0.24	0.24	0.25	0.28	0.32	0.43	0.54	1.00	1.00
95	0.27	0.26	0.26	0.26	0.27	0.28	0.30	0.32	0.36	0.48	0.55	1.00	1.00
90	0.27	0.27	0.28	0.29	0.30	0.32	0.34	0.37	0.41	0.53	0.59	1.00	1.00
85	0.28	0.29	0.30	0.32	0.34	0.36	0.39	0.42	0.47	0.59	0.64	1.00	1.00
80	0.30	0.31	0.33	0.35	0.37	0.40	0.43	0.47	0.52	0.66	0.71	1.00	1.00
75	0.32	0.34	0.36	0.39	0.41	0.44	0.48	0.52	0.58	0.74	0.80	1.00	1.00
70	0.35	0.37	0.40	0.43	0.46	0.49	0.53	0.58	0.64	0.84	1.00	1.00	1.00
65	0.38	0.40	0.43	0.47	0.50	0.54	0.58	0.64	0.71	1.00	1.00	1.00	1.00
60	0.41	0.44	0.48	0.51	0.55	0.59	0.64	0.70	0.80	1.00	1.00	1.00	1.00
55	0.45	0.48	0.52	0.56	0.60	0.64	0.70	0.78	0.95	1.00	1.00	1.00	1.00
50	0.49	0.53	0.56	0.61	0.65	0.70	0.77	0.88	1.00	1.00	1.00	1.00	1.00
45	0.53	0.57	0.61	0.66	0.71	0.77	0.86	1.00	1.00	1.00	1.00	1.00	1.00
40	0.58	0.62	0.67	0.71	0.77	0.84	1.00	1.00	1.00	1.00	1.00	1.00	1.00
35	0.63	0.67	0.72	0.77	0.84	1.00	1.00	1.00	1.00	1.00	1.00	1.00	1.00
30	0.68	0.73	0.78	0.84	0.94	1.00	1.00	1.00	1.00	1.00	1.00	1.00	1.00
25	0.73	0.79	0.84	0.92	1.00	1.00	1.00	1.00	1.00	1.00	1.00	1.00	1.00
20	0.79	0.85	0.92	1.00	1.00	1.00	1.00	1.00	1.00	1.00	1.00	1.00	1.00
15	0.85	0.92	1.00	1.00	1.00	1.00	1.00	1.00	1.00	1.00	1.00	1.00	1.00
10	0.92	1.00	1.00	1.00	1.00	1.00	1.00	1.00	1.00	1.00	1.00	1.00	1.00
5	1.00	1.00	1.00	1.00	1.00	1.00	1.00	1.00	1.00	1.00	1.00	1.00	1.00

AVERAGE INSERTION PHASE ε (deg)

-44-11897-1

Fig. 11. Computer solution for forward transmission parameter S_{21} with G magnitude <1.

24

2. Range of S_{12}

In similar fashion, Fig. 12 shows the range of values of the reverse transmission parameter as a function of the same variables. Again, each value given is the exact reciprocal of a value obtained with the first computer solution for the same variables. All S_{12} values are therefore < 1. A point of interest is that of $\epsilon = 55°$ and $\delta = 35°$, which shows the function tending to zero, the reciprocal of the previously located value obtained in the vicinity of the pole.

3. Ratio of S_{21}/S_{12}

The ratio of reciprocals is the reciprocal of the original variables. The ratio of S_{21}/S_{12}, utilizing the complex values of G (which are < 1), is everywhere the reciprocal of the values shown previously in Fig. 10.

Of special interest is the fact that significant nonreciprocity exists with this analysis, which predicts the existence of a matched differential attenuator. If the insertion loss in one direction can be kept low while the loss in the opposite direction is high, this differential attenuator might be a practical isolator. Particularly appropriate to the isolation concept is the theoretical differential loss ratio of 100:1, shown in Fig. 10 at $\epsilon = 55°$ and $\delta = 35°$.

F. Use of Non-ideal Active Device

It will now be of interest to return to the active circuit discussed on p. 11. The theoretical development to this point was predicated on the use of a special two-port active device capable of bilateral amplification while being matched both at input and output. Such a device perfectly matched is considered ideal. Several active devices are potentially applicable here, but they are considered non-ideal due to the fact that perfect matching cannot be achieved. Thus, it is of practical interest to know whether amplifier matching is really required.

The effect on the required gain and nonreciprocity of the overall differential device caused by relaxing the matched requirement (thus to produce additional internal reflections) is now to be determined. First, the mismatch to the non-ideal active device will be characterized as being entirely real in order to simplify the algebraic manipulation. Following this development, the influence that a reflection phase angle has on mismatching will be considered briefly.

1. General Scattering Matrix

Let the scattering matrix of the active element in Fig. 2 be represented by

$$S = \begin{bmatrix} R & G \\ G & R \end{bmatrix} \tag{64}$$

where R is the input and output reflection coefficient, assumed to be real. The symmetrical junction given by Eq. (32) and the matched differential phase-shift element are retained for this analysis. Equations (35) through (40) are still appropriate. Of the original assumptions made, the only one that remains is $s'_{11} = s'_{22} = 0$.

AVERAGE INSERTION PHASE ε (deg) vs. DIFFERENTIAL PHASE FACTOR δ (deg)

ε \ δ	5	10	15	20	25	30	35	40	45	50	55	60	65
180	1.00	1.00	1.00	1.00	1.00	1.00	1.00	1.00	1.00	1.00	1.00	1.00	1.00
175	1.00	1.00	1.00	1.00	1.00	1.00	1.00	1.00	1.00	1.00	1.00	1.00	1.00
170	0.92	1.00	1.00	1.00	1.00	1.00	1.00	1.00	1.00	1.00	1.00	1.00	1.00
165	0.85	0.92	1.00	1.00	1.00	1.00	1.00	1.00	1.00	1.00	1.00	1.00	1.00
160	0.79	0.85	0.92	1.00	1.00	1.00	1.00	1.00	1.00	1.00	1.00	1.00	1.00
155	0.73	0.79	0.84	0.92	1.00	1.00	1.00	1.00	1.00	1.00	1.00	1.00	1.00
150	0.68	0.73	0.78	0.84	0.94	1.00	1.00	1.00	1.00	1.00	1.00	1.00	1.00
145	0.63	0.67	0.72	0.77	0.84	0.84	1.00	1.00	1.00	1.00	1.00	1.00	1.00
140	0.58	0.62	0.67	0.71	0.77	0.77	0.86	1.00	1.00	1.00	1.00	1.00	1.00
135	0.53	0.57	0.61	0.66	0.71	0.70	0.77	0.88	1.00	1.00	1.00	1.00	1.00
130	0.49	0.53	0.56	0.61	0.65	0.64	0.70	0.78	0.95	1.00	1.00	1.00	1.00
125	0.45	0.48	0.52	0.56	0.60	0.59	0.64	0.70	0.80	0.84	1.00	1.00	1.00
120	0.41	0.44	0.48	0.51	0.55	0.54	0.58	0.64	0.71	0.74	1.00	1.00	1.00
115	0.38	0.40	0.43	0.47	0.50	0.49	0.53	0.58	0.64	0.66	0.80	1.00	1.00
110	0.35	0.37	0.40	0.43	0.46	0.44	0.48	0.52	0.58	0.59	0.71	1.00	1.00
105	0.32	0.34	0.36	0.39	0.41	0.40	0.43	0.47	0.52	0.53	0.64	1.00	1.00
100	0.30	0.31	0.33	0.35	0.37	0.36	0.39	0.42	0.47	0.48	0.59	1.00	1.00
95	0.28	0.29	0.30	0.32	0.34	0.32	0.34	0.37	0.41	0.43	0.55	1.00	1.00
90	0.27	0.27	0.28	0.29	0.30	0.30	0.30	0.32	0.36	0.39	0.54	1.00	1.00
85	0.27	0.26	0.26	0.26	0.27	0.27	0.25	0.28	0.32	0.36	0.59	1.00	1.00
80	0.28	0.26	0.25	0.24	0.24	0.24	0.21	0.23	0.27	0.37	1.00	1.00	1.00
75	0.30	0.26	0.24	0.23	0.22	0.21	0.17	0.18	0.23	0.50	1.00	1.00	1.00
70	0.32	0.27	0.25	0.22	0.20	0.18	0.12	0.13	0.23	1.00	1.00	1.00	1.00
65	0.34	0.29	0.26	0.22	0.19	0.15	0.07	0.10	0.30	1.00	1.00	1.00	1.00
60	0.38	0.31	0.27	0.23	0.18	0.13	0.01	0.16	0.76	1.00	1.00	1.00	1.00
55	0.41	0.34	0.29	0.24	0.19	0.11	0.08	0.40	1.00	1.00	1.00	1.00	1.00
50	0.45	0.37	0.32	0.26	0.19	0.11	0.26	1.00	1.00	1.00	1.00	1.00	1.00
45	0.49	0.40	0.35	0.28	0.21	0.13	1.00	1.00	1.00	1.00	1.00	1.00	1.00
40	0.53	0.44	0.38	0.31	0.23	0.22	1.00	1.00	1.00	1.00	1.00	1.00	1.00
35	0.58	0.48	0.41	0.33	0.27	1.00	1.00	1.00	1.00	1.00	1.00	1.00	1.00
30	0.62	0.52	0.44	0.37	0.55	1.00	1.00	1.00	1.00	1.00	1.00	1.00	1.00
25	0.67	0.56	0.48	0.48	1.00	1.00	1.00	1.00	1.00	1.00	1.00	1.00	1.00
20	0.73	0.60	0.53	1.00	1.00	1.00	1.00	1.00	1.00	1.00	1.00	1.00	1.00
15	0.78	0.64	1.00	1.00	1.00	1.00	1.00	1.00	1.00	1.00	1.00	1.00	1.00
10	1.00	1.00	1.00	1.00	1.00	1.00	1.00	1.00	1.00	1.00	1.00	1.00	1.00
5	1.00	1.00	1.00	1.00	1.00	1.00	1.00	1.00	1.00	1.00	1.00	1.00	1.00

DIFFERENTIAL PHASE FACTOR δ (deg)

AVERAGE INSERTION PHASE ε (deg)

Fig. 12. Computer solution for reverse transmission parameter S_{12} with G magnitude <1.

Making the necessary substitutions into the indicated equations gives, for a typical term,

$$E_i^3 = \frac{\begin{vmatrix} -\frac{1}{3} s_{21} & -(\frac{1}{3} s_{22} + 1) & -\frac{2}{3} E_i^6 & 0 \\ \frac{2}{3} s_{21} & \frac{2}{3} s_{22} & -\frac{2}{3} E_i^6 & -1 \\ -(\frac{1}{3} s_{11} + 1) & -\frac{1}{3} s_{12} & -\frac{2}{3} E_i^5 & \frac{2}{3} s'_{12} \\ \frac{2}{3} s_{11} & \frac{2}{3} s_{12} & -\frac{2}{3} E_i^5 & -\frac{1}{3} s'_{12} \end{vmatrix}}{\begin{vmatrix} -\frac{1}{3} s_{21} & -(\frac{1}{3} s_{22} + 1) & \frac{2}{3} s'_{21} & 0 \\ \frac{2}{3} s_{21} & \frac{2}{3} s_{22} & -\frac{1}{3} s'_{21} & -1 \\ -(\frac{1}{3} s_{11} + 1) & -\frac{1}{3} s_{12} & 0 & \frac{2}{3} s'_{12} \\ \frac{2}{3} s_{11} & \frac{2}{3} s_{12} & -1 & -\frac{1}{3} s'_{12} \end{vmatrix}} \tag{65}$$

where $s_{12} = s_{21} = R$. The solution of this typical term is given as

$$E_i^3 = \frac{[\frac{2}{9} s_{12}s_{21} + \frac{4}{9} s'_{12}s_{21} - \frac{2}{9} s_{11}s_{22} - \frac{2}{9} s_{22} - \frac{2}{3} s_{11} - \frac{2}{3}] E_i^5 + [\frac{6}{27} s_{12}s'_{12}s_{21} - \frac{6}{27} s_{11}s'_{12}s_{22} + \frac{6}{27} s'_{12}s_{22} - \frac{2}{9} s_{11}s'_{12} + \frac{2}{9} s'_{12} - \frac{4}{9} s_{12}] E_i^6}{\frac{1}{9} [s_{12}s_{21} + 4s'_{12}s_{21} - s_{11}s'_{12}s'_{21} + s'_{12}s_{21} - s_{11}s_{22} - 3s_{22} - 3s_{11} - 9 - s_{12}s'_{12}s_{21}s'_{21} - s'_{12}s'_{21}s_{22} + s_{11}s'_{12}s'_{21}s_{22} + 4s_{12}s'_{21}]} \tag{66}$$

The form of matrix Eq. (43) still applies; therefore, assembling all E_i terms, Eq. (44) may be rewritten as

$$S_{12}\bigg|_{\text{with } E_i^5 = 0, \; E_i^6 = 1} = J_{31}(s_{11}[E_i^6 \text{ part of } E_i^1]$$

$$+ s_{12}[E_i^6 \text{ part of } E_i^2]) + J_{32}s'_{12}[E_i^6 \text{ part of } E_i^4]$$

$$= \frac{2}{27} \{-6s_{11}s'_{12}s_{22} - 6s_{11}s'_{12} + 6s_{12}s'_{12}s_{21} + 6s_{12}s'_{12}s'_{21}$$

$$- 6s'_{12}s_{22} - 6s_{12} - 6s'_{12}\} \tag{67}$$

and Eq. (45) may be rewritten as

$$S_{21}\bigg|_{\text{with } E_i^5=1, \, E_i^6=0} = J_{31}(s_{21}[E_i^5 \text{ part of } E_i^1] + s_{22}[E_i^5 \text{ part of } E_i^2])$$

$$+ J_{32}s_{21}'[E_i^5 \text{ part of } E_i^3]$$

$$= \frac{2}{27}\{6s_{12}'s_{21}s_{21}' + 6s_{12}s_{21}s_{21}' - 6s_{11}s_{21}'s_{22} - 6s_{21}'s_{22}$$

$$- 6s_{11}s_{21}' - 6s_{21} - 6s_{21}'\} \quad . \tag{68}$$

The ratio of Eq. (67) to Eq. (68) is

$$\frac{S_{12}}{S_{21}} = \frac{s_{12}(s_{12}'s_{21}' - 1) + s_{12}'(-s_{11}s_{22} - s_{11} - s_{22} - 1 + s_{12}s_{21})}{s_{21}(s_{12}'s_{21}' - 1) + s_{21}'(s_{12}s_{21} - s_{11}s_{22} - s_{22} - s_{11} - 1)} \quad . \tag{69}$$

After making the proper substitutions indicated by

$$[S] = \begin{bmatrix} R & G\epsilon^{j\alpha} \\ G\epsilon^{j\alpha} & R \end{bmatrix} \tag{70}$$

and

$$[S'] = \begin{bmatrix} 0 & \epsilon^{j\alpha'}\epsilon^{j\varphi} \\ \epsilon^{j\alpha'}\epsilon^{-j\varphi} & 0 \end{bmatrix} \tag{71}$$

Eq. (69) becomes

$$\frac{S_{12}}{S_{21}} = \frac{G\epsilon^{j\alpha}2j \sin\alpha' + \epsilon^{j\varphi}[G^2\epsilon^{j2\alpha} - (R^2 + 2R + 1)]}{G\epsilon^{j\alpha}2j \sin\alpha' + \epsilon^{-j\varphi}[G^2\epsilon^{j2\alpha} - (R^2 + 2R + 1)]} \quad . \tag{72}$$

The form of this equation is still $\xi + \epsilon^{j\varphi}\eta/\xi + \epsilon^{-j\varphi}\eta$, which will always have a magnitude of unity whenever the ratio ξ/η is real. The ratio

$$\frac{\xi}{\eta} = \frac{G\epsilon^{j\alpha}2j \sin\alpha'}{G^2\epsilon^{j2\alpha} - (R^2 + 2R + 1)} \quad . \tag{73}$$

Substituting for the exponents and collecting terms yields

$$\frac{\xi}{\eta} = \frac{1}{\left[\dfrac{G}{2}\dfrac{\sin\alpha}{\sin\alpha'} + \dfrac{(R^2 + 2R + 1)}{2G}\dfrac{\sin\alpha}{\sin\alpha'}\right] - j\left[\dfrac{G}{2}\dfrac{\cos\alpha}{\sin\alpha'} - \dfrac{(R^2 + 2R + 1)}{2G}\dfrac{\cos\alpha}{\sin\alpha'}\right]} \quad . \tag{74}$$

It is necessary that α have values other than $n(\pi/2)$, where n is odd, to keep the ratio from being entirely real. This is part of the same sufficiency condition found before on p. 13; however, now, in addition, the restriction imposed on G must be broadened to include the effect of R. It is evident that Eq. (74) is also real whenever

$$G = \frac{R^2 + 2R + 1}{G} \quad . \tag{75}$$

Thus, $|G|$ cannot be $|R + 1|$ for differential gain to be possible.

The complete scattering matrix for the basic differential circuit with amplifier reflections is shown in Fig. 13. If R is chosen as 0, the matrix terms degenerate to those terms displayed in Fig. 3.

2. Vector Space Representation

With finite reflections R, the gain G is now a function of three variables and must be represented in three-dimensional vector space. The amplifier gain G required to provide a matched differential circuit now depends on its own reflection coefficient R, as well as ϵ and δ. G may be solved for from the s_{11} term of the matrix in Fig. 13. Making the substitutions for φ_+ and φ_-, this becomes

$$G = \frac{4\epsilon \operatorname{Re} \delta \pm \sqrt{16\epsilon^2 \operatorname{Re}^2(\delta) - (3\epsilon^2 + 1)[(-3R^2 + 2R + 1)\epsilon^2 + (-R^2 - 2R + 3)]}}{3\epsilon^2 + 1} \quad . \quad (76)$$

This result should be compared with Eq. (57), which is for the case of R = 0.

The computer program was extended to solve for the complex amplifier gain G required for various values of ϵ and δ with chosen increments of real reflection coefficients R. The program additions indicated may be found listed in Appendix B, Fig. B-3. Figure 14 shows a three-dimensional representation of all the possible solutions of this problem in reflection-insertion phase-differential phase space.

For successively larger positive values of R, the second complex term under the radical of Eq. (76) has a diminishing magnitude; thus, larger values of δ are allowable for a matched solution regardless of the value of ϵ. On the other hand, for successively larger negative values of R, the second term under the radical becomes smaller in magnitude for large values of ϵ and larger in magnitude with very small values of ϵ. A larger magnitude of this second term decreases the allowable δ, thus limiting the range over which solutions are possible. For successively larger negative values of R with ϵ near 90°, there exists a continuous range of possible values of δ without limit. If a large range of δ is desired, R should be negative, which means the amplifier should have an impedance lower than that of the feeding line. These dependences on δ are reflected in the dissymmetry of the spatial configuration.

Certainly, any value of R other than zero in Eq. (76) will cause the roots of the quadratic Eq. (76) to be different than reciprocal conjugates. Hence, the differential attenuator model will not have characteristics that are reciprocal to those of the differential gain model for any non-zero value of R.

3. Dependence on Reflection Angle

In practice, a fourth dimension is certain to be present as the phase angle on R. The effect that this angle has on the three-dimensional solution space is to be determined. A single plane was passed through the reflection phase space diagram of Fig. 14 at the point where R = +0.2 and parallel to the insertion- and differential-phase coordinate axes.

The phase angle on R = 0.2 was varied from −120° to +120° in order to determine just how susceptible the required values of G were to changes in reflection angle. Again, the computer program was rewritten. The substitutions required will be found in Appendix B, Fig. B-4.

Figure 15 shows a resulting three-dimensional configuration representing the solution space of R = 0.2 as influenced by reflection coefficient phase. The figure shows the reflection coefficient phase to vary only from −90° to +90°, and illustrates the fact that varying the phase

$$
\begin{bmatrix}
\dfrac{\{3G^2 - (3R^2 - 2R - 1)\}\,\epsilon^{-j(\varphi_+ + \varphi_-)} - 4G\epsilon^{-j\varphi_-} - 4G\epsilon^{-j\varphi_+} + G^2 - (R^2 + 2R - 3)}{\{-G^2 + (R^2 - 2R + 1)\}\,\epsilon^{-j(\varphi_+ + \varphi_-)} + 4G\epsilon^{-j\varphi_-} + 4G\epsilon^{-j\varphi_+} + G^2 - (R^2 + 6R + 9)}
&
\dfrac{4G\epsilon^{-j(\varphi_+ + \varphi_-)} + 4\{G^2 - (R^2 + 2R + 1)\}\,\epsilon^{-j\varphi_-} - 4G}{\{-G^2 + (R^2 - 2R + 1)\}\,\epsilon^{-j(\varphi_+ + \varphi_-)} + 4G\epsilon^{-j\varphi_-} + 4G\epsilon^{-j\varphi_+} + G^2 - (R^2 + 6R + 9)}
\\[3em]
\dfrac{4G\epsilon^{-j(\varphi_+ + \varphi_-)} + 4\{G^2 - (R^2 + 2R + 1)\}\,\epsilon^{-j\varphi_+} - 4G}{\{-G^2 + (R^2 - 2R + 1)\}\,\epsilon^{-j(\varphi_+ + \varphi_-)} + 4G\epsilon^{-j\varphi_-} + 4G\epsilon^{-j\varphi_+} + G^2 - (R^2 + 6R + 9)}
&
\dfrac{\{3G^2 - (3R^2 - 2R - 1)\}\,\epsilon^{-j(\varphi_+ + \varphi_-)} - 4G\epsilon^{-j\varphi_+} - 4G\epsilon^{-j\varphi_-} + G^2 - (R^2 + 2R - 3)}{\{-G^2 + (R^2 - 2R + 1)\}\,\epsilon^{-j(\varphi_+ + \varphi_-)} + 4G\epsilon^{-j\varphi_+} + 4G\epsilon^{-j\varphi_-} + G^2 - (R^2 + 6R + 9)}
\end{bmatrix}
$$

Fig. 13. Scattering matrix for basic differential circuit with amplifier reflections R.
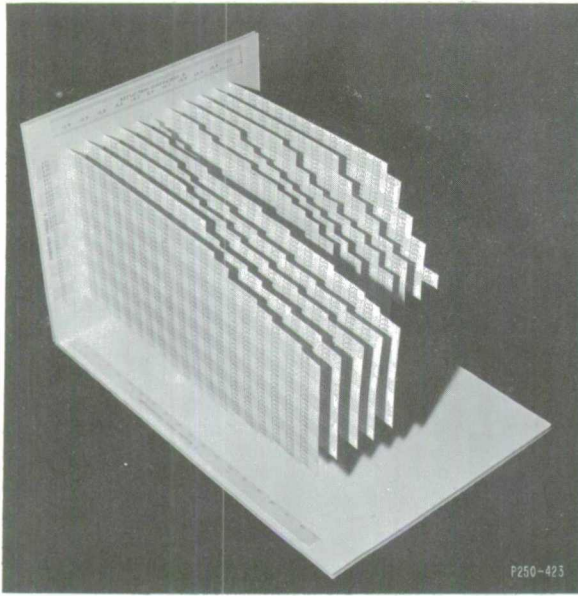
Fig. 14. Three-dimensional representation showing all possible problem solutions of $|G| > 1$ in reflection-insertion phase-differential phase space.
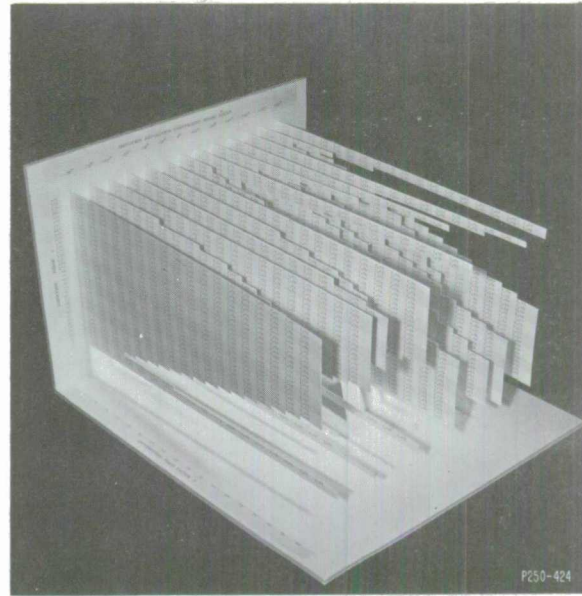
Fig. 15. Illustration showing all solutions of $|G| > 1$ as a function of amplifier reflection coefficient phase angle, insertion phase ϵ, and differential phase factor δ; amplifier reflection coefficient $|R| = 0.2$.

angle on the amplifier reflection coefficient does not limit the range of ϵ or δ for possible solutions. However, it does produce a change in symmetry about the plane $\epsilon = 90°$ with higher reflection angles. With these higher angles, the range of values of δ is extended to include a greater number of possible solutions.

By relieving conditions on the ideal amplifier, several active devices become practical. Among these is the simple reflection-type tunnel-diode amplifier consisting basically of a scattering junction and the terminating negative resistance. There is also a need for some stabilizing network[†] which will add sufficient loss to compensate for the negative resistance at unwanted frequencies.

G.   Alternate Junctions

To determine the effect that the scattering junction itself might have on nonreciprocity, two general solutions were worked out using junctions different from the symmetrical lossless junctions in the basic matched differential amplifier arrangement. One junction, formed by a 50-ohm line feeding two identical 100-ohm lines, is to be identified in the following as a balanced junction. The other junction formed by the converging of a 50-, 25-, and 100-ohm line is arbitrarily chosen and is to be identified in the following analysis as a completely nonsymmetrical junction. These junctions are shown schematically in Fig. 16(a-b). Since the theoretical development parallels the cases already treated, it will not be presented in as much detail. Suffice it to say that changing the junctions changes the numerical coefficients appearing in the various scattering matrices. The general properties of forward-to-backward differential gain and differential loss remain as before. The first configuration to be analyzed is that of the basic differential amplifier using two balanced junctions.

---

† J. H. Lepoff, "Design Procedure for a Shunt Stabilizing Circuit for Tunnel Diode Amplifiers," private communication.
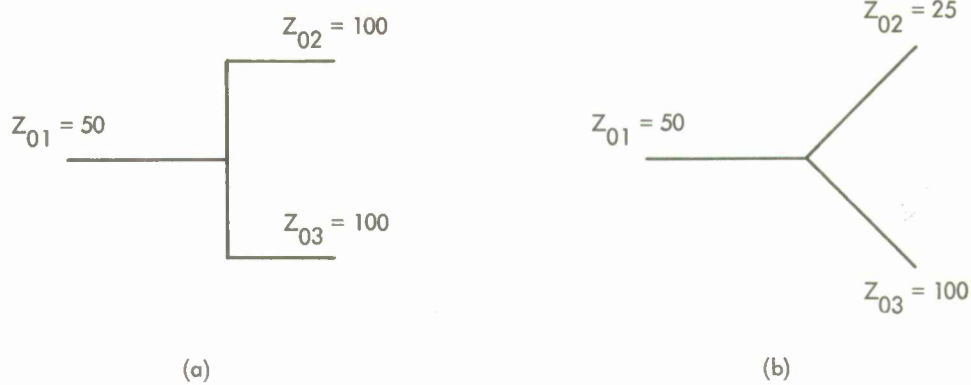
Fig. 16. Diagrammatic representation of lossless scattering junctions: (a) a balanced junction, (b) a nonsymmetrical junction.

1. Balanced Junctions

The balanced junction chosen is represented by the matrix

$$[J] = \begin{bmatrix} 0 & \dfrac{1}{\sqrt{2}} & \dfrac{1}{\sqrt{2}} \\[2mm] \dfrac{1}{\sqrt{2}} & -\dfrac{1}{2} & \dfrac{1}{2} \\[2mm] \dfrac{1}{\sqrt{2}} & \dfrac{1}{2} & -\dfrac{1}{2} \end{bmatrix} . \tag{77}$$

The resulting overall scattering matrix, utilizing two of these balanced junctions, is shown in Fig. 17. The matrix does display symmetry about the secondary diagonal, and it folds over along the principal diagonal if φ_+ and φ_- are interchanged.

The computer program was written to solve for possible amplifier gain, which would allow for the matched differential amplifier. Program substitutions are listed in Appendix B, Fig. B-5. The result of such an analysis gives a three-dimensional figure in reflection-phase space, as shown in Fig. 18. It is interesting to point out that no solution is ever possible when R = 0, due to the fact that an incoming wave splits once at the first junction, matches the input to both the upper path and the lower path, combines, and emerges as a single wave again. Thus, the separated waves just converge on the second balanced junction; there is no feedback possible.

2. Nonsymmetrical Junctions

The second alternate solution chosen was that utilizing the junction of Fig. 16(b). The scattering matrix for this completely nonsymmetrical junction of 50-, 25-, and 100-ohm lines is given as

$$[J] = \begin{bmatrix} 0.1428 & 0.5714 & 0.8081 \\ 0.5714 & -0.7142 & 0.4040 \\ 0.8081 & 0.4040 & -0.4285 \end{bmatrix} . \tag{78}$$

$$\begin{bmatrix} \dfrac{(2R+1)\,\epsilon^{-j(\varphi_+ + \varphi_-)} - G\epsilon^{-j\varphi_-} - G\epsilon^{-j\varphi_+} + G^2 - (R^2 + 2R)}{\epsilon^{-j(\varphi_+ + \varphi_-)} + G\epsilon^{-j\varphi_+} + G\epsilon^{-j\varphi_-} + G^2 - (R^2 + 4R + 4)} & \dfrac{2G\epsilon^{-j(\varphi_+ + \varphi_-)} + \{2G^2 - 2(R^2 + 2R + 1)\}\,\epsilon^{-j\varphi_+} - 2G}{\epsilon^{-j(\varphi_+ + \varphi_-)} + G\epsilon^{-j\varphi_+} + G\epsilon^{-j\varphi_-} + G^2 - (R^2 + 4R + 4)} \\[4ex] \dfrac{2G\epsilon^{-j(\varphi_+ + \varphi_-)} + \{2G^2 - 2(R^2 + 2R + 1)\}\,\epsilon^{-j\varphi_-} - 2G}{\epsilon^{-j(\varphi_+ + \varphi_-)} + G\epsilon^{-j\varphi_+} + G\epsilon^{-j\varphi_-} + G^2 - (R^2 + 4R + 4)} & \dfrac{(2R+1)\,\epsilon^{-j(\varphi_+ + \varphi_-)} - G\epsilon^{-j\varphi_-} - G\epsilon^{-j\varphi_+} + G^2 - (R^2 + 2R)}{\epsilon^{-j(\varphi_+ + \varphi_-)} + G\epsilon^{-j\varphi_+} + G\epsilon^{-j\varphi_-} + G^2 - (R^2 + 4R + 4)} \end{bmatrix}$$

Fig. 17. Scattering matrix for basic differential circuit, but with two balanced scattering junctions.

33
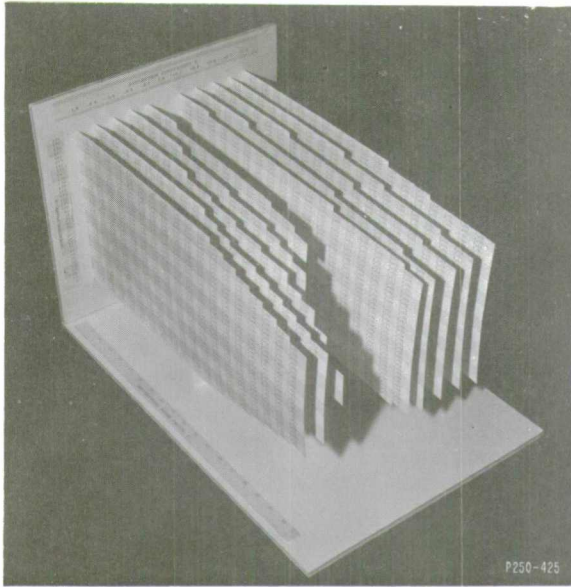
Fig. 18. Reflection-phase space representation showing possible problem solutions of $|G| > 1$ when using balanced scattering junctions.

Figure 19 shows the complete differential scattering matrix resulting from this special choice.

A computer program, altered for the use of these special junctions and still requiring a match, i.e., $S_{11} = 0$, may be found in Appendix B, Fig. B-6. The computer solution gave values of $G > 1$ within a three-dimensional field of reflection-phase space that displayed interesting characteristics. For an amplifier reflection coefficient of zero, no solution is possible; that is to say, nonreciprocity is not possible with a matched input. For successively larger negative values of R, a single lobe in solution space centered on $\epsilon = 90°$ is evident, very much like that of Fig. 14. On the other hand, with successively larger positive values of R, a double lobe is in evidence, one lobe being centered on $\epsilon = 0$ and the other on $\epsilon = 180°$.

H. Use in Active Network Synthesis

The theory developed thus far has been sufficient to predict two matched differential units — one an amplifier, and the other an attenuator. Each unit is capable of exhibiting considerable nonreciprocity with small amounts of differential phase. The use of two scattering junctions, one active element, and one element exhibiting differential phase defines the amplifier; while two scattering junctions, one passive element, and one differential phase element define the attenuator.

In the field of active network synthesis, where the requirement of reciprocity has been removed from analytic functions, there has been no way to realize the nonreciprocity except by using one or more gyrators. Starting with a given nonpositive-real immittance function, the nonreciprocity could be removed by a gyrator network to leave a positive-real remainder function which could be realized by several classical techniques. Use of the devices under discussion here could offer an alternate way of achieving the desired nonreciprocity, but with small amounts of differential phase.

1. Composite Cascade

Perhaps a more general scheme would be to achieve gain in one direction and loss in the other by cascading together one each of the previously described nonreciprocal units, thus producing a composite cascaded unit.

34

$$
\begin{bmatrix}
\dfrac{\{21(G^2 - R^2) + 38R - 5\}\,\epsilon^{-j(\varphi_+ + \varphi_-)} - 16G\epsilon^{-j\varphi_-} - 16G\epsilon^{-j\varphi_+} - (5G^2 - 5R^2 + 38R - 21)}{\{9(R^2 - G^2) - 30R + 25\}\,\epsilon^{-j(\varphi_+ + \varphi_-)} + 16G\epsilon^{-j\varphi_-} + 16G\epsilon^{-j\varphi_+} + G^2 - (R^2 - 14R + 49)} & \dfrac{32G\epsilon^{-j(\varphi_+ + \varphi_-)} + 8\{G^2 - (R^2 + 2R + 1)\}\,\epsilon^{-j\varphi_+} - 32G}{\{9(R^2 - G^2) - 30R + 25\}\,\epsilon^{-j(\varphi_+ + \varphi_-)} + 16G\epsilon^{-j\varphi_-} + 16G\epsilon^{-j\varphi_+} + G^2 - (R^2 - 14R + 49)} \\[6ex]
\dfrac{32G\epsilon^{-j(\varphi_+ + \varphi_-)} + \{8G^2 - 8(R^2 + 2R + 1)\}\,\epsilon^{-j\varphi_-} - 32G}{\{9(R^2 - G^2) - 30R + 25\}\,\epsilon^{-j(\varphi_+ + \varphi_-)} + 16G\epsilon^{-j\varphi_-} + 16G\epsilon^{-j\varphi_+} + G^2 - (R^2 - 14R + 49)} & \dfrac{\{21(G^2 - R^2) + 38R - 5\}\,\epsilon^{-j(\varphi_+ + \varphi_-)} - 16G\epsilon^{-j\varphi_-} - 16G\epsilon^{-j\varphi_+} - (5G^2 - 5R^2 + 38R - 21)}{\{9(R^2 - G^2) - 30R + 25\}\,\epsilon^{-j(\varphi_+ + \varphi_-)} + 16G\epsilon^{-j\varphi_-} + 16G\epsilon^{-j\varphi_+} + G^2 - (R^2 - 14R + 49)}
\end{bmatrix}
$$

Fig. 19. Complete scattering matrix for basic differential circuit using two special nonsymmetrical scattering junctions.

From the vast solutions of the matched differential amplifier and matched differential attenuator, it is possible to pick variables such that the cascading of one each of these presents an overall scattering matrix, given as

$$[S] = \begin{bmatrix} 0 & G_c \\ L_c & 0 \end{bmatrix} \tag{79}$$

where $1 < G_c \leqslant N$, and $0 < L_c < 1$. The value N used here is merely an upper bound. The parameters S_{12} and S_{21} may be interchanged readily by interchanging φ_+ and φ_-.

2. Iterations of Composite Cascades

If additional gain or loss is required, the entire composite network may be repeated. Figure 20 shows the iteration of two such composite cascaded networks. The terminal relations are

$$\begin{bmatrix} E_s^1 \\ E_s^2 \end{bmatrix} = \begin{bmatrix} 0 & G_c \\ L_c & 0 \end{bmatrix} \begin{bmatrix} E_i^1 \\ E_i^2 \end{bmatrix} \tag{80}$$

and

$$\begin{bmatrix} E_s^2 \\ E_s^3 \end{bmatrix} = \begin{bmatrix} 0 & G_c \\ L_c & 0 \end{bmatrix} \begin{bmatrix} E_i^2 \\ E_i^3 \end{bmatrix} . \tag{81}$$
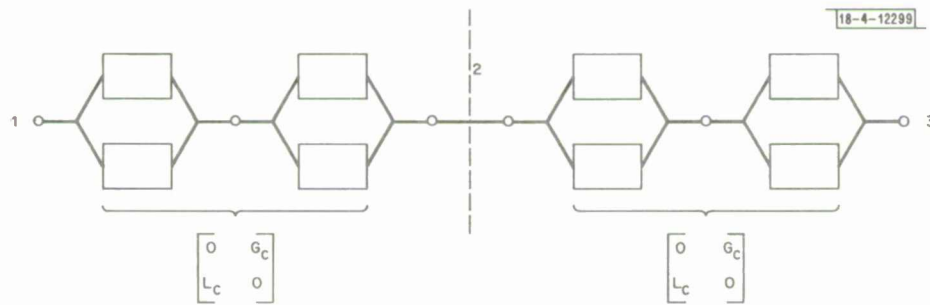
Fig. 20. Iteration of two composite cascaded differential networks.

To be conformable, these equations are rewritten in transmission or chain form as

$$\begin{bmatrix} E_i^1 \\ E_s^1 \end{bmatrix} = \begin{bmatrix} 0 & \dfrac{1}{L_c} \\ G_c & 0 \end{bmatrix} \begin{bmatrix} E_i^2 \\ E_s^2 \end{bmatrix} \tag{82}$$

36

and

$$
\begin{bmatrix} E_i^2 \\ E_s^2 \end{bmatrix} = \begin{bmatrix} 0 & \dfrac{1}{L_c} \\ G_c & 0 \end{bmatrix} \begin{bmatrix} E_i^3 \\ E_s^3 \end{bmatrix} \ . \tag{83}
$$

By substituting Eq. (83) into Eq. (82), the overall transmission matrix equation becomes

$$
\begin{bmatrix} E_i^1 \\ E_s^1 \end{bmatrix} = \begin{bmatrix} 0 & \dfrac{1}{L_c} \\ G_c & 0 \end{bmatrix} \begin{bmatrix} G_c & 0 \\ 0 & \dfrac{1}{L_c} \end{bmatrix} \begin{bmatrix} E_i^3 \\ E_s^3 \end{bmatrix} = \frac{1}{L_c^2} \begin{bmatrix} 0 & 1 \\ G_c^2 L_c^2 & 0 \end{bmatrix} \begin{bmatrix} E_i^3 \\ E_s^3 \end{bmatrix} \ . \tag{84}
$$

Converting this back to a scattering matrix equation,

$$
\begin{bmatrix} E_s^1 \\ E_s^3 \end{bmatrix} = \begin{bmatrix} 0 & G_c^2 \\ L_c^2 \cdot & 0 \end{bmatrix} \begin{bmatrix} E_i^1 \\ E_i^3 \end{bmatrix} \ . \tag{85}
$$

It is obvious that continued iterations of n of these structures can realize a scattering matrix, given by

$$
[S] = \begin{bmatrix} 0 & G_c^n \\ L_c^n & 0 \end{bmatrix} \ . \tag{86}
$$

Thus, the amount of nonreciprocity is dependent both on the number of iterations and on the differential gain and loss chosen in realizing the basic composite cascade.

It must be realized that the absolute value of G_c^n and of L_c^n indicated depends on the cascaded units being perfectly matched.

3. Immittance Relations

The desired nonreciprocity is specified by the terms of the scattering matrix of Eq. (86). Much of the network synthesis is accomplished utilizing immittance relations preferable to such scattering terms. Equation (86) will be converted to the immittance form to show that the scattering terms necessary for synthesis can easily be recognized even though the function is given in the immittance form.

The impedance matrix[1] of a two-port network may be obtained from a scattering matrix by

$$
Z = 2([U] - [S])^{-1} - [U] \tag{87}
$$

37

where [U] is the unit diagonal matrix. Thus,

$$Z = 2 \left(\begin{bmatrix} 1 & 0 \\ 0 & 1 \end{bmatrix} - \begin{bmatrix} 0 & G_c^n \\ L_c^n & 0 \end{bmatrix} \right)^{-1} - \begin{bmatrix} 1 & 0 \\ 0 & 1 \end{bmatrix}$$

$$= \frac{1}{1 - G_c^n L_c^n} \begin{bmatrix} 1 + G_c^n L_c^n & 2G^n \\ 2L_c^n & 1 + G_c^n L_c^n \end{bmatrix} \quad . \tag{88}$$

Similarly, the admittance matrix may be obtained from

$$Y = 2([U] + [S])^{-1} - [U] \quad ;$$

$$Y = 2 \left(\begin{bmatrix} 1 & 0 \\ 0 & 1 \end{bmatrix} + \begin{bmatrix} 0 & G_c^n \\ L_c^n & 0 \end{bmatrix} \right)^{-1} - \begin{bmatrix} 1 & 0 \\ 0 & 1 \end{bmatrix}$$

$$= \frac{1}{1 - L_c^n G_c^n} \begin{bmatrix} 1 + L_c^n G_c^n & -2G^n \\ -2L_c^n & 1 + G_c^n L_c^n \end{bmatrix} \quad . \tag{89}$$

An immittance matrix may be formed by combining Eqs. (88) and (89) as

$$\begin{bmatrix} \dfrac{1 + L_c^n G_c^n}{1 - L_c^n G_c^n} & \dfrac{\pm 2G}{1 - L_c^n G_c^n} \\ \\ \dfrac{\pm 2L}{1 - L_c^n G_c^n} & \dfrac{1 + L_c^n G_c^n}{1 - L_c^n G_c^n} \end{bmatrix} \tag{90}$$

where the + sign signifies an impedance matrix and the − sign signifies an admittance matrix.

Given an immittance matrix to realize, the selection would be made of G_c and L_c or G_c^n and L_c^n, where n is the number of iterations of the basic composite cascade. G_c is the product of like terms: for example, S_{12} of the matched differential amplifier section and S_{12} of the matched differential attenuator section. In similar fashion,

$$L_c = S_{21} \text{ amplifier} \times S_{21} \text{ attenuator} \quad . \tag{91}$$

In this application to synthesis, nothing has been mentioned about the phase of either L_c or G_c. Any amount of phase shift common to the two terms would be realized by a positive-real residue function. An amount of differential phase could be realized by a unit similar to that employed in the basic differential gain circuit.

III. REALIZATION OF THE MODEL

In order to demonstrate practicality and to substantiate the theoretical development, it was decided to realize one of the models predicted. It was further decided to realize the matched differential attenuator model first, thus to avoid at the outset the imbedding of an unstable active tunnel diode and its necessary stabilizing and terminating circuits. For such a realization, aside from symmetrical scattering junctions, it is necessary to have a controlling phase-shift element and a bilateral attenuator.

Several experimental procedures were carried out by the author, both in order to proceed at various points in the development and in order to verify some of the theoretical data. These experiments are described below.

A. Phase-Shift Element

The key to either device model is the use of a two-port element which can produce a different phase delay in the forward and reverse conductive directions. Only a few degrees of such differential phase are needed. Further, the desire is present of interchanging the transmission characteristics of the ports by being able to interchange φ_+ and φ_-, the phase delay in the two conductive directions.

An additional requirement of having the input and output reflection coefficients equal to zero restricts the impedance of the differential phase unit to 50 ohms, which is the present standard transmission impedance in microstrip.

Of the several devices reported in the literature which exhibit differential phase, the meander line was chosen for this application. Only a limited number of meanders would be necessary to yield a small amount of phase shift at S-band (2.0 to 4.0 GHz).

Owing to the requirement of this special application, a need exists to know how to design such a line for (a) the required 50-ohm impedance, and (b) the desired limited differential phase. Unfortunately, there presently exists no procedure for calculating the desired differential phase; thus, the following will be limited to the design of a meander line with a limited number of meanders so far as its impedance alone is concerned.

1. Design of Meander Line

An iterative-type procedure has been developed by Syracuse University Research Corporation[7] for the proper dimensions of linewidth and line spacing for a given substrate thickness to yield a matched meander line. This procedure is based on an infinite number of meanders and depends for accuracy on the reading of several sets of curves giving various fringing capacitances.

Here, a new approach will be used to determine the meander-line impedance characteristics. This will be accomplished by modifying all-pass filter equations to properly account for changing propagation velocities, and by using recent data on such velocities in coupled microstrips. Where only a few meanders will be needed, such a scheme will be more direct.

Theory of Coupled Strips:— The problem of conducting strips in close proximity has been solved for a general transmission scheme. Jones and Bolljahn[18] present several

39

solutions of two such parallel coupled lines with various terminations. However, their development is for the stripline, transmission-line system, with a ground plane above as well as below the coupled strips (such a configuration is illustrated in Fig. 21). Certainly, propagation along the strips is in the TEM mode.
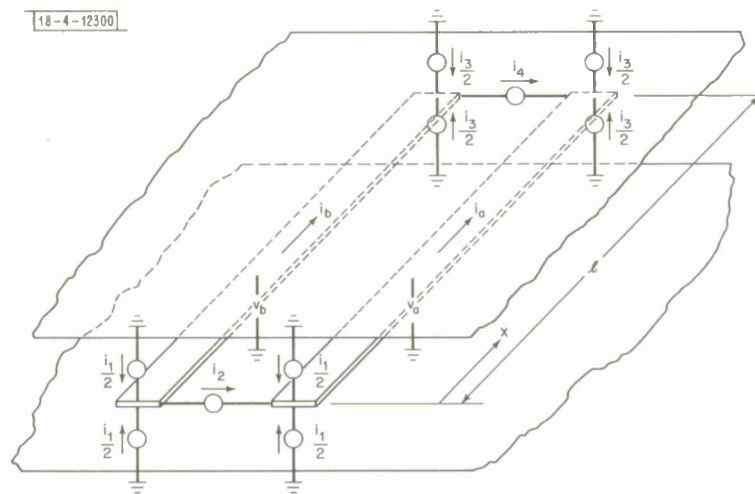
Fig. 21. Notation used in deriving all-pass filter characteristics in stripline transmission system. After E. M. T. Jones and J. T. Bolljahn.[18]

The indicated sets of current generators can excite a so-called even or odd mode of propagation. Each normal mode has a characteristic impedance defined by Bolljahn as follows:

Z_{oe} = characteristic impedance of one wire to ground with equal current (flowing) in the same directions,

Z_{oo} = characteristic impedance of one wire to ground with equal current (flowing) in opposite directions.

Results are presented in Ref. 18 for two coupled strips connected together at the far end, thus presenting a single meander line. This is classified as an all-pass filter.

The image impedance of such a derived filter in the TEM mode is given as

$$Z_I = \sqrt{Z_{oe} Z_{oo}} \tag{92}$$

and its insertion phase shift φ can be obtained from

$$\cos \varphi = \frac{\dfrac{Z_{oe}}{Z_{oo}} - \tan^2 \beta l}{\dfrac{Z_{oe}}{Z_{oo}} + \tan^2 \beta l} \quad . \tag{93}$$

The solution that follows is a modification for microstrip transmission.

Theory of Coupled Strips in Microstrip:— Figure 22 shows two parallel lines coupled in the microstrip transmission system where now the upper ground plane is removed, leaving air dielectric above the strip and a solid high dielectric substrate below. Wave propagation along the strip is no longer truly in the TEM mode.

Owing to the fact that all transverse dimensions are much smaller than the wavelength within the operating frequency range, the simplifying assumption is made that the TEM mode still persists.

40
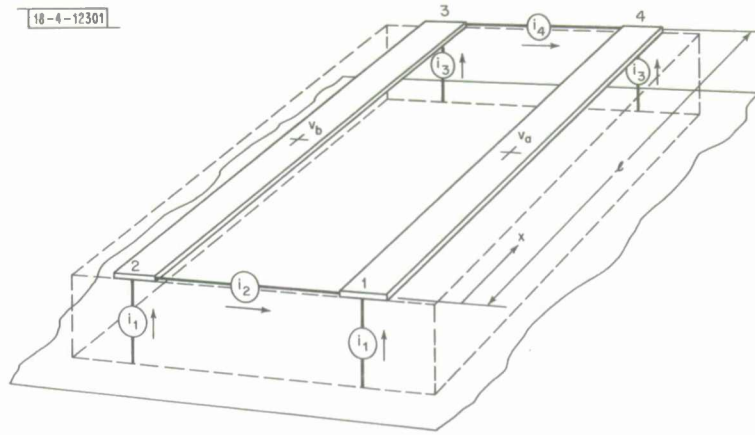
Fig. 22. Notation used in deriving image impedance characteristic for microstrip meander line.

A recent analysis by Weiss and Bryant[17] presents data for the even- and odd-mode velocities along pairs of coupled microstrips. Data[†] for dielectric constants of 16.0 and 14.4 are reproduced in Appendix B, Figs. B-7(b) and B-8(b). These data are directly applicable to the derivation of the meander-line impedance.

<u>Modification of All-Pass Equations</u>:— The equations derived for the all-pass filter or meander line in stripline may now be rederived taking into account the different mode velocities for microstrip transmission.

Referring to Fig. 22, the input current to each of the terminals may be related to the current sources indicated as

$$I_1 = i_1 + i_2$$

$$I_2 = i_1 - i_2$$

$$I_3 = i_3 - i_4$$

$$I_4 = i_3 + i_4 \quad . \tag{94}$$

The generator currents are, in turn, related to the terminal currents by

$$i_1 = \frac{1}{2} (I_1 + I_2)$$

$$i_2 = \frac{1}{2} (I_1 - I_2)$$

$$i_3 = \frac{1}{2} (I_3 + I_4)$$

$$i_4 = \frac{1}{2} (I_4 - I_3) \quad . \tag{95}$$

Since infinite impedance current generators are employed, the strip voltage to the ground plane v_{a1} may be obtained from transmission-line theory as

---

† These data are reproduced with special permission from J. A. Weiss and T. G. Bryant.[17]

41

$$v_{a1} = \frac{-jZ_{oe}i_1 \cos\beta_e(\ell - x)}{\sin\beta_e\ell} \tag{96}$$

where Z_{oe} is the even-mode characteristic impedance, and β_e is the even-mode phase velocity along the strip. Similar expressions exist for the contributions to v_a and v_b by the remaining current sources.

The terminal voltages for the coupled strips become

$$V_1 = (v_{a1} + v_{a2} + v_{a3} + v_{a4})|_{x=0}$$

$$V_2 = (v_{b1} + v_{b2} + v_{b3} + v_{b4})|_{x=0}$$

$$V_3 = (v_{b1} + v_{b2} + v_{b3} + v_{b4})|_{x=\ell}$$

$$V_4 = (v_{a1} + v_{a2} + v_{a3} + v_{a4})|_{x=\ell} \quad . \tag{97}$$

Substituting Eq. (96) and similar expressions into Eq. (97) yields a set of equations, one of which is illustrated here as

$$V_1 = -jZ_{oe}i_1 \frac{\cos\beta_e\ell}{\sin\beta_e\ell} - jZ_{oo}i_2 \frac{\cos\beta_o\ell}{\sin\beta_o\ell} - jZ_{oe}i_3 \frac{1}{\sin\beta_e\ell} - jZ_{oo}i_4 \frac{1}{\sin\beta_o\ell} \quad . \tag{98}$$

In order to effect a simplification of the derivation, it will be helpful to define

$$A = \frac{j}{2} Z_{oe} \frac{\cos\beta_e\ell}{\sin\beta_e\ell}$$

$$B = \frac{j}{2} Z_{oo} \frac{\cos\beta_o\ell}{\sin\beta_o\ell}$$

$$C = \frac{j}{2} Z_{oe} \frac{1}{\sin\beta_e\ell}$$

$$D = \frac{j}{2} Z_{oo} \frac{1}{\sin\beta_o\ell} \quad . \tag{99}$$

The relation between the terminal currents and terminal voltages may be expressed in matrix form as

$$\begin{bmatrix} V_1 \\ V_2 \\ V_3 \\ V_4 \end{bmatrix} = [Z] \begin{bmatrix} I_1 \\ I_2 \\ I_3 \\ I_4 \end{bmatrix} \quad . \tag{100}$$

For the case of a single meander line, the boundary conditions require that $I_3 = -I_4$ and $V_4 = V_3$.

This matrix equation reduces to two equations of the form

$$V_1 = \left[-A - B + \frac{D^2}{B}\right] I_1 + \left[-A + B - \frac{D^2}{B}\right] I_2 \tag{101}$$

42

and

$$V_2 = \left[-A + B - \frac{D^2}{B}\right] I_1 + \left[-A - B + \frac{D^2}{B}\right] I_2 \quad . \tag{102}$$

These terms may be compared with those of a general network described by the open-circuit driving point and transfer impedances z_{11}, z_{12}, and z_{22} where

$$V_1 = z_{11} I_1 + z_{12} I_2 \tag{103}$$

and

$$V_2 = z_{21} I_1 + z_{22} I_2 \quad . \tag{104}$$

If a boundary condition is now applied to this circuit such that it is terminated at port 2 by its image impedance, $V_2 = -I_2 Z_I$, Eq. (104) may be solved for I_2 as

$$I_2 = \frac{z_{21}}{-Z_I - z_{22}} I_1 \quad . \tag{105}$$

With this result substituted, Eq. (103) becomes

$$V_1 = z_{11} I_1 + \frac{z_{12} z_{21}}{-Z_I - z_{22}} I_1 \quad . \tag{106}$$

With the circuit so terminated in its image impedance Z_I, the ratio of V_1/I_1 is also Z_I. Thus,

$$Z_I = z_{11} + \frac{z_{12} z_{21}}{-Z_I - z_{22}} \quad . \tag{107}$$

If z_{11} is identical to z_{22}, and symmetry has been preserved to guarantee this condition, then

$$Z_I = \sqrt{z_{11} z_{22} - z_{12} z_{21}} \quad . \tag{108}$$

The terms of Eqs. (101) and (102) may be identified with z_{11}, z_{22}, z_{12}, and z_{21} and substituted into Eq. (108) to give

$$Z_I = \left(4AB - \frac{4AD^2}{B}\right)^{1/2} \quad . \tag{109}$$

Upon substituting from the defining equation of Eq. (100) and simplifying, the final image impedance is given as

$$Z_I = \sqrt{Z_{oe} Z_{oo}} \sqrt{\frac{\tan \beta_o \ell}{\tan \beta_e \ell}} \quad . \tag{110}$$

This result may be compared with the Johns and Bolljahn result of Eq. (92).

The image transfer constant for any two-port network is defined in impedance terms as

$$\cosh \varphi = \frac{(z_{11} z_{22})^{1/2}}{z_{12}} \quad . \tag{111}$$

Substituting for z_{11}, z_{12}, and z_{22}, and making use of the fact that $z_{11} = z_{22}$,

$$\cosh \varphi = \frac{-A - B + (D^2/B)}{-A + B - (D^2/B)} \quad . \tag{112}$$

If the Z_{oe} and Z_{oo} are assumed to be real, i.e., lossless lines, Eq. (112) may be reduced to

$$\cos \varphi = \frac{(Z_{oe}/Z_{oo}) - \tan \beta_e \ell \, \tan \beta_o \ell}{(Z_{oe}/Z_{oo}) + \tan \beta_e \ell \, \tan \beta_o \ell} \quad . \tag{113}$$

Equations (110) and (113) show the alterations necessary in the Jones and Bolljahn all-pass equations to properly take into account the different normal-mode velocities.

Theoretical Impedance Curves:— An examination of the Weiss and Bryant data[17] reveals that $\beta_o < \beta_e$ for coupled strips. Equation (110) then will no longer predict an image impedance which is constant at all frequencies, for when $\beta_o \ell < \pi/2 < \beta_e \ell$, the image impedance is imaginary or the filter is in cutoff. Coupling in microstrip makes the meander line then a band-pass filter.

Figure 23 shows both the image impedance Z_I and the insertion phase φ calculated for a magnesium titanate (K = 16) dielectric at frequencies in L-, S-, and C-bands. The length ℓ was chosen so that $\beta_e \ell$ would be $\pi/2$ at 4 GHz, the end of S-band. The W/H ratio, i.e., width of the conducting strip to the thickness of the substrate, was chosen to provide a 50-ohm image impedance at 3.0 GHz. The dashed curves were intended to show the character of Z_I and of φ if the effect of the even- and odd-mode velocities was not taken into account.
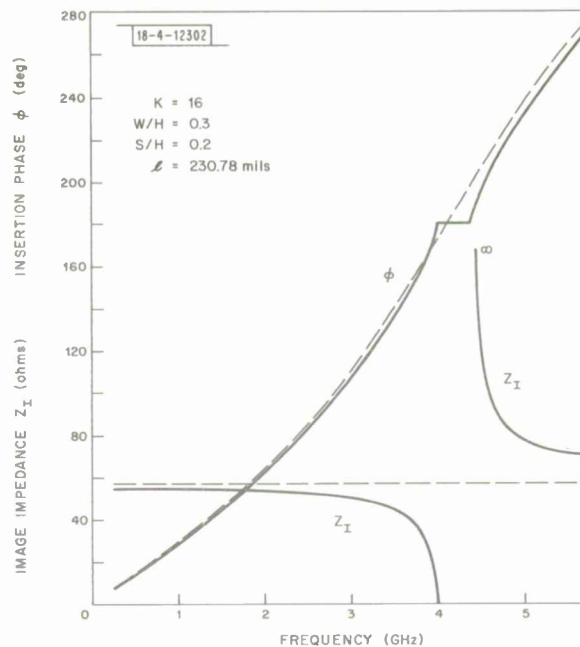
Fig. 23. Theoretical image impedance and insertion phase
of microstrip meander line on dielectric (K = 16) substrate.

Assumption of Coupled Meanders:— Although accurate information is available concerning the effect of coupling one strip to a second strip, no information is available on the effect of a second or third coupling offered when more than one meander is included. In order to proceed, it is assumed that there is no additional effect on the image impedance presented

by a second coupling meander. Although this is certainly erroneous, only a few meanders are necessary in this case, and such an assumption serves as a starting point.

Experimental Meander-Line Impedance:— Before attempting to determine accurate image impedance measurements on either a single or coupled meander line, the reflections introduced by various connectors must be known. In this case, reflections were minimized by using special OSM[†] connectors with the projecting center pin flattened and its extension beyond the plane of the shell limited to 15 mils. A special plexiglass hold-down gives rigidity to the center pin. These OSM connectors, as redesigned by D. H. Temme, may be seen in place in the photograph of Fig. 36. With the best 50-ohm line available, the measured reflection coefficient of line plus connectors was 0.05 or less over the 2.0- to 4.0-GHz S-band.

A single meander line was cut from indium to the dimensions indicated in Fig. 23, the width W = 12 mils, separation S = 8 mils, and length of 257 mils for a 40-mil-thick dielectric. Sheet indium 2 mils thick was used for temporary circuits because it has low resistivity, can be readily cut, is very pliable, and will stay in place with good electrical contact without the use of adhesives. The meander line was then just pressed in place over an 8-mil gap cut in a gold-deposited 22-mil line on a substrate of magnesium titanate (K = 16). The result of the input scattering measurement showed a reflection coefficient of 0.08 or less below a frequency of 3.0 GHz and showed a tendency to cutoff by having a reflection value of 0.5 at 4.0 GHz.

Two indium meander lines were made and tightly coupled with a spacing of 8 mils. Although the second line was supposed to be identical to the first, the line was actually slightly shorter and was not exactly uniform in separation. The input scattering parameter S_{11} for this two-meander line was $\leqslant 0.16$ over the entire S-band range. The point for an indication of cutoff ($S_{11} = 0.5$) occurred at a slightly higher frequency of 5.0 GHz. The coefficient becomes 0.93 at 6 GHz, indicating definite cutoff.

2. Influence of Ferrite

The previous results were sufficiently encouraging to proceed with the design of meander lines on 40-mil-thick ferrite substrates. Ferrite material maintains good dielectric properties while at the same time exhibiting the desired ferrimagnetism necessary for the generation of differential phase shift. The ferrite chosen for these experiments was a gadolinium and aluminum-doped yttrium-iron garnet (YIG) having a magnetic saturation moment $4\pi M_s$ of 550 G.

Demagnetized Permeability:— In such a ferrite medium of infinite and unbounded extent, the application of a weak high-frequency magnetic field along with a static magnetic field produces a permeability that has the properties of a tensor. The tensor nature of the permeability relating the harmonic induction of the ferrite to the microwave field intensity was first given by Polder.[19] One diagonal term from the Polder tensor is

$$\mu = 1 - \frac{4\pi\gamma^2 MH}{\omega^2 - \gamma^2 H^2} \tag{114}$$

where γ is the gyromagnetic ratio for electron spin, $e/mc = 17.6 \times 10^6$ rad/sec/Oe, or $\gamma/2\pi =$ 2.8 MHz/sec/Oe, M is the magnetic moment, and H is the static magnetic field intensity. It is evident not only that μ can be frequency-dependent, but also that its magnitude can be <1 in an infinite medium.

---

†Trade name of Omni Spectra, Inc.

The most elementary ferrite geometry is that of the ellipsoid whose dimensions are small with respect to wavelength. If a small sample of such an ellipsoidal-shaped ferrite is immersed in a static uniform magnetic field H_{ex}, the main field induces "magnetic charges" on the ellipsoidal surface. The presence of these surface charges creates a field intensity component within the ferrite in opposition to that of the main field, thus to alter the internal field intensity. Internally, H_i is uniform and is given by

$$H_i = H_{ex} - \overleftrightarrow{N}M \tag{115}$$

where $-\overleftrightarrow{N}M$ is the demagnetizing field caused by the presence of the surface charges, $\overleftrightarrow{N}$ is the demagnetization tensor, and M is the magnetic moment of the ferrite. Even with the application of an external field H_{ex}, which is directed only along the z-direction, it is possible that the uniform internal field H_i has x and y as well as z components. If the direction of the external magnetic field is aligned with one of the principal axes of the ellipsoid, $\overleftrightarrow{N}$ becomes a diagonal tensor whose elements are demagnetization factors N_x, N_y, N_z.

In a lossless ferrite medium, with the alignment of ellipsoid coordinates such that one coordinate is coincident with the direction of the applied static field, the magnetic moment M precesses about the static magnetic field vector. The natural frequency of such a precession is given in terms of the demagnetization factors by Kittel[20] as

$$\omega_o = \gamma \left\{ [H_{ex} + (N_x - N_z) M] [H_{ex} + (N_y - N_z) M] \right\}^{1/2} \tag{116}$$

where γ is the gyromagnetic ratio for electron spin.

Normally, such a sample of ferrite would be subjected to a weak high-frequency magnetic field together with the steady field component. The presence of high-frequency field components in directions other than along the static field direction generates magnetic moments in these directions. The precessing magnetic moment influenced by the high-frequency field may be described by a tensor permeability $\overleftrightarrow{\mu}$. One of the diagonal terms of this tensor is given by

$$\mu = 1 + 4\pi \left[\frac{M}{H_{ex} + (N_x - N_z) M} \right] \Big/ \left[1 + \left(\frac{\omega}{\omega_o} \right)^2 \right] \tag{117}$$

where ω_o is given by the Kittel resonance of Eq. (116). By making this substitution, the single permeability term considered becomes

$$\mu = 1 + \frac{4\pi M \gamma^2 \cdot [H_{ex} + (N_y - N_z) M]}{\gamma^2 \left\{ [H_{ex} + (N_x - N_z) M] [H_{ex} + (N_y - N_z) M] \right\} - \omega^2} . \tag{118}$$

Aside from the fact that the expression indicates a resonance in the second term, it is evident that, even in the demagnetized state with $H_{ex} = 0$, the permeability is frequency-dependent due to the presence of the demagnetizing fields.

For a geometry different than the fundamental ellipsoid, e.g., the substrate with its magnetizing yoke, the view may be taken that the ferrite is composed of many macroscopic crystallites, each with a saturation magnetization $4\pi M_s$, but each arbitrarily directed. Now, even with a zero applied field H_{ex}, many demagnetizing field components are present and the permeability cannot easily be described without resorting to artificial schemes to make a solution tractable. Owing to the fact that the resultant permeability obtained for the infinite medium and for the

elementary geometry demonstrated a dependence on frequency, it is recognized that μ for any geometry would have this property. It is also evident that μ can be < 1 even in the demagnetized state.

The effect of frequency on the demagnetized μ for the particular G500 ferrite material used in these experiments is illustrated in Fig. 24. These data[†] were obtained from measurements on straight-line and circular resonators.
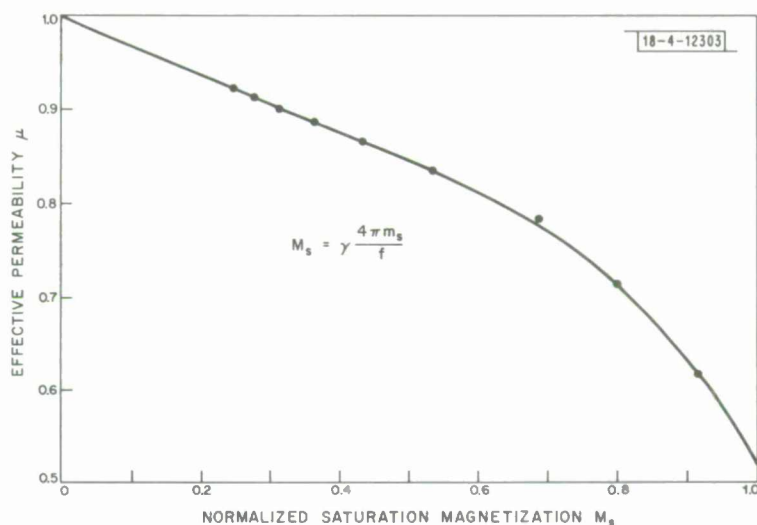
Fig. 24. Curve af effective permeability vs normolized saturatian magnetizotion far a micrastrip line on demognetized ferrite substrate.

Expected SWR:– Because of this low-frequency effect in the demagnetized ferrite, standing-wave ratio measurements made over S-band with this material would be expected to vary from 1 to 1.1. This is assuming, of course, that everything else is perfectly matched.

Theoretical Impedance Curves:– Utilizing such a frequency-dependent μ,[†] as shown in Fig. 24, and the data on even- and odd-mode velocities from the Weiss and Bryant[17] analysis, calculations may now be made with Eqs. (110) and (113) for the image impedance and insertion phase of a meander line deposited on a ferrite substrate.

Figure 25 shows the theoretical results computed for frequencies in L-, S-, and C-bands sufficient to show the bandpass characteristic of the meander line. Evident in the figure is a severe drop in image impedance caused by the changing permeability of the ferrite. The width-to-height ratio W/H is selected to provide an impedance of approximately 50 ohms near the 3.0 GHz point. The dashed curves are intended to illustrate the effect of not taking the changing velocity into account. In this case, as in the previous calculations, the length l is chosen so that $\beta_e l$ is $\pi/2$ at 4.0 GHz.

Permeability in Latched State:– In practice, the ferrite will not be demagnetized, but rather will be latched in one of its two remanent states with a zero applied magnetic field. This extra complexity arises both by the mechanism of creating the necessary differential phase and by the requirement that the test model have two switchable states. The effect of such a

---

[†] The data are reproduced with permission from E. J. Denlinger of the Lincoln Laboratory staff.
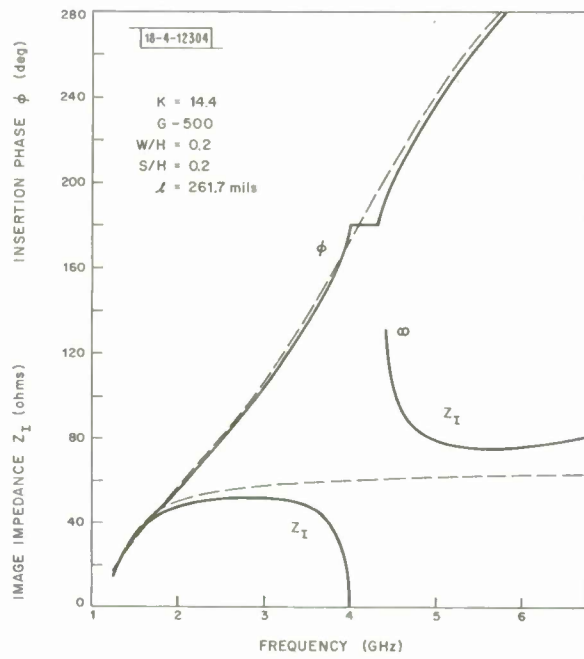
Fig. 25. Theoretical image impedance and insertion phase of a microstrip meander line on demagnetized ferrite (G500) substrate.

Fig. 26. Spatial configuration used in deriving requirements for magnetic field circular polarization.
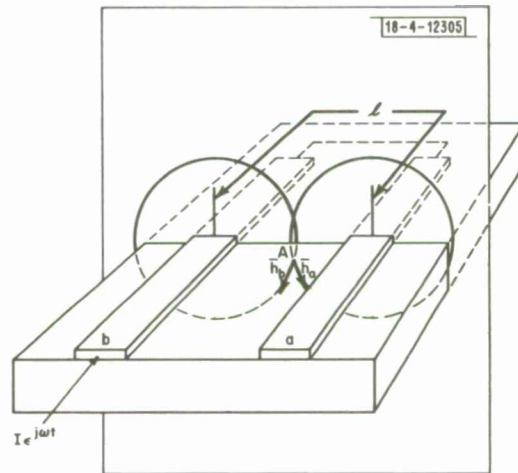
latching state on the permeability is unknown, so it was decided on further calculations to utilize the arithmetic mean between the projected completely demagnetized permeability and unity.

Field Interaction for Differential Phase:— Figure 26 shows the spatial configuration of two magnetic field vectors $\bar{h}_a$ and $\bar{h}_b$ under a single meander line. Point A represents a location where $\bar{h}_a$ and $\bar{h}_b$ are in space quadrature. The quadrature directions are identified by unit vectors $\bar{i}_a$ and $\bar{i}_b$. The effective propagating magnetic field at point A is given in complex exponential form by

$$H_A = (\bar{i}_a h_a + \bar{i}_b h_b)\, \epsilon^{-j\beta x} \quad . \tag{119}$$

If now h_b can be related to h_a in time quadrature such that $h_b = -jh_a$, then

$$H_A = (\bar{i}_a h_a - j\bar{i}_b h_a)\, \epsilon^{-j\beta x} \tag{120}$$

and the resulting instantaneous magnetic field is

$$h = \mathrm{Re}\, H_A \epsilon^{j\omega t} = \bar{i}_a h_a \cos(\omega t - \beta x) + \bar{i}_b h_a \sin(\omega t - \beta x) \quad . \tag{121}$$

The indicated space and time quadratures provide for circular polarization of the magnetic field.

It should be observed that the needed time quadrature may easily be obtained by making the meander path length ℓ a quarter-wavelength. In the ferrite-filled space under a meander line, the actual polarization will vary from linear at the ends through elliptical to circular at the mid-plane.

If a steady internal magnetic field H_i is present in a direction indicated along the meander line, the magnetic moments in the ferrite will precess in a circular orbit about the vector H_i, that is to say, in coincidence with or opposite the signal circular polarization just established. Such coincidence produces strong coupling for signals propagating, say, from left to right, but very weak coupling for propagation in the opposite sense. This is an aid to phase delay for propagation in one direction, and an opposition to phase delay for propagation in reverse. This kind of coupling produces the desired differential phase. Such an interaction has not yet been analyzed; thus, there is no known direct way with which to calculate the differential phase factor δ — it must be determined experimentally.

Two Meander Lines on G500 Ferrite:— Since interest was in utilizing a small amount of differential phase shift, it was decided to determine experimentally just how much differential phase would be possible using only two coupled meander lines deposited on ferrite.

In order to have a 50-ohm single microstrip line feeding the meander line at 3 GHz, the width of the strip must be selected with due regard for the permeability of the ferrite while in the latched state. By using the approximation of $1/2(1 + \mu_{demag})$, the permeability becomes $1/2(1 + 0.84) = 0.92$. The impedance will be degraded by $\sqrt{\mu}$; so, the dimension W should be selected from the Weiss-Bryant data for ferrite (K = 14.4) to produce a 52.1-ohm line. For this condition, W/H is 0.5975, or, on a 40-mil substrate, the line width should be 23.9 mils.

For the meander line itself, the spacing was selected as 8 mils to provide close coupling with a ratio S/H = 0.2. Selecting a W/H of 0.3 resulted in a calculated image impedance of 51.4 ohms at 3 GHz. The length of the meander legs (250 mils) was selected to give $\beta_e \ell = \pi/2$ at the band limit of 4 GHz. With the order of the approximations involved, it was felt that 51.4 ohms was close enough for a first attempt.

49
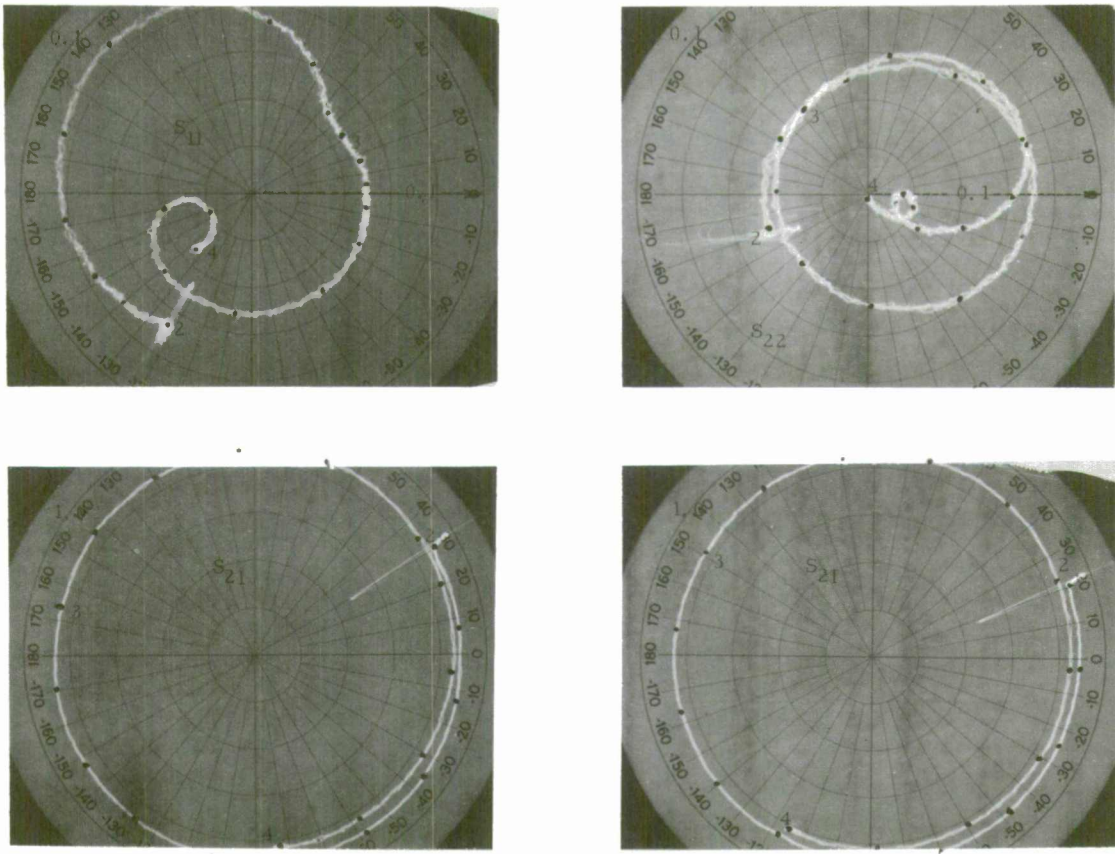
Fig. 27.   Polar display of complex reflection coefficients and transmission coefficients for two-meander, chrome-gold line on G500 ferrite.   Graphs are swept from 2 to 4 GHz.
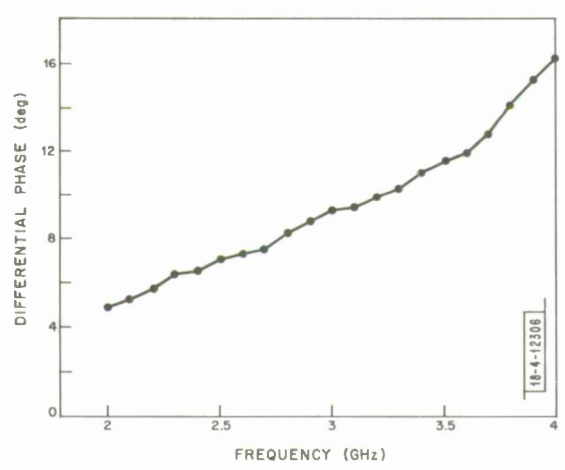
Fig. 28.   Curve of differential phase shift vs frequency for two-meander, chrome-gold line on G500 ferrite.

Measurements:— Experience with indium lines on ferrite indicated the optimum width to be 22 rather than 23.9 mils for straight lines. A part of this discrepancy may be attributed to the fact that the thickness of the conducting strip was not considered. Caulton, et al.,[21] developed an approximate relation for such a thickness correction. With a deposited strip thickness of 0.3 mil, the width correction amounts to slightly less than 0.7 mil.

Because of inaccuracies in the involved printing process and in the etching process, the deposited meander line had dimensions quite different from the expected 12-mil lines with 8-mil spacings. The meander leg widths varied from 10.50 to 9.63 mils, the average being only 10.13 mils. On the other hand, spacing was increased to an average 9.36 mils with a variation about this average value of ±0.44 mil. The width of the straight feed line was reduced to 20.67 mils. All deposited conducting strips had a thickness of 0.354 mil.

The set of measured scattering parameters for this experimental meander line is shown in Fig. 27, where frequency intervals of 0.1 GHz are marked with dots along the graphs; these data show the largest reflection coefficient of S_{11} to be 0.087 and that of S_{22} to be 0.071. In both of these views, the scale has been expanded to a reflection of 0.1 full scale. It is doubtful that further adjustment of line width or meander-line width would show a startling improvement with the order of reflections from the connectors involved. The line did show cutoff at 5.25 GHz. Also shown in Fig. 27 is the transmission coefficient S_{21} for the two latched directions of magnetization, thus to illustrate and be able to measure the differential phase. Although the S_{12} measurements are not shown, they were within experimental error of 1° from the measurements of S_{21}, but, of course, with the latching reversed.

A very careful measurement of the differential phase possible at the various frequencies of S-band was made on this same experimental meander line. The data are shown in Fig. 28. By taking measurements on a straight 22-mil-wide line, deposited on the same substrate, the insertion phase of the meander alone was obtained. Figure 29 shows the result of these measurements from lines on the G500 substrate.
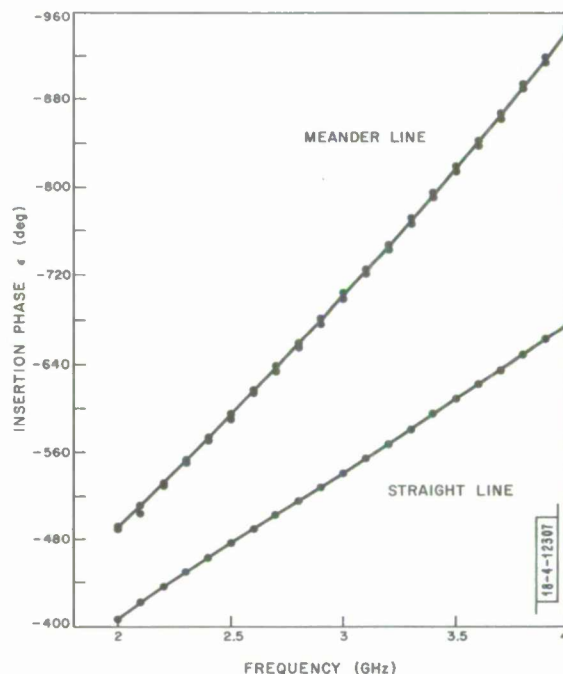
Fig. 29. Curves of insertion phase vs frequency for line with two meanders and straight line both on 2-inch ferrite G500 substrate.

51
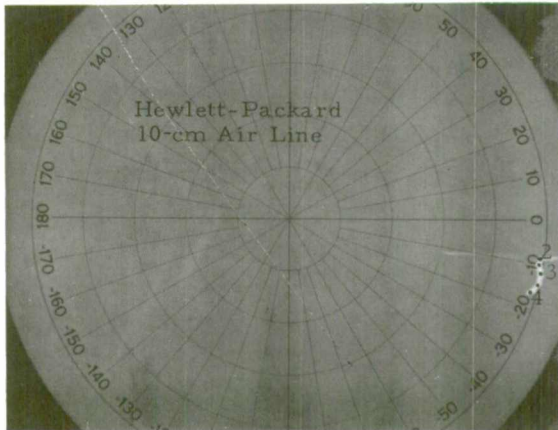
Fig. 30. Polar display of phase correction to be added to all transmission coefficient measurements. Curve is shown swept from 2 to 4 GHz.
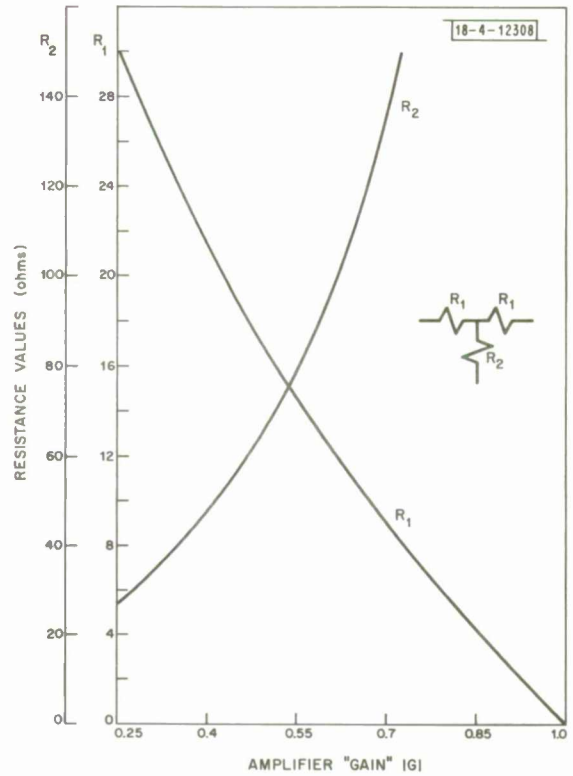
Fig. 31. Resistance values for T networks with various "gains."
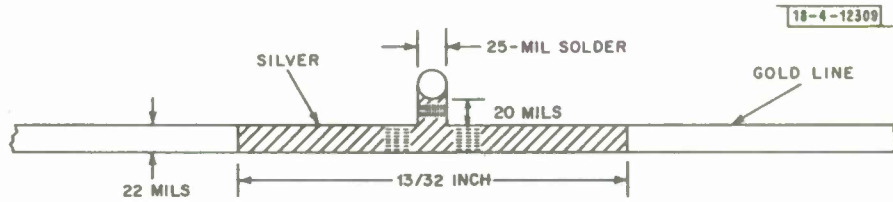
Fig. 32. Enlarged diagram of experimental bilateral attenuator.

In measuring the transmission parameters with the Network Analyzer, great care was taken to balance out the insertion phase of adapters, OSM connectors, and line extenders, to give measurements on the substrate circuit alone. Figure 30 shows the only remaining phase correction that must be added to all insertion measurements, that of a Hewlett-Packard 10-cm length of air line.

B. Bilateral Microstrip Attenuator

A bilateral matched attenuator must be realizable in microstrip form prior to initiating the final design of the differential attenuator model. It would be desirable to have some simple structure like a T or Π network with as few elements as possible. Unfortunately, no commercial units are available yet for the microstrip transmission system. Thin-film resistors are available, but, for this application, they must be made to order with deposited silver-strip contacts to be useful. Even these elements are not available in dimensions suitable for microstrip work.

1. Range of Attenuation Needed

A survey of Fig. 4 shows the range of $|G|$ needed for the differential attenuator model to be from 0.27 to 0.92, inclusive. The values of series and shunt resistances required to realize a simple T network are shown in Fig. 31 as a function of the attenuation factor $|G|$. Since resistors of these values are not available in small size, it was decided to make them.

2. Technique of Silver-Sprayed Resistors

An experimental procedure being investigated in the laboratory consists of spraying silver paint on substrates to achieve the microstrip transmission line. Such a sprayed line is susceptible to variations caused by the thickness of the deposition, and at present is considered lossy. It was decided to attempt to realize the necessary resistances by spraying a short section of line and then scraping off a sufficient amount of silver, increasing the resistance to the value desired.

Figure 32 shows an enlarged view of the experimental attenuator. The ground post was a piece of 25-mil solder pushed into a 25-mil hole and soldered to the substrate (magnesium titanate) ground plane. The choice of resistance values was $R_1 = 15.5$ and $R_2 = 72$ ohms. The actual values scraped were 13 and 72 ohms. An ohmmeter was simply connected across the appropriate terminals and the scraping performed until the proper value was acquired.

3. Experimental Results

Figure 33 shows the scattering parameters of this experimental bilateral attenuator. The reflection coefficients are less than 0.2 over the entire S-band. It is felt that if the resistors could be closer together, using shorter sprayed sections, the reflection might be reduced still further. The transmission parameter shows an attenuation of exactly 6 dB over the lower part of S-band and an increase of about 1 dB at the top near 4 GHz. Certainly, the presence of the ground post so near the line plus the layer of silver adds some inductance into the circuit which could cause such a variation.

C. Differential Attenuator Model

The design of the model may now be undertaken knowing that a meander line giving the desired differential phase is possible, and a bilateral attenuator with reasonable resistance values is realizable. Inasmuch as the preference in this case is to show a realization based on small differential phase, the choices of ϵ, G magnitude, and the argument of G are to be made with

S_{11}: scole 0.2 at auter circle.
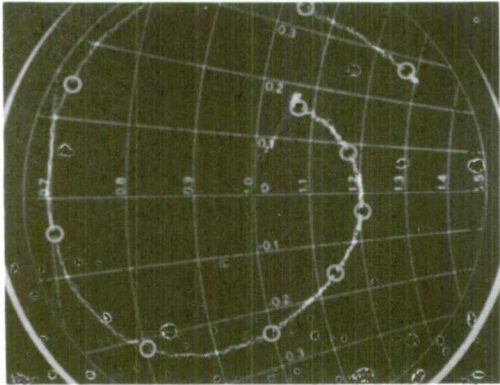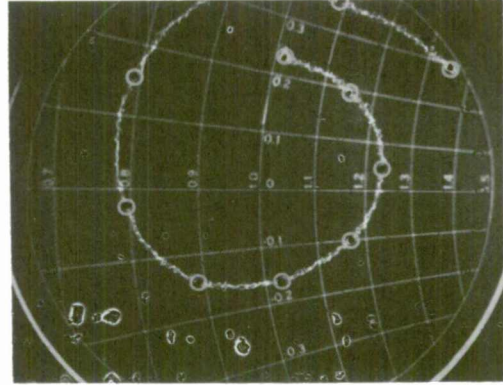
S_{22}: scale 0.2 at outer circle.
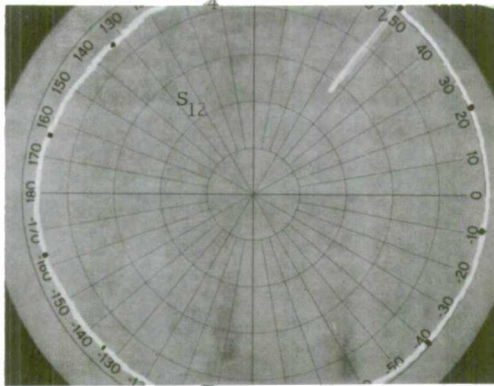
S_{12} calibrated to 6.0-dB attenuation at outer circle.

Fig. 33.   Polar display of complex reflection ond transmissian caefficients of bilateral attenuotor on dielectric substrate.   Graphs are swept from 2 ta 4 GHz.

this in mind. Actually, the choice of δ and ϵ fixes the complex value of G required for a match since

$$G(I) = f(\epsilon, \delta) \quad . \tag{122}$$

1. Proper Phase Lengths

Figure 28 showed the amount of differential phase possible with the meander line operating near 3 GHz to be approximately 10°. Thus, the frequency of operation was chosen as 3.25 GHz where the differential phase shift is exactly 10°. The selection of frequency allowed all phase lengths to be determined.

The value of the insertion phase ϵ for the differential phase unit was chosen as 45°. This selection was made in keeping with a reasonably large ratio of S_{21}/S_{12} at $\delta = 10°$, as may be seen in Fig. 10. It is also in keeping with a required attenuation "$|G|$" that would be practical to make with the scraped-down silver-line technique.

Reference to Fig. 29 shows that the meander line alone at 3.25 GHz presents $754.75 - 573.23$ or $181.52°$ of phase delay; consequently, ϵ must be raised to $45 + 360 = 405°$. The total electrical length of lines feeding the meander from the two symmetrical scattering junctions must be restricted to $405 - 181.52$ or $223.48°$. Since the single-line phase of $573.23°$ was obtained at 3.25 GHz on an exact 2.0-inch length of substrate, a simple ratio suffices to show the length of the feed line to be

$$\frac{2000}{Y} = \frac{573.23}{223.48} \tag{123}$$

or

$$Y = 779.7 \, \text{mils} \quad . \tag{124}$$

With the selection of $\delta = 10°$ and $\epsilon = 45°$, the complex G required of the bilateral attenuator is fixed. Reference to Fig. 5 shows the required insertion phase of the attenuator to be $+26.57°$. Thus, the phase delay through the attenuator path must be $-333.43°$. A simple ratio will again suffice to show the required total length of the attenuator legs from scattering junction to scattering junction to be

$$\frac{2000}{X} = \frac{573.23}{333.43} \tag{125}$$

or

$$X = 1163.3 \, \text{mils} \quad . \tag{126}$$

Figure 34 summarizes the design so far by showing schematically the layout of the final matched differential attenuator model with all dimensions.

2. Attenuator Resistances

The magnitude of G required for the chosen δ and ϵ is 0.5. It may be determined from Fig. 31 that the series resistances of the silver-painted line must each be 16.7 ohms, and the shunt resistance to the ground pin must be 66.7 ohms to provide the proper bilateral loss.

3. Construction Details

Following is a brief description of just how the integrated microwave circuit was formed on the ferrite substrate.
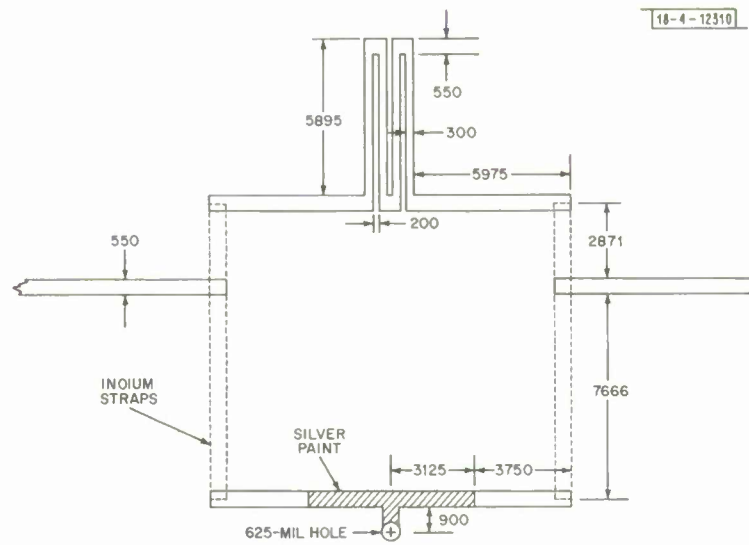
Fig. 34. Layout of differential attenuator model as cut from a Rubylith; all dimensions are in mils magnified by 25.
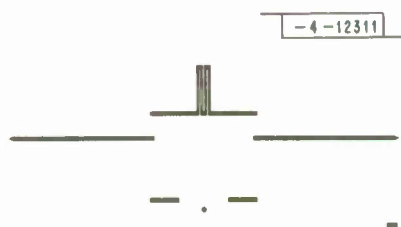
Fig. 35. Photo-etch positive master of differential attenuator model; actual size.
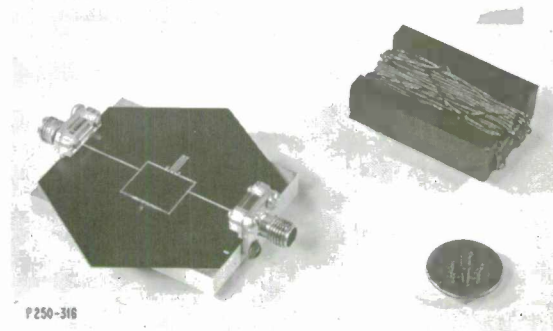
Fig. 36. Microstrip differential attenuator shown with microstrip latching yoke.

56

The layout of Fig. 34 was cut from a Rubylith with a 25-to-1 magnification of dimensions in order to make such a hand-cutting process tractable. The diagram was then photoreduced to a glass plate, which served as the final contact negative. A contact print of this plate is shown in Fig. 35.

A 2-inch hexagonal substrate of gadolinium and aluminum-doped YIG 40 mils thick was prepared for photo-etching. First, a layer a few angstroms thick of chromium and then gold was evaporated on the two flat surfaces, the chromium to form a good bond between the ferrite and gold. Each surface was then plated with gold to a 0.3-mil thickness which is several skin depths at S-band. A photo resist was then spun on one of the gold surfaces and baked ready for exposure. After the contact negative exposure (two minutes) and development, the excess gold was chemically etched away and then the chromium, leaving the desired circuit with a gold ground plane beneath.

A 25-mil hole was drilled through the brittle ferrite and filled with silver epoxy, thus forming a conducting post to the ground plane. Finally, after masking off the rest of the circuit, a layer of silver paint was sprayed over the area of the attenuator resistors.

It was necessary to use indium straps on the sides rather than print the entire circuit, due to the fact that there might be reason to test each branch of the circuit separately. Also, it was necessary to open the circuit at some point so that conductivity through the attenuator section alone existed for the scraping of resistors.

The finished product may be seen in the photograph of Fig. 36, where also shown is the latching yoke which was actually placed beneath the substrate when operating in order not to interfere with either the meander line or the silver resistors.

4. Measured Scattering Parameters

A microscopic examination of the final circuit shows all dimensions to be approximately 1.5-percent low. This uniform change in dimension is undoubtedly due to undercutting in the etching process. Such small changes probably affect only the phase lengths of the various circuit arms and probably would not seriously affect the overall scattering parameters. Measurement with the microscope also revealed the thickness of the gold-deposited lines to be 0.354 mil.

Meander-Line Branch:— Inaccuracies in the final dimensions of the meander line are attributed to the cutting of the Rubylith. The several meander leg widths vary from 11.6 to 12.15 mils, with an average of 11.83 mils. Spacing between the legs varies from 7.28 to 7.88 mils, the average being 7.52 mils. The fact that these dimensions are close to the desired 12-mil legs with an 8-mil spacing is due to the 25:1 magnification used in preparing the Rubylith. The first experimental meander line referred to on p. 51 was obtained from a Rubylith with only a 10:1 magnification.

It was experimentally determined that this second meander line produced 10° of differential phase at a frequency slightly below 3.2 GHz with the ferrite magnetization latched in its two remanence states. Based on the first meander line, the 10° differential phase shift was predicted to occur at 3.25 GHz. Such a difference was probably due to the different spacing and the different leg widths of the two experimental meander lines which affected the generation of the differential phase.

Two methods were used to control the differential phase shift at 3.2 GHz. First, a 5-A current pulse flowing through the 26-turn coil wound on the ferrite yoke was more than sufficient to latch the ferrite magnetization in one of its two remanence states, thus producing 10° of
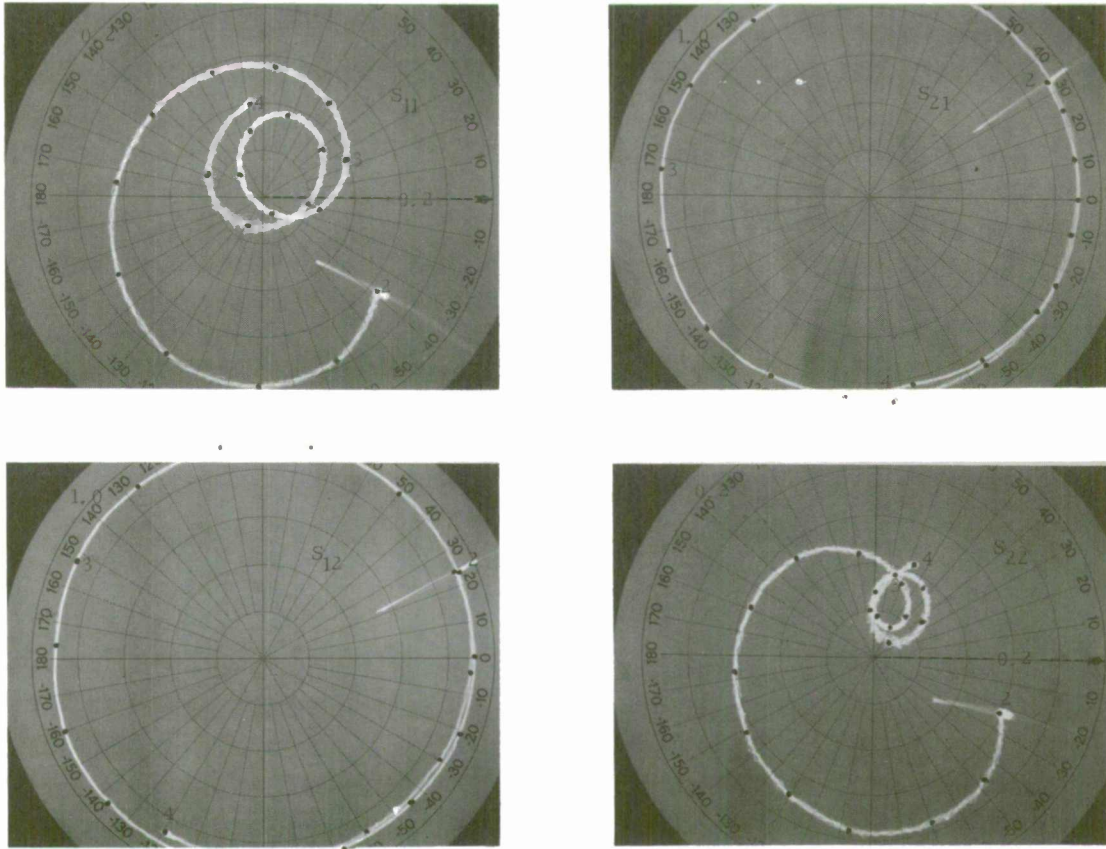
Fig. 37.   Polar display of complex reflection and transmission coefficients of meander-line section of differential attenuator.   Graphs are shown swept from 2 to 4 GHz.

differential phase. Second, a continuous current flow of limited amperage was employed to produce smaller amounts of differential phase shift. It was determined that a 0.2-A current, when switched, could generate 6° of differential phase shift. A 0.26-A current was required to produce 8° of differential phase.

Since the physical dimensions of this meander line were quite different from those of the first experimental line described on p. 51, it would be expected that the impedance also would be subject to change. Actually, the impedance match with this line was not nearly as good. An attempt was made to improve the match by attaching two stubs, each 20 mils in length, to the meander-line branch. The match further improved by using 17-mil-wide indium side straps to connect the meander line to the 21.7-mil feed lines. Approximately 3 mils of the indicated reduction in dimension from the 21.7-mil size are needed to correct for the 2.2-mil thickness of the indium. The remaining decrease in width means the characteristic impedance of the indium straps is 51 or 52 ohms. Thus, the side straps are providing some transforming action between the mismatched meander line and the 50-ohm feed lines.

Figure 37 shows the complete set of meander-line scattering parameters measured with a Hewlett-Packard Network Analyzer which offers a very convenient way to measure such scattering parameters directly and continuously over an octave band of frequencies. This particular unit measures the phase angle and magnitude ratio of two signals: a test signal and a reference signal. By converting these test and reference signals to deflection signals, a dynamic polar display of both phase and amplitude information of a reflection or transmission coefficient is presented. For reflection measurements, the incident and reflected signals of the device being tested are, respectively, the reference and test signals. For transmission measurements, the analyzer splits an input signal, allowing the test signal alone to pass through the device being tested. Referring to Fig. 37, it should be noted both the reflection coefficients S_{11} and S_{22} are shown with an expanded scale of 0.2 maximum. It is further noted that the final matching is fairly good, for the clustered points defining the reflection coefficients S_{11} or S_{22} are each equal to or less than a value of 0.08 in the frequency range of 3 to 4 GHz. On the other hand, the transmission coefficients S_{12} and S_{21} are nearly of unit magnitude. By the fact that these coefficients are not equal to 1, some small transmission loss is indicated. This measured loss is less than a decibel and shows a slight increase at the high end of the band.

Bilateral Attenuator Branch:— In contrast to the predicted resistance values shown in Fig. 31 for a bilateral attenuator to present a "gain" of 0.5, the experimentally determined best values were as follows: R_{series} = 11.1 ohms, R_{shunt} = 71.15 ohms. These values were obtained by adjusting DC resistances to give the best impedance match while keeping the gain at 0.5. The discrepancy between the best value of series resistance and the theoretical value of 16 ohms was probably caused by a combination of skin effect and the fact that the relatively thick layer of silver paint would introduce inductance into the circuit. The shunt resistance DC value is higher than the theoretical 66 ohms, for this element is subject not only to skin effect but also to a bypass capacitance to the ground plane which effectively lowers the resistance.

Shortening the physical dimension of the series resistance from 15/64 inch on the first model to 1/8 inch produced a noticeable improvement in matching to begin with over most of the frequency band. It was determined by experiment that connecting side straps of indium only 14 mils wide reduced the reflection coefficient still further. Such narrow side straps connecting the attenuator to the feed lines act as quarter-wave transformers over that portion of the frequency band near 3.5 GHz, where the 300-mil strap length is a quarter-wavelength. The set of measured
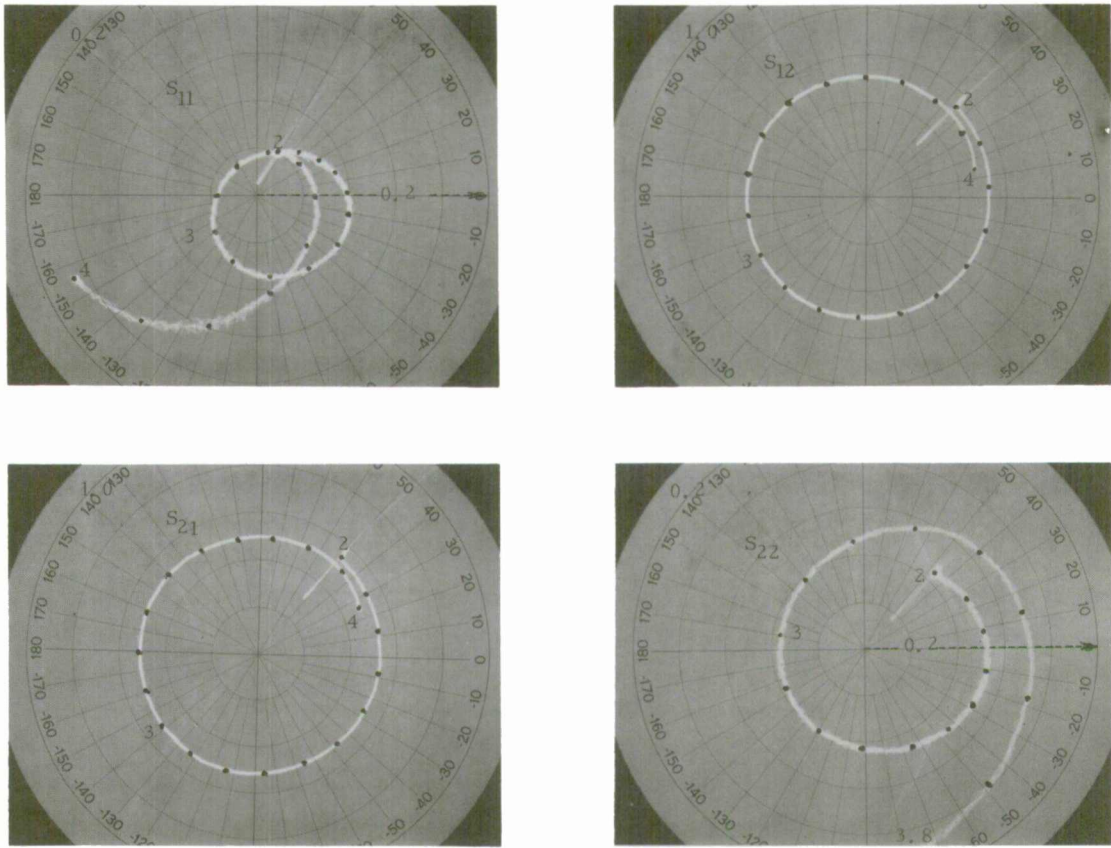
Fig. 38. Polar display of complex reflection and transmission coefficients of bilateral attenuator section from differential attenuator. Graphs are shown swept from 2 to 4 GHz.

scattering parameters for the attenuator section is shown in Fig. 38, where both S_{11} and S_{22} are recorded on a scale expanded to 0.2 maximum. The final match shown is superior to that obtained with the first bilateral attenuator described on p. 53, having the characteristics shown in Fig. 33.

The measured transmission parameters S_{12} and S_{21}, also illustrated in Fig. 38, show a value of transmission gain of 0.51 over the frequency range of interest. This is to be compared with the needed theoretical value of 0.50.

Complete Differential Attenuator:— Figure 39 shows the overall scattering parameters for the complete differential attenuator. The overall reflection coefficient parameter S_{11} indicates that an excellent match exists at a frequency of 3.275 GHz. A value of 0.02 was actually measured at this frequency, which demonstrates the fact that the differential attenuator can be designed to have a matched input at the operating frequency. The overall match at this frequency is not quite as good for transmission in the reverse direction indicated by the S_{22} reflection coefficient data. Presumably, this is caused by the poorer match provided by the bilateral attenuator branch in this transmission direction. The Smith Chart graticule overlay is used in displaying S_{22} merely to show what standing-wave ratio might be expected on a 50-ohm line feeding the differential attenuator. It is estimated that such a standing-wave ratio would be 1.3 at 3.275 GHz. Other than the difference in reflection coefficients noted near the 3.2-GHz frequency, the data display similar reflection characteristics at the two ports of the differential attenuator.

Both the transmission coefficients S_{12} and S_{21}, shown in Fig. 39, display the desired nonreciprocity. Each parameter is shown with the ferrite magnetization latched in both of its two remanent states. Observe from the pair of curves defining S_{12} that the curve with the pronounced dent was obtained as a result of an applied magnetic field directed along the meander line pointing away from the bilateral attenuator. The smoother curve without the severe dent shown in S_{21} was obtained with exactly the same direction of magnetization. The maximum nonreciprocity seems to occur at a frequency slightly below 3.2 GHz, where the differential phase shift was exactly 10°. The fact that such a peak does not occur closer to the design frequency is due collectively to the slight uniform changes in dimensions, the nonperfect match of elements which required the use of reactive stubs on the critical phase-shift branch, and especially the fact that the meander line itself is quite different from the first experimental model on which the design was based.

The measured differential loss given in decibels as a function of frequency is shown in Fig. 40. Data for these curves were read from the curves of the scattering parameters S_{12} and S_{21} of Fig. 39, and from similar curves taken when limiting the differential phase shift to 6° and 8°, respectively. These data were then converted to the desired decibel transmission loss. The theoretical differential loss maximum was predicted to be 3.0 dB at 3.25 GHz, while the actual loss obtained would be nearer 2.5 dB at 3.175 GHz. No account was taken of small losses either in the ferrite or along the deposited lines. Losses along the deposited lines are expected to be negligible; however, losses in the ferrite medium are different for the two directions of transmission through the device, and could contribute to a change in the differential loss expected.

The difference between similar shaped curves defining the transmission parameters S_{12} and S_{21}, as indicated in Fig. 39, is to be observed. Although there seems to be approximately a 5° difference in phase of one parameter compared with the other, the difference in magnitude of the two parameters is negligible at a given frequency. This demonstrates that the amplitude
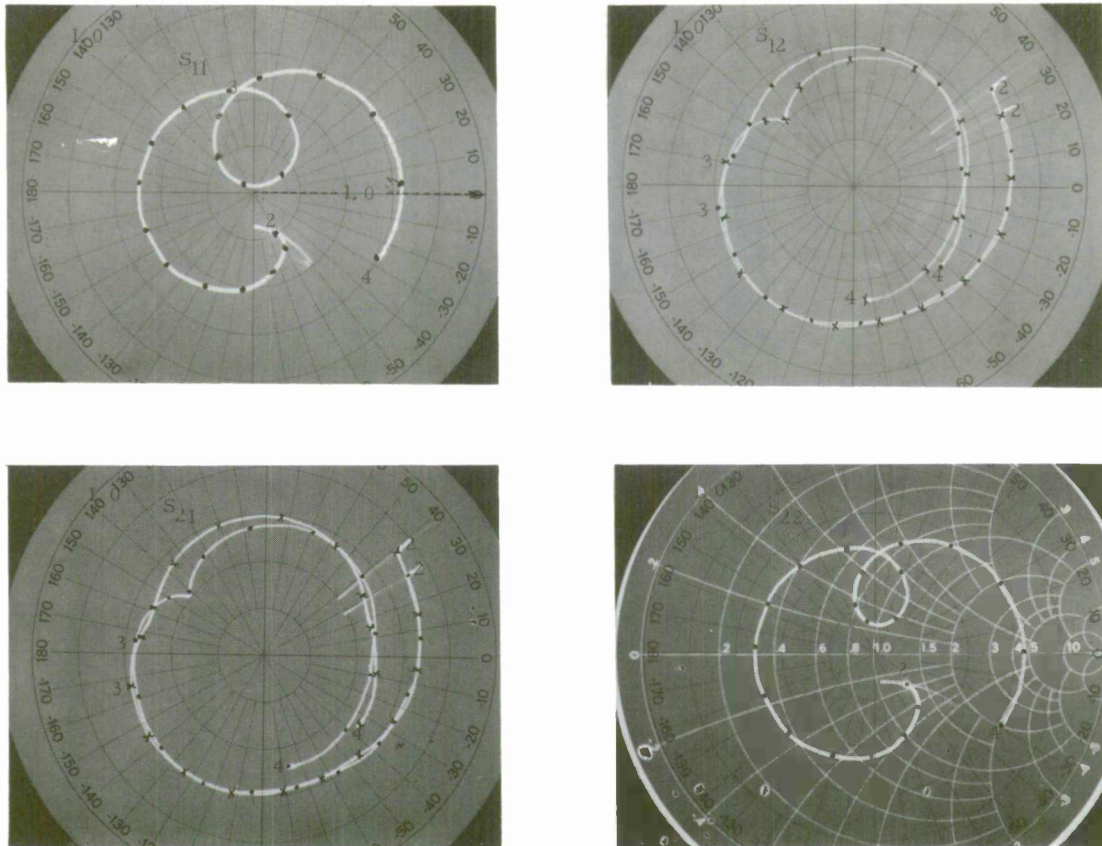
Fig. 39.   Polar display of complex scattering coefficients for differential attenuator.   Graphs are shown swept from 2 to 4 GHz.
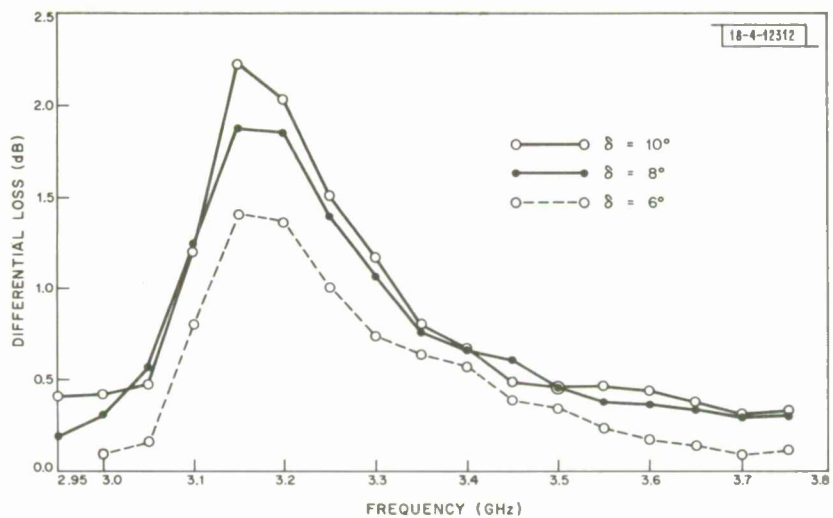
Fig. 40.   Curves of differential loss in decibels vs frequency for differential attenuator with 6°, 8°, and 10° of differential phase shift.
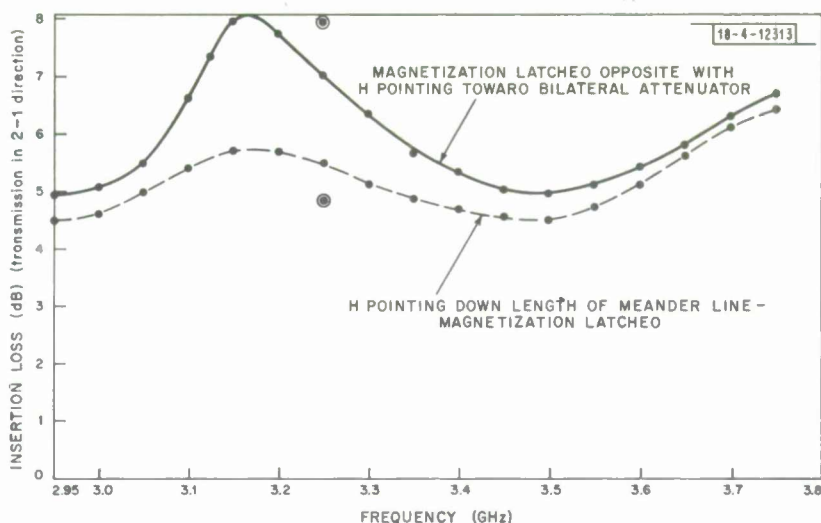
Fig. 41. Differential attenuator insertion loss vs frequency with ferrite magnetization latched in both remanent states.

nonreciprocity is symmetrical; however, there is a small amount of residual differential phase shift present. Data from the curves of S_{12} alone were used to illustrate the insertion loss of the differential attenuator model at various frequencies in S-band. This loss is shown for the two latched states in Fig. 41. The two encircled points at the 3.25-GHz design frequency are included to represent the theoretical loss predicted by the computer solution. A comparison shows the loss in one latched state to be the value expected, while the loss in the other latched state is approximately 0.5 dB high. Thus, the measured performance of the model agrees within reasonable error with the predicted performance.

IV. CONCLUSIONS

This final section is devoted to the conclusions drawn from both the theoretical development and the experimental work of this investigation. Also discussed here are areas for further investigation which seem to be promising in light of the work thus far accomplished.

The theoretical development of active nonreciprocal two-port networks of potentially periodic structure, which was presented in Sec. II, has shown conclusively that forward-to-backward amplitude nonreciprocity is possible. Furthermore, such nonreciprocity may be achieved with a relatively simple configuration. At least some degree of nonreciprocal gain may be achieved by the proper interconnection of an active negative resistance device and a passive element exhibiting but a small amount of differential phase shift.

The desired amplitude nonreciprocity cannot be attained with a tandem connection of the active device, the differential phase-shift element, and various lossless scattering obstacles. Accordingly, to have amplitude nonreciprocity at all with the cascade connection, one or more of the individual devices cascaded must possess the nonreciprocity. On the other hand, the parallel-parallel connection, utilizing two scattering junctions with which to interconnect the active device and the differential phase-shift element, does provide for nonreciprocal amplitudes. Although the basic analysis of the parallel-parallel connection utilized symmetrical scattering junctions, the conclusion is that any scattering junction will work with but one exception — that of a pair of perfectly balanced junctions matched to both the active device and to the differential phase-shift device. With the use of such balanced junctions matched, no amplitude nonreciprocity is ever

63

possible. It is further concluded that the active negative resistance device need not have an input impedance to match the impedance of that branch of the circuit in which it is used. Moreover, it is possible to select the characteristics of such an active device, together with the characteristics of the phase-shift device, so that the parallel-parallel connected differential gain configuration presents a matched input and output at the chosen operating frequency.

In order to realize the differential amplifier, projected by the theory, a two-port amplifying device is required giving the same amplification in both conductive directions. Additional research is needed to determine how an active element such as a tunnel or an avalanche diode may be simply integrated with other microstrip components to achieve such an amplifying device. If a reflection-type tunnel-diode amplifier is desired, some form of scattering junction must be specified which, when connected to the tunnel diode, forms a physically symmetrical two-port device. Because of the fact that the active negative resistance is unstable, some simple stabilizing network must also be specified which would be much easier to realize as a series type in the microstrip system, minimizing the need for shunting through the substrate material to the ground plane. Finally, a circuit must be designed with which to terminate the tunnel diode at all frequencies outside the desired operating band.

As far as the differential phase-shift element alone is concerned, it is concluded that a single meander line can be designed quite easily to present a desired impedance by using the bandpass characteristic equations derived, and the even- and odd-mode velocities from the theory of coupled microstrips. The experimental results of Sec. III clearly verify these designs. It is demonstrated that the minimum practical amount of differential phase shift required is such that a line with two meanders is needed. Therefore, a need does exist for additional information on the exact effect that more than one coupling has on the impedance of a conducting strip. Only when this information on multi-coupled strips is available will it be possible to design meander lines of several meanders without resorting to some trial and error.

Having once determined the impedance characteristic, it then would be desirable to be able to predict accurately the number of meanders necessary for a required differential phase shift at a given frequency. This requires information not presently available. Precise design information on differential phase per meander would probably depend upon such factors as substrate thickness, ferrite material characteristics, meander-line separation, and meander-leg length.

The theory of Sec. II showed that nonreciprocal loss could be achieved very simply by interconnecting a bilateral attenuator with a device exhibiting differential phase. It was possible to construct such a differential attenuator, described in Sec. III, that realized both the desired matched input impedance and the desired nonreciprocity while still utilizing a minimum amount of differential phase shift from a meander line. It is concluded that the very close agreement between measured results and theoretical results serves to fully substantiate the theory.

In the construction of the bilateral attenuator device, it was concluded that small resistance values such as those required for series arms of a T configuration could easily be made by scraping a silver-deposited line. It is recommended that, in the future, these silver-deposit resistors be even smaller in physical dimension than those utilized in the first model. Great difficulty was encountered in realizing the relatively high resistance for the shunt arm of the T network by scraping the silver paint. It is therefore recommended that such resistances of values much greater than 10 ohms be made by some other technique.

An important extension of the differential attenuator concept is that of the isolator. Theory predicts such an isolator to be possible, giving upwards of 40 dB of differential loss with an

64

insertion loss in the direction of least attenuation of only 3 dB. To achieve this operation requires a differential phase shift of approximately 35°. It is estimated that a line of at least six meanders could produce this amount of phase shift at a frequency near 3 GHz. Of course, no theoretical estimate of bandwidth has been calculated for this device.

It was demonstrated that the transmission characteristics of the simple parallel configuration, including the forward-to-backward gain or loss, could be interchanged by the simple expedient of latching the magnetic state of the ferrite in the reverse direction. This switching of nonreciprocity is clearly illustrated in the transmission characteristic measurements made on the differential attenuator model.

Questions that have not been considered in the present initial investigation, but which are certainly important to microwave transmission, include those of power-handling capacity, bandwidth, and especially noise figure. Moreover, the incidental losses, characteristic of these projected differential devices, will only be really known when each device has been realized and tested.

In conclusion, then, it should be observed that this report describes a way of achieving amplitude nonreciprocity at microwave frequencies which is both simpler than existing methods and alternate to presently employed techniques. This simple straightforward design, derived from active network theory, can exhibit a degree of unidirectional and switchable gain or loss using relatively small amounts of differential phase. The realized microstrip differential attenuator model demonstrated the practicality of nonreciprocal devices based on such a design. Thus, the objectives of this research endeavor have been achieved.

REFERENCES

1. K. L. Su, Active Network Synthesis (McGraw-Hill, New York, 1965).

2. H. J. Carlin and A. B. Giordano, Network Theory: An Introduction to Reciprocal and Nonreciprocal Circuits (Prentice-Hall, Inc., New York, 1964).

3. H. J. Carlin, "Synthesis of Nonreciprocal Networks," in Proceedings of Symposium on Modern Network Synthesis, Vol. 5, MRI Symposia Series (Polytechnic Institute of Brooklyn, New York, 1955).

4. _____, "On the Physical Realizability of Linear Non-Reciprocal Networks," Proc. IRE 43, No. 5, 608 (1955).

5. _____, "Theory and Application of Gyrator Networks," Report No. R-355-53, PIB-289, Rome Air Development Center (March 1954).

6. R. J. Wenzel, "Design of TEM Microwave Filters Using Modern Network Theory," Bendix Corporation, Research Laboratory Division, Southfield, Michigan (14 May 1963).

7. H. A. Hair and G. T. Roome, "Thin Ferrites for Integrated Microwave Devices," 2nd Quarterly Technical Report (covering 1 January through 31 March 1966), Syracuse University Research Corporation, Special Projects Laboratory, Syracuse, New York.

8. J. B. Gunn, "Instabilities of Current in III-V Semiconductors," IBM J. Res. Develop. 8, No. 2, 141 (1964).

9. W. T. Read, "A Proposed High-Frequency Negative Resistance Diode," Bell System Tech. J. 37, No. 2, 401 (1958).

10. J. A. Copeland, "L.S.A. Oscillator Diode Theory," J. Appl. Phys. 38, 3096 (1967).

11. H. S. Sommers, Jr., "Tunnel Diodes as High-Frequency Devices," Proc. IRE 47, 1201 (1959).

12. G. Gibbons and R. E. Davis, "A Beam-Lead Planar Ge Esaki Diode," Proc. IEEE (Correspondence) 54, 814 (1966).

13. L. Esaki, "New Phenomenon in Narrow Ge p-n Junctions," Phys. Rev. 109, 603 (1958).

14. J. O. Scanlan, Analysis and Synthesis of Tunnel Diode Circuits (John Wiley and Sons, Inc., New York, 1966).

15. R. D. Gallagher, "A Microwave Tunnel Diode Amplifier," Microwave J. 8, 62 (1965).

16. H. A. Wheeler, "Transmission-Line Properties of Parallel Strips Separated by a Dielectric Sheet," IEEE Trans. Microwave Theory Tech. MTT-13, 172 (1965).

17. J. A. Weiss and T. G. Bryant, "Parameters of Microstrip Transmission Lines and of Coupled Pairs of Microstrip Lines," paper presented at the International Microwave Symposium, Detroit, Michigan, 20-22 May 1968.

18. E. M. T. Jones and J. T. Bolljahn, "Coupled-Strip-Transmission-Line Filters and Directional Couplers," Trans. IRE, PGMTT MTT-4, 75 (1956).

19. D. Polder, "On the Theory of Ferromagnetic Resonance," Phil. Mag. 40, 99 (1949).

20. C. Kittel, "On the Theory of Ferromagnetic Resonance Absorption," Phys. Rev. 73, 155 (1948).

21. M. Caulton, J. J. Hughes, and H. Sobol, "Measurements on the Properties of Microstrip Transmission Lines for Microwave Integrated Circuits," RCA Review (September 1966), p. 377.

APPENDIX A
IMPERFECT CIRCULATORS

Here, circuits are treated that can be considered as modified forms of the basic parallel-parallel connected circuit of Fig. 2. They are modified forms in that they do not conform to the required minimum number of elements. The analysis is carried out as a three-port device rather than the two-port type considered in the main text. The devices discussed here are capable of providing perfect circulation if circuit conditions are properly chosen; that is, full simultaneous scattering can be achieved into, say, port 2 from port 1, into port 3 from port 2, and into port 1 from port 3, no other coupling being possible. However, these devices can also exhibit non-reciprocity without requiring perfect circulation. With an active element terminating one of the three ports, nonreciprocity can be produced while the input and output ports remain perfectly matched. Since these devices are under control of one or more differential phase elements, the name Diphalator has been coined to describe them.

Two theoretical developments are treated: one utilizing two differential phase elements, and the other utilizing only a single differential element.

I. GENERAL THEORETICAL CONSIDERATIONS

A circuit configuration shown in Fig. A-1 is very similar to that shown in Fig. 2, with the exception that a third port has been brought out to be externally available. That portion of the
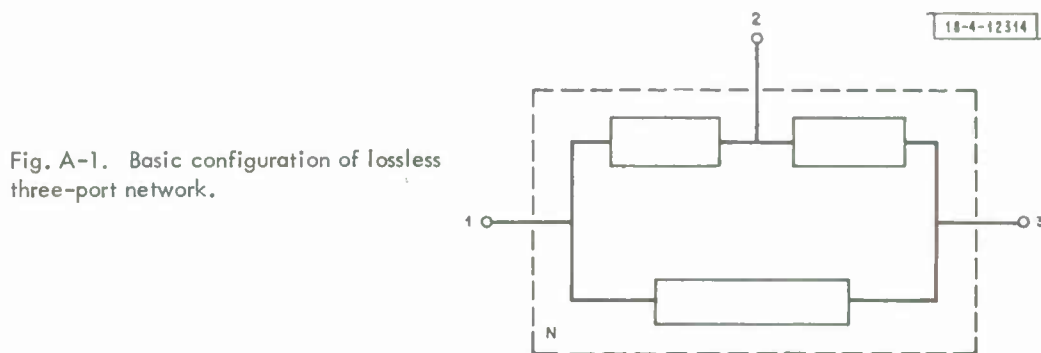
Fig. A-1. Basic configuration of lossless three-port network.

network contained within the dashed boundary (designated by N) is characterized as being loss-less, physically symmetrical with respect to ports 1 and 3, but electrically nonreciprocal. Although nonreciprocal since it is lossless, unitarity of the matrix may be relied upon.

A. Desired Matrix Constraints

The condition of unitarity given by Eq. (6) when applied symbolically to the three-port network of Fig. A-1 becomes

$$
\begin{bmatrix} s_{11}^* & s_{21}^* & s_{31}^* \\ s_{12}^* & s_{22}^* & s_{32}^* \\ s_{13}^* & s_{23}^* & s_{33}^* \end{bmatrix}
\begin{bmatrix} s_{11} & s_{12} & s_{13} \\ s_{21} & s_{22} & s_{23} \\ s_{31} & s_{32} & s_{33} \end{bmatrix}
=
\begin{bmatrix} 1 & 0 & 0 \\ 0 & 1 & 0 \\ 0 & 0 & 1 \end{bmatrix} .
\tag{A-1}
$$

There are nine condition equations resulting from the indicated product. Similarly, by starting with Eq. (7), there are nine more related condition equations.

The desirability of having a matched input and output of a network to facilitate iterations prompts the setting of both s_{11} and s_{33} in Eq. (A-1) to zero. Further, if an active element such as a tunnel diode is to be attached to terminal 2 to provide reflection-type amplification, it would be desirable to isolate terminal 1 from 2. This isolation is achieved by setting $s_{12} = 0$, i.e., the waves scattered into terminal 1 from 2 are zero. Now, with both s_{11} and s_{12} chosen as zero, one of the nine indicated constraining equations demands that s_{13} be 1.0. Although this allows any wave entering terminal 3 to be scattered into terminal 1, it must be remembered that a per-fectly matched load on terminal 3 will prevent such feedback. Thus far, the general scattering matrix for the three-port network is

$$[S] = \begin{bmatrix} 0 & 0 & 1 \\ & & 0 \end{bmatrix} \quad . \tag{A-2}$$

The fact that s_{13} is 1.0 implies that all other terms in column 3 including s_{23} are zero. The remaining condition equations specify that

$$|s_{21}|^2 + |s_{31}|^2 = 1$$

$$|s_{22}|^2 + |s_{32}|^2 = 1$$

$$|s_{21}|^2 + |s_{22}|^2 = 1$$

and

$$|s_{31}|^2 + |s_{32}|^2 = 1 \quad . \tag{A-3}$$

Such an interrelationship of scattering terms may be represented by

$$[S] = \begin{bmatrix} 0 & 0 & 1 \\ j\sin\gamma\epsilon^{-j\alpha} & \cos\gamma\epsilon^{-j\alpha} & 0 \\ \cos\gamma\epsilon^{-j\alpha} & j\sin\gamma\epsilon^{-j\alpha} & 0 \end{bmatrix} \tag{A-4}$$

where γ and α are unknown linking coefficients. It is noted if γ were zero, there would result the scattering matrix of a straight line. If, on the other hand, γ were $\pi/2$, there would result another degeneracy, the matrix of a perfect circulator.

An alternate solution exists, also satisfying the same condition equations, and is given by

$$[S] = \begin{bmatrix} 0 & j\sin\gamma\epsilon^{-j\alpha} & \cos\gamma\epsilon^{-j\alpha} \\ 0 & \cos\gamma\epsilon^{-j\alpha} & j\sin\gamma\epsilon^{-j\alpha} \\ 1 & 0 & 0 \end{bmatrix} \quad . \tag{A-5}$$

It is interesting to see if now, with the inclusion of a simple active device, either of these matrices may be molded in such a way as to show two-port nonreciprocity.

B. Reduction to Two-Port Active Network

The application of a simple negative resistance to terminal 2 of the lossless network is shown in Fig. A-2. Let it be assumed that a wave incident on the lossless network from the

Fig. A-2. Two-port active network obtained from negative resistance and basic lossless three-port circuit.
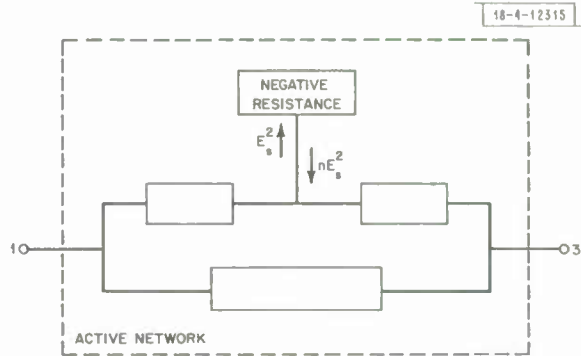
amplifier is nE_s^2, where n is the reflection coefficient of the tunnel-diode amplifier and is >1. E_s^2 is the input to the amplifier, i.e., the scattered wave coming out of port 2.

This overall active network may be adequately described by the matrix equation

$$\begin{bmatrix} E_s^1 \\ E_s^2 \\ E_s^3 \end{bmatrix} = \begin{bmatrix} 0 & 0 & 1 \\ j\sin\gamma\epsilon^{-j\alpha} & \cos\gamma\epsilon^{-j\alpha} & 0 \\ \cos\gamma\epsilon^{-j\alpha} & j\sin\gamma\epsilon^{-j\alpha} & 0 \end{bmatrix} \times \begin{bmatrix} E_i^1 \\ nE_s^2 \\ E_i^3 \end{bmatrix} . \tag{A-6}$$

One of the variables is no longer independent. If these equations are written out, factored, and reassembled in matrix form, then there results

$$\begin{bmatrix} E_s^1 \\ E_s^3 \end{bmatrix} = \begin{bmatrix} 0 & 1 \\ \dfrac{\cos\gamma\epsilon^{-j\alpha} - n\epsilon^{-j2\alpha}}{1 - n\cos\gamma\epsilon^{-j\alpha}} & 0 \end{bmatrix} \begin{bmatrix} E_i^1 \\ E_i^3 \end{bmatrix} . \tag{A-7}$$

The possibility of selecting γ, α, and n to produce nonreciprocity in the overall scattering matrix of such an active network is obvious.

If the alternate network whose scattering matrix is given by Eq. (A-5) had been used, the terms in the matrix of Eq. (A-7) merely change places across the main diagonal. Nonreciprocity and the matching are preserved.

II. DIPHALATOR WITH TWO DIFFERENTIAL PHASE-SHIFT ELEMENTS

Having determined that the circuit arrangement of Fig. A-1 is capable of exhibiting non-reciprocity, we now must determine under what internal circuit constraints these conditions can be realized.
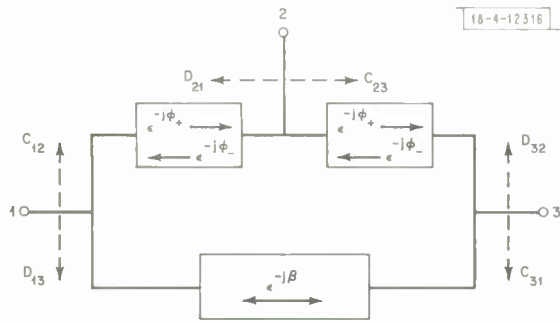
Fig. A-3. Schematic diagram of Diphalator with two differential phase-shift elements.

The schematic diagram of one possible internal circuit is shown in Fig. A-3 which depicts a Diphalator using two differential phase-shift elements in a tandem orientation, i.e., the φ_+ delays are both in a left-to-right sense, and a single transmission line of phase length β degrees. The possible individual waves are indicated by C and D in the figure and their direction of travel is designated by double subscripts.

A. Derivation of the Scattering Matrix

With an input of unit amplitude incident on terminal 1, and with the assumption that all junctions are symmetrical such that their scattering matrices are given by Eq. (32), the relations between the internal waves become

$$C_{23} = -\frac{1}{3} D_{32} \epsilon^{-j\varphi_-} + \frac{2}{3} C_{12} \epsilon^{-j\varphi_+}$$

$$D_{21} = \frac{2}{3} D_{32} \epsilon^{-j\varphi_-} - \frac{1}{3} C_{12} \epsilon^{-j\varphi_+}$$

$$C_{12} = \frac{2}{3} \times 1 + \frac{2}{3} C_{31} \epsilon^{-j\beta} - \frac{1}{3} D_{21} \epsilon^{-j\varphi_-}$$

$$D_{13} = \frac{2}{3} \times 1 + \frac{2}{3} D_{21} \epsilon^{-j\varphi_-} - \frac{1}{3} C_{31} \epsilon^{-j\beta}$$

$$C_{31} = -\frac{1}{3} D_{13} \epsilon^{-j\beta} + \frac{2}{3} C_{23} \epsilon^{-j\varphi_+}$$

$$D_{32} = \frac{2}{3} D_{13} \epsilon^{-j\beta} - \frac{1}{3} C_{23} \epsilon^{-j\varphi_+} \quad . \tag{A-8}$$

In matrix form, Eq. (A-8) is

$$
\begin{bmatrix}
1 & -\frac{2}{3}\epsilon^{-j\beta} & 0 & 0 & 0 & \frac{1}{3}\epsilon^{-j\varphi_-} \\
0 & \frac{1}{3}\epsilon^{-j\beta} & 0 & 1 & 0 & -\frac{2}{3}\epsilon^{-j\varphi_-} \\
0 & 1 & -\frac{2}{3}\epsilon^{-j\varphi_+} & \frac{1}{3}\epsilon^{-j\beta} & 0 & 0 \\
0 & 0 & \frac{1}{3}\epsilon^{-j\varphi_+} & -\frac{2}{3}\epsilon^{-j\beta} & 1 & 0 \\
-\frac{2}{3}\epsilon^{-j\varphi_+} & 0 & 1 & 0 & \frac{1}{3}\epsilon^{-j\varphi_-} & 0 \\
\frac{1}{3}\epsilon^{-j\varphi_+} & 0 & 0 & 0 & -\frac{2}{3}\epsilon^{-j\varphi_-} & 1
\end{bmatrix}
\begin{bmatrix}
C_{12} \\ C_{31} \\ C_{23} \\ D_{13} \\ D_{32} \\ D_{21}
\end{bmatrix}
=
\begin{bmatrix}
\frac{2}{3} \\ \frac{2}{3} \\ 0 \\ 0 \\ 0 \\ 0
\end{bmatrix}
\quad . \tag{A-9}
$$

70

The scattering parameters associated with terminal 1 are defined in terms of these internal waves by

$$s_{11} = \frac{2}{3}\left(D_{21}\epsilon^{-j\varphi_-} + C_{31}\epsilon^{-j\beta}\right) - \frac{1}{3} \times 1 \tag{A-10}$$

$$s_{21} = \frac{2}{3}\left(C_{12}\epsilon^{-j\varphi_+} + D_{32}\epsilon^{-j\varphi_-}\right) \tag{A-11}$$

and

$$s_{31} = \frac{2}{3}\left(D_{13}\epsilon^{-j\beta} + C_{23}\epsilon^{-j\varphi_+}\right) \quad . \tag{A-12}$$

The various C and D parameters must be obtained from solutions of Eq. (A-9) and then substituted into the appropriate defining equation. These terms require considerable algebraic manipulation; consequently, only a typical term will be shown here. Such a term representing one of the internal waves needed is

$$D_{21} = \frac{-\dfrac{8}{27}\epsilon^{-j(\beta+\varphi_-)} + \dfrac{6}{81}\epsilon^{-j(2\varphi_++2\beta+\varphi_-)} + \dfrac{2}{27}\epsilon^{-j(2\varphi_++\varphi_-)}}{-\dfrac{1}{27}\epsilon^{-j2(\varphi_++\beta+\varphi_-)} + \dfrac{2}{27}\epsilon^{-j(\varphi_++2\beta+\varphi_-)} + \dfrac{1}{27}\epsilon^{-j2(\varphi_++\varphi_-)}}$$

$$\frac{-\dfrac{2}{27}\epsilon^{-j(\varphi_++2\beta)} + \dfrac{2}{9}\epsilon^{-j\varphi_+}}{+\dfrac{2}{9}\epsilon^{-j(\varphi_++\varphi_-)} + \dfrac{8}{27}\epsilon^{-j(2\varphi_++\beta)} + \dfrac{8}{27}\epsilon^{-j(\beta+2\varphi_-)} + \dfrac{1}{9}\epsilon^{-j2\beta} - 1} \quad . \tag{A-13}$$

It should be recognized that Eqs. (A-10) through (A-12) can also define parameters s_{33}, s_{23}, and s_{13}, respectively, provided $\epsilon^{-j\varphi_+} \rightarrow \epsilon^{-j\varphi_-}$ and vice-versa. The possibility of such a simplification is due to the physical symmetry of the configuration and the fact that the phase-shift elements are oriented in tandem.

The final defining equations necessary to complete the overall scattering matrix are those resulting from the application of a unit amplitude signal on terminal 2:

$$s_{22} = \frac{2}{3}\left(D_{32}\epsilon^{-j\varphi_-} + C_{12}\epsilon^{-j\varphi_+}\right) - \frac{1}{3} \times 1 \tag{A-14}$$

$$s_{12} = \frac{2}{3}\left(D_{21}\epsilon^{-j\varphi_-} + C_{31}\epsilon^{-j\beta}\right) \tag{A-15}$$

$$s_{32} = \frac{2}{3}\left(C_{23}\epsilon^{-j\varphi_+} + D_{13}\epsilon^{-j\beta}\right) \quad . \tag{A-16}$$

These particular C and D parameters may be obtained from a modified form of Eq. (A-9). Due to the fact that the excitation is now on terminal 2, the right-hand column matrix of Eq. (A-9) must be changed to $[0\ \ 0\ \ 0\ \ 0\ \ 2/3\ \ 2/3]_t$.

Figure A-4 displays the final overall 3×3 scattering matrix for this Diphalator. It is especially important to recognize the fundamental dissymmetry about the matrix principal diagonal indicating the nonreciprocity present. Equally important is the recognition that interchanging φ_+ and φ_- everywhere folds the matrix about the main diagonal, indicating the switchable states

Fig. A-4. Scattering matrix for lossless Diphalator using two differential phase-shift elements.

whereby the transmission characteristics are exchanged. The rows and columns of terms satisfy the conditions of unitarity since the Diphalator is, of course, lossless.

B. Computer Solutions

A computer program was written to determine relationships between the variables φ_+, φ_-, and β that would allow the s_{13} term to be of unit magnitude; this program appears in Appendix B as Fig. B-9. Since unitarity still prevails, the limiting of s_{13} to unit magnitude automatically guarantees zero values for s_{11}, s_{12}, s_{23}, and s_{33}.

The results of the computer analysis are shown in Fig. A-5. For a given line length β, two solutions are possible: one consists of paired values of φ_+ and φ_- that represent a cross-type
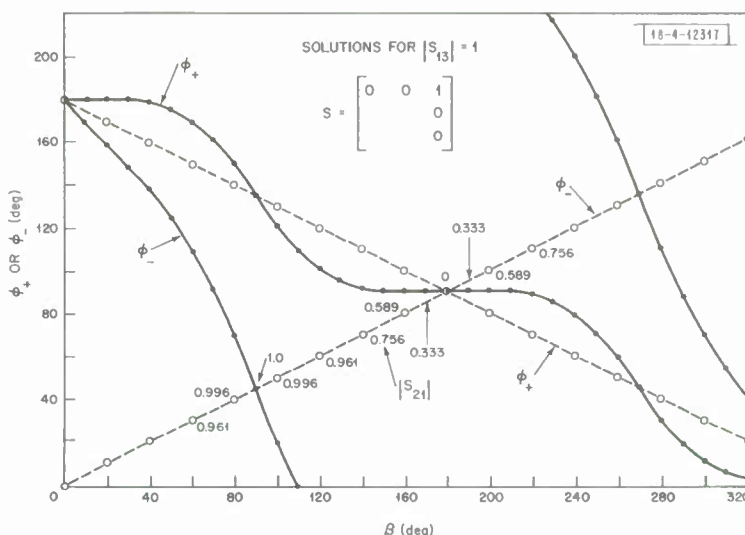
Fig. A-5. Relations among variables required for $|S_{13}| = 1.0$ in scattering matrix of two phase-shift Diphalator.

linear relationship, shown by the dashed curves; for the other solution, paired values of φ_+ and φ_- define a more elaborate function, as shown by the solid curves. Of special interest are two areas represented by small values of β for which nonreciprocity is possible with small δ, and a more practical area near $\beta = 180°$, for which nonreciprocity is also possible with small differential phase shift. The solution indicated for $\beta = 90°$ or $270°$ is that for perfect circulation where $s_{13} = s_{21} = s_{32} = 1$. Another degeneracy is apparent with $\beta = 180°$ and $\varphi_+ = \varphi_- = 90°$. This solution is for a straight line where $s_{13} = s_{22} = s_{31} = 1$. It is evident that nonreciprocity in this device does not depend entirely on the existence of circulation.

A second computer program was written to determine the entire complex scattering matrix for discrete data points; this program is listed as Fig. B-10 in Appendix B. The variations of $|s_{21}|$ are indicated along the dashed curve of Fig. A-5.

C. Invariant Identities

Care must be exercised in altering the curves of Fig. A-5 by adding or subtracting increments such as 180° or 360°, for the periodicity of these curves is peculiar. For the linear relationship

$$\varphi_- = \frac{1}{2}\,\beta$$

when

$$\varphi_+ = \pi - \frac{1}{2}\,\beta \tag{A-17}$$

and no special precautions are needed. However, for the solution involving the solid curves with a constant value of β

$$\varphi_- \rightarrow \varphi_- \pm 180°$$

and

$$\varphi_+ \rightarrow \varphi_+ \pm 180° \qquad . \tag{A-18}$$

More important is the pairing of curves with the recycling of β, for if

$$\beta \rightarrow \beta + 180°$$

then

$$\varphi_- \rightarrow \varphi_- + 90°$$

and

$$\varphi_+ \rightarrow \varphi_+ - 90° \qquad . \tag{A-19}$$

Two incidental sets of invariances are obtained by holding either φ_+ or φ_- constant: (a) for a constant φ_-

$$\beta \rightarrow \beta + 360° \tag{A-20}$$

when $\varphi_+ \rightarrow \varphi_+ + 360°$, and (b) for a constant φ_+

$$\beta \rightarrow \beta + 360° \tag{A-21}$$

which requires $\varphi_- = \varphi_-$.

Thus, it has been demonstrated that this lossless circuit arrangement is capable of exhibiting the desired property of nonreciprocity without requiring circulation. Such nonreciprocity can be achieved with a small amount of differential phase shift and can be achieved while preserving the desired matching.

III. DIPHALATOR WITH ONE DIFFERENTIAL PHASE-SHIFT ELEMENT

An alteration of the basic configuration is shown in Fig. A-6, with two dissimilar line lengths α and β and a single phase-shift element. The only elements preserved in juxtaposition from
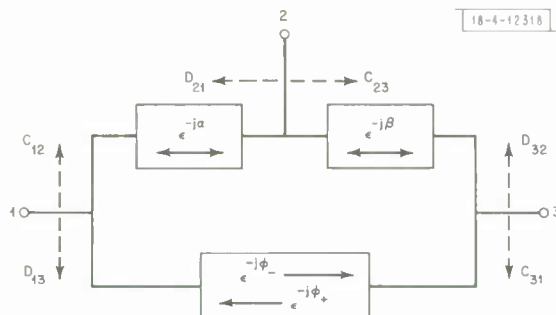
Fig. A-6. Schematic diagram af Diphalator with single differential phase-shift element.

the previous analysis are the symmetrical scattering junctions. The following shows that this lossless circuit can also demonstrate nonreciprocity without requiring complete circulation.

A. Derivation of the Scattering Matrix

Although basically the solution parallels that of the previous section, there are sufficient algebraic differences that should at least be indicated. In matrix form, the relations between the internal waves of Fig. A-6 are given by

$$
\begin{bmatrix}
1 & -\frac{2}{3}\epsilon^{-j\varphi_+} & 0 & 0 & 0 & \frac{1}{3}\epsilon^{-j\alpha} \\
0 & \frac{1}{3}\epsilon^{-j\varphi_+} & 0 & 1 & 0 & -\frac{2}{3}\epsilon^{-j\alpha} \\
0 & 1 & -\frac{2}{3}\epsilon^{-j\beta} & \frac{1}{3}\epsilon^{-j\varphi_-} & 0 & 0 \\
0 & 0 & \frac{1}{3}\epsilon^{-j\beta} & -\frac{2}{3}\epsilon^{-j\varphi_-} & 1 & 0 \\
-\frac{2}{3}\epsilon^{-j\alpha} & 0 & 1 & 0 & \frac{1}{3}\epsilon^{-j\beta} & 0 \\
\frac{1}{3}\epsilon^{-j\alpha} & 0 & 0 & 0 & -\frac{2}{3}\epsilon^{-j\beta} & 1
\end{bmatrix}
\begin{bmatrix}
C_{12} \\ C_{31} \\ C_{23} \\ D_{13} \\ D_{32} \\ D_{21}
\end{bmatrix}
=
\begin{bmatrix}
\frac{2}{3} \\ \frac{2}{3} \\ 0 \\ 0 \\ 0 \\ 0
\end{bmatrix}
. \quad (A-22)
$$

Each of the C and D coefficients must be determined in terms of $\epsilon^{-j\varphi_+}$, $\epsilon^{-j\varphi_-}$, $\epsilon^{-j\alpha}$, and $\epsilon^{-j\beta}$ for substitution into the defining equations for the scattering parameters. For a unit amplitude applied to terminal 1, these defining equations are

$$
s_{11} = \frac{2}{3}\left(D_{21}\epsilon^{-j\alpha} + C_{31}\epsilon^{-j\varphi_+}\right) - \frac{1}{3} \times 1 \tag{A-23}
$$

$$
s_{21} = \frac{2}{3}\left(D_{32}\epsilon^{-j\beta} + C_{12}\epsilon^{-j\alpha}\right) \tag{A-24}
$$

and

$$
s_{31} = \frac{2}{3}\left(D_{13}\epsilon^{-j\varphi_-} + C_{23}\epsilon^{-j\beta}\right) . \tag{A-25}
$$

Because of physical symmetry about terminal 2, these same equations define s_{33}, s_{23}, and s_{13}, respectively, when φ_+ and φ_- are interchanged along with an interchange of α and β.

With the excitation on terminal 2, the right-hand matrix in Eq. (A-22) must be changed to $[0\ 0\ 0\ 0\ 2/3\ 2/3]_t$ to be applicable. The remaining defining equations for the scattering parameters are

$$
s_{22} = \frac{2}{3}\left(D_{32}\epsilon^{-j\beta} + C_{12}\epsilon^{-j\alpha}\right) - \frac{1}{3} \times 1 \tag{A-26}
$$

$$
s_{12} = \frac{2}{3}\left(D_{21}\epsilon^{-j\alpha} + C_{31}\epsilon^{-j\varphi_+}\right) \tag{A-27}
$$

Fig. A-7. Scattering matrix for lossless Diphalator with single differential phase-shift element.

-44-11892-1

and

$$s_{32} = \frac{2}{3} \left(C_{23} \epsilon^{-j\beta} + D_{13} \epsilon^{-j\varphi_-} \right) \tag{A-28}$$

where the C and D coefficients are to be obtained from the modified matrix Eq. (A-22).

The final matrix for this Diphalator is shown in Fig. A-7. Dissymmetry is in evidence about the principal diagonal. If $\alpha = \beta$, symmetry is recognized about the minor diagonal, indicating the physical symmetry of the device about port 2. An interchange of φ_+ and φ_- effects a folding of terms across the principal diagonal. These indications are in agreement with the desired nonreciprocal but switchable states of the lossless network.

B. Computer Solutions

Two computer programs were written for this case: one to determine the values of β, φ_+, and φ_- to satisfy the unitarity condition with $|s_{13}| = 1$, and the other to evaluate the entire magnitude scattering matrix for discrete values of the variables. These programs may be found in Appendix B as Figs. B-11 and B-12.

Two ranges of solutions are evident for this circuit, as may be seen by referring to Fig. A-8. For one solution type, both φ_+ and β are required to be invariant, φ_+ at 180° and β at 90°; thus,
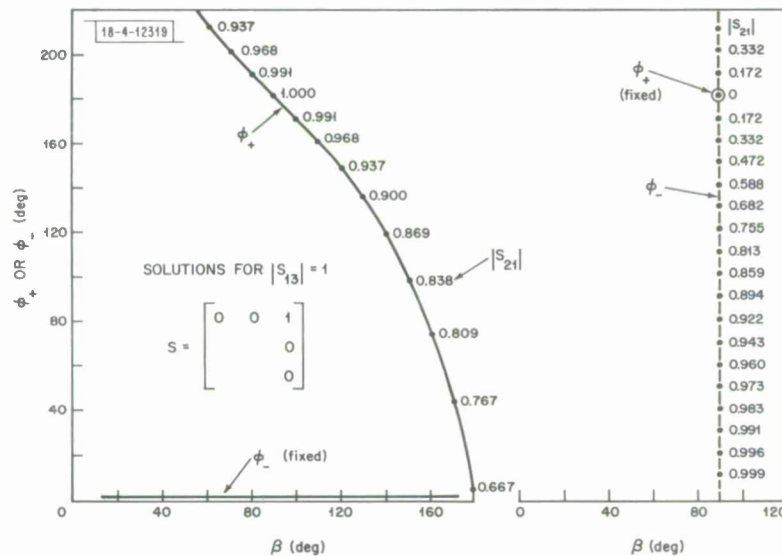
Fig. A-8. Relations among variables required for $|S_{13}| = 1.0$ in scattering matrix of single phase-shift Diphalator.

φ_- is the only active variable. The condition required on the second type solution is that φ_- remain fixed at 0°. For this case, two variables are effective, i.e., φ_+ and β. Numerical values indicated along the curves of the figure represent the magnitudes of s_{21}. These data are included merely to indicate how the parameter magnitudes are subdivided within the overall scattering matrix. It is evident that perfect circulation can occur only by restricting φ_- to 0° or 360°, by requiring $\beta = 90°$, and by limiting φ_+ to 180°.

A typical computer calculation of the magnitude scattering matrix for $\varphi_+ = 180°$, $\beta = 90°$, and $\varphi_- = 90°$ is

$$\begin{bmatrix} 0.0000 & 0.0000 & 1.0000 \\ 0.8944 & 0.4472 & 0.0000 \\ 0.4472 & 0.8944 & 0.0000 \end{bmatrix} \quad .$$

C. Invariant Identities

It may be determined that holding both φ_+ and φ_- constant allows β to be increased by 180°, leaving the same solution. Thus,

$$\varphi_+ = \varphi_+$$

$$\varphi_- = \varphi_-$$

$$\beta \rightarrow \beta + 180° \quad . \tag{A-29}$$

Alternately, if β be held constant, invariance in the solution requires

$$\beta = \beta$$

$$\varphi_+ \rightarrow \varphi_+ + 360°$$

$$\varphi_- \rightarrow \varphi_- + 360° \quad . \tag{A-30}$$

Thus, the single phase-shift Diphalator also exhibits the desirable properties set forth for this lossless device.

APPENDIX B

This appendix comprises a listing of programs written specifically for the IBM-360 computer installation at Lincoln Laboratory, together with graphical data used in some of the computations. All programs are written in Fortran H language. Several of the figures show only substitutions or modifications needed in other programs for a given application. Each program listed and each graph is referred to in either the main body of the report or in Appendix A.

```
//E38848 JOB    S360,                                                       C
//             '8LAKE/LI8BEY,UIO5',MSGLEVEL=1
//START   EXEC   PROC=DUMMY
//COM     EXEC   PROC=FORTRANH
//SYSIN   DD    *
C THIS PROGRAM DESIGNATES VALUES OF G COMPLEX, S12, AND S21 FOR MINIMUM
C              DIFFERENTIAL GAIN CIRCUIT  -   FE8RUARY 9, 1968
C                       h. M. LI8BEY              GRCUP 44
C
C          1          2          3          4          5          6          7
C234567890123456789012345678901234567890123456789012345678901234567890123456789012
C
      COMPLEX PHA,PHN,EPSLN,DELTA,ATLED,X,XX,Y,YY,G,GG,Z,ZZ,GFO,G8A,GGFO
     1,GG8A,DEN,DDEN,R
       DIMENSION G(648),GFO(648),GGFOR(648),G8A(648),GG8AK(648),GG(648),
     1 V(648),H(648),PHI(648),GGG(648),PHIM(648),VV(648),HH(648),ZU(648)
     2,ZUM(648),VVV(648),HHH(648),AMDA(648),AMDAM(648),GGFO(648),GG8A(64
     38),L8L(180),CEN(648),DDEN(648),DDDEN(648),RATIO(648)
  116 READ (5,117,END=45) R
  117 FORMAT (F10.0,F10.0)
      I = 0
    1 CO 28 J=5,180,5
      JSUM = -185
      JSUM = JSUM + J
      A = JSUM
      L8L(J) = -JSUM
    2 CO 27 K=5,90,5
      I = I + 1
      KSUM = 0
      KSUM = KSUM + K
      8 = -KSUM
      PHA = CMPLX(0.C,A)
      PHA = (2.*3.1415927*PHA)/360.
      EPSLN = CEXP(PHA)
      PHN = CMPLX(0.C,8)
      PHN = (2.*3.1415927*PHN)/360.
      CELTA = CEXP(PHN)
      ATLED = CONJG(DELTA)
    3 X = (16.*(EPSLN**2)*REAL(DELTA)*REAL(DELTA)-(3.*(EPSLN**2)+1.)*(((
     1 -3.*(R**2)+2.*R+1.)*(EPSLN**2))+(-(R**2)-2.*R+3.)))
    4 XX = CSQRT(X)
    5 Y = (4.*EPSLN*REAL(DELTA)+XX)/(3.*(EPSLN**2)+1.)
    6 Z = (4.*EPSLN*REAL(DELTA)-XX)/(3.*(EPSLN**2)+1.)
    7 YY = CA8S(Y)
    8 YYY = REAL(YY)
    9 ZZ = CA8S(Z)
   10 ZZZ = REAL(ZZ)
   11 IF(YYY-ZZZ)12,12,14
   12 G(I) = Z
   13 GO TO 15
   14 G(Ii = Y
```

Fig. B-1. Fortron list of program for evoluation of $|G|$, org G, $|S_{12}|$, $|S_{21}|$, and rotio S_{12}/S_{21} for basic nonreciprocol goin network.

```
 15   GFO (I) = (4.*(G(I)**2)*EPSLN*DELTA+4.*G(I)*(EPSLN**2)-4.*G(I)-4.*
      1 ((R**2)+2.*R+1.)*EPSLN*DELTA)/(-(G(I)**2)*(EPSLN**2)+(G(I)**2)+4.
      2 *G(I)*EPSLN*DELTA+4.*G(I)*EPSLN*(ATLED)+((R**2)-2.*R+1.)*(EPSLN**
      3 2)-((R**2)+6.*R+9.))
 16   GGFO (I) = CABS (GFO(I))
 17   GGFOR (I) = REAL (GGFO(I))
 18   GBA (I) = (4.*(G(I)**2)*EPSLN*(ATLED)+4.*G(I)*(EPSLN**2)-4.*G(I)-4
      1 .*((R**2)+2.*R+1.)*EPSLN*(ATLED))/(-(G(I)**2)*(EPSLN**2)+(G(I)**2
      2 )+4.*G(I)*EPSLN*DELTA+4.*G(I)*EPSLN*(ATLED)+((R**2)-2.*R+1.)*(EPS
      3 LN**2)-((R**2)+6.*R+9.))
115   DEN (I) = (-(G(I)**2)*(EPSLN**2)+(G(I)**2)+4.*G(I)*EPSLN*DELTA+4.*
      1 G(I)*EPSLN*(ATLED)+((R**2)-2.*R+1.)*(EPSLN**2)-((R**2)+6.*R+9.))
      DDEN(I) = CABS(DEN(I))
      DDDEN(I) = REAL(DDEN(I))
 19   GG8A (I) = CA8S (GBA(I))
 20   GGBAK (I) = REAL (GGBA(I))
103   RATIO(I) = (GG8AK(I))/(GGFOR(I))
 21   GG(I) = CA8S (G(I))
 22   GGG(I) = REAL (GG(I))
 23   V(I) = AIMAG (G(I))
 24   H(I) = REAL (G(I))
 25   PHI (I) = ATAN2 (V(I),H(I))
 26   PHIM(I) = (360.*PHI(I))/(2.*3.1415927)
 54   VV(I) = AIMAG (GFO(I))
 55   HH(I) = REAL (GFO(I))
 86   IF(HH(I))56,87,56
 87   HH(I) = HH(I) + 999.
 56   ZU(I) = ATAN2 (VV(I),HH(I))
 57   ZUM(I) = (360.*ZU(I))/(2.*3.1415927)
 58   VVV(I) = AIMAG (GBA(I))
 59   HHH(I) = REAL (G8A(I))
 88   IF(HHH(I))60,89,60
 89   HHH(I) = HHH(I) + 999.
 60   AMDA(I) = ATAN2 (VVV(I),HHH(I))
 61   AMDAM(I) = (360.*AMDA(I))/(2.*3.1415927)
 27   CONTINUE
 28   CONTINUE
      WRITE (6,29)
 29   FORMAT ('1',39X,'AMPLIFIER GAIN AS FUNCTION OF AVE PHASE AND DIFF
      1PHASE'/)
      ISTART = 1
      IEND = 18
 74   DO 32 J=5,180,5
 30   WRITE (6,31) LBL(J),(GGG(I),I=ISTART,IEND)
 31   FORMAT (I4,(' ',18F7.2))
      ISTART = ISTART + 18
      IEND = IEND + 18
 32   CONTINUE
 46   WRITE (6,47)
 47   FORMAT (130HO          5      10      15      20      25      30      35
      1      40      45      50      55      60      65      70      75      80
      2 85      90)
 80   CONTINUE
      WRITE (6,33)
 33   FORMAT ('1',29X,'AMPLIFIER ANGLE AS FUNCTION OF AVE INSERTION PHAS
      1E AND DIFFERENTIAL PHASE'/)
```

Fig. B-1. Continued.

```
      ISTART = 1
      IEND = 18
 75   DO 36 J=5,180,5
 34   WRITE (6,35) LBL(J),(PHIM(I),I=ISTART,IEND)
 35   FORMAT (I4,(' ',18F7.2))
      ISTART = ISTART + 18
      IEND = IEND + 18
 36   CONTINUE
 48   WRITE (6,49)
 49   FORMAT (130H0            5        10       15       20       25       30       35
     1    40       45       50       55       60       65       70       75       80
     2 85        90)
 81   CONTINUE
      WRITE (6,98)
 98   FORMAT ('1',45X,'COMMON DENOMINATOR MAGNITUDE FOR S12 AND S21'/)
      ISTART = 1
      IEND = 18
      DO 100 J=5,180,5
      WRITE (6,99) L8L(J),(DDDEN(I),I=ISTART,IEND)
 99   FORMAT (I4,(' ',18F7.2))
      ISTART = ISTART + 18
      IEND = IEND + 18
 100  CONTINUE
      WRITE (6,101)
 101  FORMAT (130H0            5        10       15       20       25       30       35
     1    40       45       50       55       60       65       70       75       80
     2 85        90)
 102  CONTINUE
      WRITE (6,37)
 37   FORMAT ('1',39X,'S12 MAGNITUDE AS FUNCTION OF AVE PHASE AND DIFF P
     1HASE'/)
      ISTART = 1
      IEND = 18
 76   DO 40 J=5,180,5
 38   WRITE (6,39) L8L(J),(GGFOR(I),I=ISTART,IEND)
 39   FORMAT (I4,(' ',18F7.2))
      ISTART = ISTART + 18
      IEND = IEND + 18
 40   CONTINUE
 50   WRITE (6,51)
 51   FORMAT (130H0            5        10       15       20       25       30       35
     1    40       45       50       55       60       65       70       75       80
     2 85        90)
 82   CONTINUE
      WRITE (6,41)
 41   FORMAT ('1',39X,'S21 MAGNITUDE AS FUNCTION OF AVE PHASE AND DIFF P
     1HASE'/)
      ISTART = 1
      IEND = 18
 77   DO 44 J=5,180,5
 42   WRITE (6,43) L8L(J),(GGBAK(I),I=ISTART,IEND)
 43   FORMAT (I4,(' ',18F7.2))
      ISTART = ISTART + 18
      IEND = IEND + 18
 44   CONTINUE
 52   WRITE (6,53)
```

Fig. B-1. Continued.

81

```
  53  FORMAT (130H0                  5         10        15        20        25        30        35
     1     40        45        50        55        60        65        70        75        80
     2 85         90)
  83  CONTINUE
      WRITE (6,62)
  62  FORMAT ('1',35X,'S12 ANGLE AS FUNCTION CF AVE PHASE AND DIFFERENTI
     1AL PHASE'/)
      ISTART = 1
      IEND = 18
  78  CO 67 J=5,180,5
  63  WRITE (6,64) LBL(J),(ZUM(I),I=ISTART,IEND)
  64  FORMAT (I4,(' ',18F7.2))
      ISTART = ISTART + 18
      IEND = IEND + 18
  67  CONTINUE
  65  WRITE (6,66)
  66  FORMAT (130H0                  5         10        15        20        25        30        35
     1     40        45        50        55        60        65        70        75        80
     2 85         90)
  84  CONTINUE
      WRITE (6,68)
  68  FORMAT ('1',35X,'S21 ANGLE AS FUNCTION CF AVE PHASE AND DIFFERENTI
     1AL PHASE'/)
      ISTART = 1
      IEND = 18
  79  CO 73 J=5,18C,5
  69  WRITE (6,70) LBL(J),(AMDAM(I),I=ISTART,IEND)
  70  FORMAT (I4,(' ',18F7.2))
      ISTART = ISTART + 18
      IEND = IEND + 18
  73  CONTINUE
  71  WRITE (6,72)
  72  FORMAT (130H0                  5         10        15        20        25        30        35
     1     40        45        50        55        60        65        70        75        80
     2 85         90)
  85  CONTINUE
 104  WRITE (6,105)
 105  FORMAT ('1',15X,'RATIO OF S21 TO S12 MAGNITUDE AS A FUNCTION OF AV
     1ERAGE INSERTION PHASE AND AVERAGE DIFFERENTIAL PHASE'/)
      ISTART = 1
      IEND = 18
 106  CO 109 J=5,180,5
 107  WRITE (6,108) LBL(J),(RATIO(I),I=ISTART,IEND)
 108  FORMAT (I4,(' ',18F7.2))
      ISTART = ISTART + 18
      IEND = IEND + 18
 109  CONTINUE
 110  WRITE (6,111)
 111  FORMAT (130H0                  5         10        15        20        25        30        35
     1     40        45        5C        55        60        65        70        75        80
     2 85         90)
C
C        1         2         3         4         5         6         7
C234567890123456789012345678901234567890123456789012345678901234567890123456789012
 112  CONTINUE
 118  GO TO 116
  45  STOP
      END
/*
//LINK   EXEC   PROC=LINKSRCN
//GO    EXEC   PROC=EXECUTE
//FT05F001   DD   *
   0.C       0.0
/*
```

Fig. B-1. Continued.

```
C THIS PROGRAM DESIGNATES VALUES OF GCOMPLEX, S12, AND S21 FOR MINIMUM
C              DIFFERENTIAL GAIN CIRCUIT   -   FEBRUARY 9, 1968
C       *   *   *   *   *   USING NEGATIVE ROOT OF G  *   *   *   *   *   *   *   *
C
C
C
   11   IF(ZZZ-YYY)12,12,14
```

****

Fig. B-2. Modification necessary in Fortran program of Fig. B-1 to evaluate $|G|$, arg G, $|S_{12}|$, $|S_{21}|$, and ratio S_{12}/S_{21} for basic nonreciprocal loss network.

```
C THIS PROGRAM DESIGNATES VALUES OF G COMPLEX, S12, AND S21 FOR MINIMUM
C              DIFFERENTIAL GAIN CIRCUIT AND DEPENDS ON
C                  THE AMPLIFIER REFLECTION COEFFICIENT
C              R = 0.0 TO R = + AND - 1.0 IN 0.2 INCREMENTS
C
C
C
C
      0.2       0.0
      0.4       0.0
      0.6       0.0
      0.8       0.0
     1.0        0.0
    -0.2        0.0
    -0.4        0.0
    -0.6        0.0
    -0.8        0.0
    -1.0        0.0
```

****

Fig. B-3. Additions required for Fortran program of Fig. B-1 to evaluate $|G|$, arg G, $|S_{12}|$, $|S_{21}|$, and ratio S_{12}/S_{21} for basic nonreciprocal gain network with amplifier reflections R.

83

```
C THIS PROGRAM DESIGNATES VALUES OF G COMPLEX, S12, ANO S21 FOR MINIMUM
C            OIFFERENTIAL GAIN CIRCUIT ANO OEPENDS ON
C            THE AMPLIFIER REFLECTION COEFFICIENT R = 0.2
C            WITH ANGLES FROM -120 TO +120 IN 15 DEGREE INCREMENTS
C
C
C
C
C
   +0.2000    +0.0000
   +0.0517    +0.1931
   +0.0517    -0.1931
   +0.1732    +0.1000
   +0.1732    -0.1000
   +0.1414    +0.1414
   +0.1414    -0.1414
   +0.1000    +0.1732
   +0.1000    -0.1732
   +0.1931    +0.0517
   +0.1931    -0.0517
   +0.0000    +0.2000
   +0.0000    -0.2000
   -0.1000    +0.1732
   -0.1000    -0.1732
   -0.1732    +0.1000
   -0.1732    -0.1000
                            ************************
```

Fig. B-4. Additions required far Fartran pragram af Fig. B-1 ta evaluate $|G|$, arg G, $|S_{12}|$, $|S_{21}|$, and ratia S_{12}/S_{21} for basic nonreciprocal gain network with amplifier reflectian coefficient $R = 0.2$ with angles fram $-120°$ ta $+120°$.

84

```
C
C          * * * * * * * * * * * * * * * * * * * * * * * * *
C          *                                               *
C          *               THIS PROGRAM                    *
C          *    DETERMINES COMPLEX VALUES IN POLAR FORM     *
C          *     FOR G, S12, S21, COMMCN DENOMINATOR        *
C          *              AND THE S RATIO                   *
C          *                   FOR                          *
C          *                THE BASIC                       *
C          *    DIFFERENTIAL GAIN CIRCUIT MATRIX            *
C          *       USING BALANCED JUNCTIONS                 *
C          *    DEPENDING ON THE AMPLIFIER REFLECTION       *
C          *    COEFFICIENT R VARYING FROM 0 TO +AND-       *
C          *              I BY 0.2 INCREMENTS               *
C          *                                               *
C          *                                               *
C          *                                               *
C          *                                               *
C          * * * * * * * * * * * * * * * * * * * * * * * * *
C
C
    3  X = ((EPSLN**2)*REAL(DELTA)*REAL(DELTA)+(R**2)-2.*R*(EPSLN**2)+2.*
      1 R-(EPSLN**2))
    5  Y = (EPSLN*REAL(DELTA)+XX)
    6  Z = (EPSLN*REAL(DELTA)-XX)
   15  GFO (I) = (2.*((G(I)**2)*EPSLN*DELTA+G(I)*(EPSLN**2)-G(I)-((R**2)+
      1 2.*R+1.)*EPSLN*DELTA))/((G(I)**2)+G(I)*EPSLN*DELTA+G(I)*EPSLN*(AT
      2 LED)+(EPSLN**2)-((R**2)+4.*R+4.))
   18  GBA (I) = (2.*((G(I)**2)*EPSLN*(ATLED)+G(I)*(EPSLN**2)-G(I)-((R**2
      1 )+2.*R+1.)*EPSLN*(ATLED)))/((G(I)**2)+G(I)*EPSLN*DELTA+G(I)*EPSLN
      2 *(ATLED)+(EPSLN**2)-((R**2)+4.*R+4.))
  II5  DEN (I) = ((G(I)**2)+G(I)*EPSLN*DELTA+G(I)*EPSLN*(ATLED)+(EPSLN**2
      1 )-((R**2)+4.*R+4.))
                         ************************
```

Fig. B-5. Substitutions far Fartran pragram of Fig. B-1 to evaluate $|G|$, arg G, $|S_{12}|$, $|S_{21}|$, and ratia S_{12}/S_{21} when using balanced scattering junctians.

```
C                * * * * * * * * * * * * * * * * * * * * * * * *       C
C                *                                             *       C
C                *              THIS PROGRAM                   *       C
C                *     DETERMINES COMPLEX VALUES IN POLAR FORM *       C
C                *       FOR G, S12, S21, COMMON DENOMINATOR   *       C
C                *             AND THE S RATIO                 *       C
C                *                  FOR                        *       C
C                *               THE BASIC                     *       C
C                *     DIFFERENTIAL GAIN CIRCUIT MATRIX        *       C
C                * USING COMPLETELY NON-SYMMETRICAL JUNCTIONS  *       C
C                *     DEPENDING ON THE AMPLIFIER REFLECTION   *       C
C                *    COEFFICIENT R VARYING FROM 0 TO +AND-    *       C
C                *          1 BY 0.2 INCREMENTS                *       C
C                *                                             *       C
C                *                                             *       C
C                *                                             *       C
C                *                                             *       C
C                *                                             *       C
C                * * * * * * * * * * * * * * * * * * * * * * * *       C
C
C
   3   X = (256.*(EPSLN**2)*REAL(DELTA)*REAL(DELTA)-(21.*(EPSLN**2)-5.)*(
      1 -(R**2)*(21.*(EPSLN**2)-5.)+R*(38.*(EPSLN**2)-1.)-5.*(EPSLN**2)+
      2 21.))
   5   Y = (16.*EPSLN*REAL(DELTA)+XX)/(21.*(EPSLN**2)-5.)
   6   Z = (16.*EPSLN*REAL(DELTA)-XX)/(21.*(EPSLN**2)-5.)
  15   GFO (I) = (8.*((G(I)**2)*EPSLN*DELTA+4.*G(I)*((EPSLN**2)-1.)-EPSLN
      1 *DELTA*((R**2)+2.*R+1.)))/((G(I)**2)*(1.-9.*(EPSLN**2))+G(I)*32.*
      2 EPSLN*REAL(DELTA)+(R**2)*(9.*(EPSLN**2)-1.)-R*(30.*(EPSLN**2)-14.
      3 )+(25.*(EPSLN**2)-49.))
  18   GBA (I) = (8.*((G(I)**2)*EPSLN*(ATLED)+4.*G(I)*((EPSLN**2)-1.)-EPS
      1 LN*(ATLED)*((R**2)+2.*R+1.)))/((G(I)**2)*(1.-9.*(EPSLN**2))+G(I)*
      2 32.*EPSLN*REAL(DELTA)+(R**2)*(9.*(EPSLN**2)-1.)-R*(30.*(EPSLN**2)
      3 -14.)+(25.*(EPSLN**2)-49.))
 115   DEN (I) = ((G(I)**2)*(1.-9.*(EPSLN**2))+G(I)*32.*EPSLN*REAL(DELTA)
      1 +(R**2)*(9.*(EPSLN**2)-1.)-R*(30.*(EPSLN**2)-14.)+(25.*(EPSLN**2)
      2 -49.))
                      ************************
```

Fig. B-6.   Substitutions for Fortran program of Fig. B-1 to evaluate $|G|$, org G, $|S_{12}|$, $|S_{21}|$, and ratio S_{12}/S_{21} when using nonsymmetrical scattering junctions.

Fig. B-7(o). Even- ond odd-mode impedonces for coupled microstrips with porameter S/H: substrote K = 16 (dielectric).

Fig. B-7(b). Even- and odd-mode velocities for coupled microstrips with parameter S/H: substrate K = 16 (dielectric).
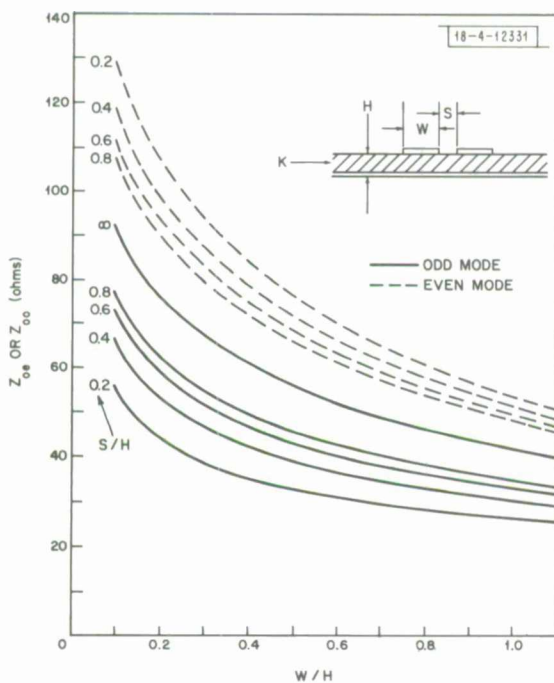
Fig. B-8(a). Even- and odd-mode impedances for coupled microstrips with porameter S/H: substrote K = 14.4 (dielectric).

Fig. B-8(b). Even- and odd-mode velocities for coupled microstrips with porameter S/H: substrate K = 14.4 (dielectric).

```
//E32283 JOB    S360,                                                          C
//              'BLAKE/LIBBEY,UI05',MSGLEVEL=1
//START   EXEC   PROC=DUMMY
//COM    EXEC   PROC=FORTRANH
//SYSIN   DD    *
C      THIS PROGRAM DESIGNATES VALUES OF S13 FOR IMPERFECT CIRCULATOR
C
C
       COMPLEX PHP, BTA, PHM, R
       DIMENSION R(600),RR(600)
   20  DO 21 M = 10,270,130
    1  DO 14 J = 10,360,10
       JSUM = -10
       JSUM = JSUM + J
       B = JSUM
   17  WRITE (6,15)
   15  FORMAT(51H1                                           BETA = ////)
       I = 0
    2  DO 11 K = 10,360,10
       KSUM = -360
       KSUM = KSUM + K
       A = -KSUM
    3  DO 10 L = 10,140,10
       I = I + 1
       LSUM = M - 20
       LSUM = LSUM + L
       C = LSUM
       PHP = CMPLX(0.0,-A)
       BTA = CMPLX(0.0,-B)
       PHM = CMPLX(0.0,-C)
    4  PHP = (2.*3.1415927*PHP)/360.
    5  BTA = (2.*3.1415927*BTA)/360.
    6  PHM = (2.*3.1415927*PHM)/360.
    7  R(I) = (4.*(CEXP(2.*PHP+BTA+2.*PHM)+2.*CEXP(PHP+BTA+PHM)+2.*CEXP
      1  (2.*BTA+2.*PHM)-2.*CEXP(2.*PHM)-3.*CEXP(BTA))/27.)/((-CEXP(2.*
      2  PHP+2.*BTA+2.*PHM)+2.*CEXP(PHP+2.*BTA+PHM)+CEXP(2.*PHP+2.*PHM)
      3  +6.*CEXP(PHP+PHM)+8.*CEXP(2.*PHP+BTA)+8.*CEXP(BTA+2.*PHM)+3.*
      4  CEXP(2.*BTA)-27.)/27.)
    8  R(I) = CABS (R(I))
    9  RR(I) = REAL (R(I))
   10  CONTINUE
   11  CONTINUE
   12  WRITE (6,13) (RR(I),I=1,504)
   13  FORMAT (14F9.4)
   14  CONTINUE
   21  CONTINUE
   16  STOP
       END

//LINK   EXEC   PROC=LINKSRCN
//GO     EXEC   PROC=EXECUTE
                         ***********************
```

Fig. B-9. Fortran list of program for evaluation of $|S_{13}|$ for Diphalator
with two differential phase-shift elements.

```
//E31827 JOB    S360,                                                      C
//             'BLAKE/LIBBEY,UI05',MSGLEVEL=1
//START   EXEC   PROC=DUMMY
//COM     EXEC   PROC=FORTRANH
//SYSIN   DD     *
C THIS PROGRAM CALCULATES THE COMPLEX SCATTERING MATRIX FOR THE
C              IMPERFECT CIRCULATOR -- OCTOBER 25, 1967
C
       COMPLEX PHP,BTA,PHM,R,Z,Y,X,Q,W
       CALL MSGOP
    1  READ (5,2,END=11) A,B,C
    2  FORMAT (F10.0,F10.0,F10.0)
       PHP = CMPLX (0.0,-A)
       BTA = CMPLX (0.0,-B)
       PHM = CMPLX (0.0,-C)
    3  PHP = (2.*3.1415927*PHP)/360.
    4  BTA = (2.*3.1415927*BTA)/360.
    5  PHM = (2.*3.1415927*PHM)/360.
    6  R = (4.*(CEXP(2.*PHP+2.*BTA+PHM)+2.*CEXP(PHP+BTA+2.*PHM)+CEXP(2.*
   1   PHP+PHM)+CEXP(PHP+2.*BTA)-2.*CEXP(BTA+PHM)-3.*CEXP(PHP))/27.)/
   2   ((-CEXP(2.*PHP+2.*BTA+2.*PHM)+2.*CEXP(PHP+2.*BTA+PHM)+CEXP(2.*
   3   PHP+2.*PHM)+6.*CEXP(PHP+PHM)+B.*CEXP(2.*PHP+BTA)+B.*CEXP(BTA+
   4   2.*PHM)+3.*CEXP(2.*BTA)-27.)/27.)
   16  W = (4.*(CEXP(2.*PHP+BTA+2.*PHM)+2.*CEXP(PHP+BTA+PHM)+2.*CEXP
   1   (2.*BTA+2.*PHM)-2.*CEXP(2.*PHM)-3.*CEXP(BTA))/27.)/((-CEXP(2.*
   2   PHP+2.*BTA+2.*PHM)+2.*CEXP(PHP+2.*BTA+PHM)+CEXP(2.*PHP+2.*PHM)
   3   +6.*CEXP(PHP+PHM)+B.*CEXP(2.*PHP+BTA)+B.*CEXP(BTA+2.*PHM)+3.*
   4   CEXP(2.*BTA)-27.)/27.)
   19  Z = ((3.*CEXP(2.*PHP+2.*BTA+2.*PHM)-2.*CEXP(PHP+2.*BTA+PHM)+CEXP(
   1   2.*PHP+2.*PHM)+2.*CEXP(PHP+PHM)-B.*CEXP(2.*PHP+BTA)-8.*CEXP(BTA+2
   2   .*PHM)+3.*CEXP(2.*BTA)+9.)/27.)/((-CEXP(2.*PHP+2.*BTA+2.*PHM)+2.*
   3   CEXP(PHP+2.*BTA+PHM)+CEXP(2.*PHP+2.*PHM)+6.*CEXP(PHP+PHM)+8.*CEXP
   4   (2.*PHP+BTA)+B.*CEXP(BTA+2.*PHM)+3.*CEXP(2.*BTA)-27.)/27.)
   22  Y = (4.*(CEXP(PHP+2.*BTA+2.*PHM)+2.*CEXP(2.*PHP+BTA+PHM)+CEXP(2.*
   1   BTA+PHM)-2.*CEXP(PHP+BTA)+CEXP(PHP+2.*PHM)-3.*CEXP(PHM))/27.)/((
   2   -CEXP(2.*PHP+2.*BTA+2.*PHM)+2.*CEXP(PHP+2.*BTA+PHM)+CEXP(2.*PHP+
   3   2.*PHM)+6.*CEXP(PHP+PHM)+B.*CEXP(2.*PHP+BTA)+B.*CEXP(BTA+2.*PHM)
   4   +3.*CEXP(2.*BTA)-27.)/27.)
   25  X = ((3.*CEXP(2.*PHP+2.*BTA+2.*PHM)+2.*CEXP(PHP+2.*BTA+PHM)-3.*CEX
   1   P(2.*PHP+2.*PHM)+6.*CEXP(PHP+PHM)-B.*CEXP(2.*PHP+BTA)-B.*CEXP(BTA
   2   +2.*PHM)-CEXP(2.*BTA)+9.)/27.)/((-CEXP(2.*PHP+2.*BTA+2.*PHM)+2.*
   3   CEXP(PHP+2.*BTA+PHM)+CEXP(2.*PHP+2.*PHM)+6.*CEXP(PHP+PHM)+B.*CEXP
   4   (2.*PHP+BTA)+B.*CEXP(BTA+2.*PHM)+3.*CEXP(2.*BTA)-27.)/27.)
   13  Q = (4.*(CEXP(2.*PHP+BTA+2.*PHM)+2.*CEXP(PHP+BTA+PHM)+2.*CEXP(2.*
   1   PHP+2.*BTA)-2.*CEXP(2.*PHP)-3.*CEXP(BTA))/27.)/((-CEXP(2.*PHP+2.*
   2   BTA+2.*PHM)+2.*CEXP(PHP+2.*BTA+PHM)+CEXP(2.*PHP+2.*PHM)+6.*CEXP
   3   (PHP+PHM)+B.*CEXP(2.*PHP+BTA)+B.*CEXP(BTA+2.*PHM)+3.*CEXP(2.*BTA)
   4   -27.)/27.)
    B  WRITE (6,9) A,B,C,Z,Y,W,R,X,Y,C,R,Z
    9  FORMAT (3F9.4//6F9.4/6F9.4/6F9.4/////)
   10  GO TO 1
   11  STOP
       END
/*
//LINK    EXEC   PROC=LINKSRCN
//GO    EXEC   PROC=EXECUTE
//FT05F001   DD    *
   150.0        60.0        30.0
/*
```

Fig. B-10. Fortron list of program for evaluotion of entire camplex scottering matrix far Diphalator with two differentiol phose-shift elements using discrete doto points.

```
C THIS PROGRAM DESIGNATES VALUES OF S13 FCR IMPERFECT CIRCULATOR WITH
C          BUT ONE DIFFERENTIAL PHASE SHIFT ELEMENT
C
C
C
   7  R(I) = (4.*(2.*CEXP(PHP+2.*BTA+PHM)+CEXP(PHP+4.*BTA)-2.*CEXP(2.*B
  1 TA)+2.*CEXP(PHP+2.*BTA)-3.*CEXP(PHP))/27.)/((-CEXP(PHP+4.*BTA+PHM
  2 )+2.*CEXP(PHP+2.*BTA+PHM)+B.*CEXP(PHP+2.*BTA)+B.*CEXP(2.*BTA+PHM)
  3 +CEXP(4.*BTA)+3.*CEXP(PHP+PHM)+6.*CEXP(2.*BTA)-27.)/27.)
                     ***********************
```

Fig. B-11. Substitutian far Fartran pragram af Fig. B-9 to evaluate $|S_{13}|$ far Diphalator with anly ane differential phase-shift element.

```
//E35640 JOB   S360,                                                    C
//            'BLAKE/LIBBEY,UI05',MSGLEVEL=1
//START   EXEC   PROC=DUMMY
//COM     EXEC   PROC=FORTRANH
//SYSIN   DD   *
C THIS PROGRAM CALCULATES THE MAGNITUDE SCATTERING MATRIX FOR THE SECOND
C            IMPERFECT CIRCULATOR WITH BUT ONLY ONE DIFFERENTIAL
C                PHASE SHIFT ELEMENT - OCTCBER 31, 1967
C
      COMPLEX PHP,BTA,PHM,R,Z,Y,X,Q,W
      CALL MSGDP
   1  READ (5,2,END=11) A,B,C
   2  FORMAT (F1C.0,F10.0,F10.0)
      PHP = CMPLX (0.0,-A)
      BTA = CMPLX (0.0,-B)
      PHM = CMPLX (0.0,-C)
   3  PHP = (2.*3.1415927*PHP)/360.
   4  BTA = (2.*3.1415927*BTA)/360.
   5  PHM = (2.*3.1415927*PHM)/360.
   6  R = (4.*(CEXP(PHP+3.*BTA+PHM)+2.*CEXP(3.*BTA+PHM)+CEXP(PHP+BTA+PHM
  1 )+CEXP(3.*BTA)-2.*CEXP(BTA+PHM)-3.*CEXP(BTA))/27.)/((-CEXP(PHP+4.
  2 *BTA+PHM)+2.*CEXP(PHP+2.*BTA+PHM)+8.*CEXP(PHP+2.*BTA)+B.*CEXP(2.*
  3 BTA+PHM)+CEXP(4.*BTA)+3.*CEXP(PHP+PHM)+6.*CEXP(2.*BTA)-27.)/27.)
   7  R = CABS (R)
  12  RR = REAL (R)
  16  W = (4.*(2.*CEXP(PHP+2.*BTA+PHM)+CEXP(PHP+4.*BTA)-2.*CEXP(2.*B
  1 TA)+2.*CEXP(PHP+2.*BTA)-3.*CEXP(PHP))/27.)/((-CEXP(PHP+4.*BTA+PHM
  2 )+2.*CEXP(PHP+2.*BTA+PHM)+B.*CEXP(PHP+2.*BTA)+B.*CEXP(2.*BTA+PHM)
  3 +CEXP(4.*BTA)+3.*CEXP(PHP+PHM)+6.*CEXP(2.*BTA)-27.)/27.)
  17  W = CABS (W)
  18  WW = REAL (W)
  19  Z = ((CEXP(PHP+2.*BTA+PHM)+3.*CEXP(PHP+PHM)-8.*CEXP(PHP+2.*BTA)+3.
  1 *CEXP(PHP+4.*BTA+PHM)-3.*CEXP(PHP+2.*BTA+PHM)-B.*CEXP(2.*BTA+PHM)
  2 +CEXP(4.*BTA)+3.*CEXP(2.*BTA)-CEXP(2.*BTA)+9.)/27.)/((-CEXP(PHP+4
  3 .*BTA+PHM)+2.*CEXP(PHP+2.*BTA+PHM)+8.*CEXP(PHP+2.*BTA)+8.*CEXP(2.
  4 *BTA+PHM)+CEXP(4.*BTA)+3.*CEXP(PHP+PHM)+6.*CEXP(2.*BTA)-27.)/27.)
  20  Z = CABS (Z)
  21  ZZ = REAL (Z)
  22  Y = (4.*(2.*CEXP(PHP+3.*BTA)+CEXP(PHP+3.*BTA+PHM)+CEXP(PHP+BTA+PHM
  1 )+CEXP(3.*BTA)-2.*CEXP(PHP+BTA)-3.*CEXP(BTA))/27.)/((-CEXP(PHP+4.
  2 *BTA+PHM)+2.*CEXP(PHP+2.*BTA+PHM)+B.*CEXP(PHP+2.*BTA)+B.*CEXP(2.*
  3 BTA+PHM)+CEXP(4.*BTA)+3.*CEXP(PHP+PHM)+6.*CEXP(2.*BTA)-27.)/27.)
```

Fig. B-12. Fartran list of program far evaluatian af magnitude scattering matrix af Diphalatar with anly ane differential phase-shift element using discrete data paints.

```
23   Y = CABS (Y)
24   YY = REAL (Y)
25   X = ((3.*CEXP(PHP+4.*BTA+PHM)+CEXP(PHP+2.*BTA+PHM)-8.*CEXP(PHP+2.*
    1 BTA)+CEXP(PHP+2.*BTA+PHM)-8.*CEXP(2.*BTA+PHM)-3.*CEXP(4.*BTA)-CEX
    2 P(PHP+PHM)+6.*CEXP(2.*BTA)+9.)/27.)/((-CEXP(PHP+4.*BTA+PHM)+2.*
    3 CEXP(PHP+2.*BTA+PHM)+8.*CEXP(PHP+2.*BTA)+8.*CEXP(2.*BTA+PHM)+CEXP
    4 (4.*BTA)+3.*CEXP(PHP+PHM)+6.*CEXP(2.*BTA)-27.)/27.)
26   X = CABS (X)
27   XX = REAL (X)
13   Q = (4.*(2.*CEXP(PHP+2.*BTA+PHM)+CEXP(4.*BTA+PHM)-2.*CEXP(2.*BTA)+
    1 CEXP(2.*BTA+PHM)+CEXP(2.*BTA+PHM)-3.*CEXP(PHM))/27.)/((-CEXP(PHP+
    2 4.*BTA+PHM)+2.*CEXP(PHP+2.*BTA+PHM)+B.*CEXP(PHP+2.*BTA)+8.*CEXP(2
    3 .*BTA+PHM)+CEXP(4.*BTA)+3.*CEXP(PHP+PHM)+6.*CEXP(2.*BTA)-27.)/27.
    4 )
14   Q = CABS (Q)
15   QQ = REAL (Q)
 8   WRITE (6,9) A,B,C,ZZ,YY,WW,RR,XX,YY,QQ,RR,ZZ
 9   FORMAT (3F9.4//3F9.4/3F9.4/3F9.4////)
10   GO TO 1
11   STOP
     END
/*
//LINK    EXEC    PROC=LINKSRCN
//GO    EXEC    PROC=EXECUTE
//FT05F001    DD    *
  18C.0         90.0          90.0
/*
```

Fig. B-12. Continued.

APPENDIX C
BIBLIOGRAPHY

Belevitch, V., "Elementary Applications of the Scattering Formalism in Network Design," Trans. IRE, PGCT CT-3, 97 (1956).

Butcher, P. N., "Les Impédances de Couplage dans Les Structures EN Bandes (On the Coupling Impedance of Tape Structures)," Numéro Spécial du Congrès Tubes Hyperfréquences, No. 4.2.08, Paris, 1956.

Chang, K. K. N., Parametric and Tunnel Diodes (Prentice-Hall, New York, 1964).

Chow, W. F., Principles of Tunnel Diode Circuits (John Wiley and Sons, Inc., New York, 1964).

Cunningham, W. J., Nonlinear Analysis (McGraw-Hill, New York, 1958), pp. 106-114 and 93-101.

Farney, G. K., "Slow Wave Circuits for Electronic Interaction Derived from Two-Wire Transmission Lines by Geometrical Meandering and/or Reactive Loading," S. F. D. Laboratory, Inc., Union, New Jersey (April 1964).

Firestone, W. L., "Analysis of Transmission Line Directional Couplers," Proc. IRE 42, 1529 (1954).

Harrison, G. R., and J. L. Allen, "Integrated Circuit Technology Applicable to Functional Microwave Modules," paper presented for a Special Microwave Session at the International IEEE Convention, New York, 18-21 March 1968.

Henock, B. T., and Y. Kvaerna, "Broadband Tunnel-Diode Amplifiers," Technical Report 213-2, Stanford Electronics Laboratories, Stanford, California, SEL-62-099 (August 1962).

Ince, W. J., et al., "Phased Array Radar Studies, 1 July 1961 to 1 January 1963," Technical Report 299, Lincoln Laboratory, M.I.T. (20 February 1963), Part 2, Ch. II, DDC 417572.

Kuo, F. F., Network Analysis and Synthesis, Second Edition (John Wiley and Sons, Inc., New York, 1966), Chapter 14.

Lax, B., and K. J. Button, Microwave Ferrites and Ferrimagnetics (McGraw-Hill, New York, 1962).

Lepoff, J. H., "Design Procedure for a Shunt Stabilizing Circuit for Tunnel Diode Amplifiers," private communication.

_____, "How to Design Stable, Broadband Tunnel Diode Amplifiers," Microwaves (November 1964), p. 38.

Miller, B. A., T. P. Miles, and D. C. Cox, "A Design Technique for Realizing a Microwave Tunnel-Diode Amplifier in Stripline," IEEE Trans. Microwave Theory Tech. MTT-15, No. 10, 554 (1967).

Newcomb, R. W., T. N. Rao, and J. Woodard, "A Minimal Capacitor Cascade Synthesis for Integrated Circuits," Microelectronics and Reliability 6, No. 2, 113 (May 1967).

Okean, H. C., "Synthesis of Negative Resistance Reflection Amplifiers Employing Band-Limited Circulators," IEEE Trans. Microwave Theory Tech. MTT-14, No. 7, 323 (1966).

Oliver, B. M., "Directional Electromagnetic Couplers," Proc. IRE 42, 1686 (1954).

Oono, Y., "Application of Scattering Matrices to the Synthesis of n-Ports," Trans. IRE, PGCT CT-3, 111 (1956).

Richards, P. I., "Resistor Transmission-Line Circuits," Proc. IRE 36, 217 (1948).

Roome, G. T., H. A. Hair, and C. W. Gerst, "Thin Ferrites for Integrated Microwave Devices," 3rd Quarterly Technical Report (covering 1 April 1966 through 30 June 1966), Syracuse University Research Corporation, Special Projects Laboratory, Syracuse, New York.

Schiffman, B. M., "A New Class of Broad-Band Microwave 90-Degree Phase Shifters," Trans. IRE, PGMTT MTT-6, 232 (1958).

Sokolnikoff, I. S., Tensor Analysis (John Wiley and Sons, Inc., New York, 1957).

Thourel, L., The Use of Ferrites at Microwave Frequencies (Macmillan, New York, 1964).

Weiss, J. A., "An Interference Effect Associated with Faraday Rotation, and Its Application to Microwave Switching," presented at Conference on Magnetism and Magnetic Materials, Boston, Massachusetts, 16-18 October 1956.

_____, "Circulator Synthesis," IEEE Trans. Microwave Theory Tech. MTT-13, No. 13, 38 (1965), DDC 616432.

_____, "Reciprocal and Nonreciprocal Microstrip Periodic Networks," Final Report prepared by Worcester Polytechnic Institute under subcontract to Lincoln Laboratory, M.I.T. (15 July 1967).

Welch, J. D., and H. J. Pratt, "Losses in Microstrip Transmission Systems for Integrated Microwave Circuits," NEREM Record (1966), DDC 648055.

Wheeler, H. A., "Skin Resistance of a Transmission-Line Conductor of Polygon Cross Section," Proc. IRE 43, No. 7, 805 (1955).

Young, L., "Microwave Filters and Diplexers," Stanford Research Institute, New York (IEEE International Convention Digest, 1967).

DOCUMENT CONTROL DATA - R&D

(Security classification of title, body of abstract and indexing annotation must be entered when the overall report is classified)

1. ORIGINATING ACTIVITY (Corporate author)	2a. REPORT SECURITY CLASSIFICATION
Lincoln Laboratory, M.I.T.	Unclassified
	2b. GROUP None

3. REPORT TITLE

Theory of Active Nonreciprocal Networks

4. DESCRIPTIVE NOTES *(Type of report and inclusive dates)*

Technical Report

5. AUTHOR(S) *(Last name, first name, initial)*

Libbey, Waldo M.

6. REPORT DATE	7a. TOTAL NO. OF PAGES	7b. NO. OF REFS
4 February 1969	98	53

8a. CONTRACT OR GRANT NO. AF 19(628)-5167	9a. ORIGINATOR'S REPORT NUMBER(S)
b. PROJECT NO. ARPA Order 498	Technical Report 455
c.	9b. OTHER REPORT NO(S) *(Any other numbers that may be assigned this report)*
d.	ESD-TR-69-5

10. AVAILABILITY/LIMITATION NOTICES

This document has been approved for public release and sale; its distribution is unlimited.

11. SUPPLEMENTARY NOTES	12. SPONSORING MILITARY ACTIVITY
None	Advanced Research Projects Agency, Department of Defense

13. ABSTRACT

This investigation sets forth theory and experimental data for active nonreciprocal networks. A simple way is shown of achieving nonreciprocity using a magnetic field device exhibiting small amounts of differential phase shift. In the theoretical treatment, use is made of scattering parameters. The effect on nonreciprocity of having cascaded and parallel connected elements is considered. How matching and scattering from various junctions influences non-reciprocity is included. Two simple devices exhibiting nonreciprocity are discussed in detail: a differential amplifier, and a differential attenuator; and a procedure is given for their use in active network synthesis. For these devices, the meander line is the nonreciprocal element utilizing a magnetic field. A new meander-line design is presented, realizing a desired impedance, based on recent data on odd- and even-mode velocities along coupled microstrips.

From the experimental work, data are reported on a meander line showing impedance characteristics which are in good agreement with theory and showing the amount of differential phase shift possible. To realize an element with loss, an experimental bilateral microstrip attenuator is described whose resistances are short silver-deposited lines. Measurements show satisfactory matching for a 6-dB model. A complete design is given for a microstrip differential attenuator using the loss and nonreciprocal elements mentioned operating near 3 GHz. Scattering parameters measured on a model differential attenuator show very close agreement with theory. Data are presented on both the differential attenuation and the insertion loss of this realized model.

A theoretical analysis is given in Appendix A of two lossless three-port circuits capable of exhibiting nonreciprocity using small amounts of differential phase shift. The analysis demonstrates that relations between variables exist that will allow perfect matching at input and output ports and will allow the desired nonreciprocity without depending entirely on the existence of circulation.

14. KEY WORDS

network theory	attenuators	circulators
magnetic fields	nonreciprocity	differential phase
phase shift	impedance	ferrites
amplifiers	Diphalator	